

THESIS FOR THE DEGREE OF DOCTOR OF PHILOSOPHY

**Wind Farm Configuration and Energy Efficiency Studies
- Series DC versus AC Layouts**

STEFAN LUNDBERG



Department of Energy and Environment
CHALMERS UNIVERSITY OF TECHNOLOGY
Göteborg, Sweden 2006

Wind Farm Configuration and Energy Efficiency Studies - Series DC versus AC Layouts
STEFAN LUNDBERG
ISBN 978-91-7291-884-9

© STEFAN LUNDBERG, 2006.

Doktorsavhandlingar vid Chalmers tekniska högskola
Ny serie nr. 2565
ISSN 0346-718X

Department of Energy and Environment
Chalmers University of Technology
SE-412 96 Göteborg
Sweden
Telephone +46 (0)31-772 1000

Chalmers Bibliotek, Reproservice
Göteborg, Sweden 2006

To my family

Abstract

In this thesis, the design and control of a wind farm utilizing series-connected wind turbines with a DC output has been evaluated. The advantage is that a suitable DC voltage level, appropriate for transmission of the generated power directly, without using a large centralized DC/DC converter, can be obtained. This is achieved by series-connecting a number of wind turbines. In addition, the energy production using various wind turbines and wind park layouts have been investigated. Furthermore, the energy production costs have been determined. Finally, the limiting factors for the installation of smaller wind parks have been evaluated. For instance, when dynamic power pulsations have to be considered, from a power quality point of view, when a wind energy installation is to be connected to the grid.

The results found are that the uneven power production from the individual wind turbines creates design as well as control difficulties for the wind farm with series-connected wind turbines. A control scheme for the wind turbines is proposed and investigated in this thesis. It is found that the proposed control scheme manages to safely operate the wind farm, even when large deviations in the individual power production of the turbines exist. A down-scaled prototype has been built, representing one wind turbine unit, and the base current control ability was verified experimentally.

Moreover, it is found that it is necessary to design the individual wind turbine converters for a voltage level of about 35 % higher than the nominal voltage. Otherwise there will be a substantial energy loss due to the uneven power production from the individual wind turbines that occurs in actual installation.

In addition, it is found that the series dc wind park has a good economical potential, since it eliminates the need for an offshore platform in the wind park.

Finally, the electrical limiting factors for the installation of wind farms is determined using field experimental data. For instance, it is shown that for a wind park of about 10 wind turbines, the power pulsations are "smoothened" sufficiently so that the flicker emission never will be the limiting factor, even for fixed-speed turbines, when a wind energy installation is connected to a network. Worth mentioning is that it was found that the summation formula for flicker given in IEC 61400-21 can give a flicker prediction that is too low.

Acknowledgements

This work has been carried out at the Department of Energy and Environment at Chalmers University of Technology. The financial support given by the National Energy Administration (Energimyndigheten), E.ON Sweden foundation for research as well as ABB Power Technologies is gratefully acknowledged.

I would like to thank my supervisor Dr. Torbjörn Thiringer for his supervision, his patience and support and especially for his encouragement and positive attitude. Without his help this work would not have been finished. I would also like to thank my fellow Ph.D students and coworkers: Massimo Bongiorno, Jimmy Ehnberg, Magnus Ellsén, Lena Max, Robert Karlsson, Andreas Petersson and Oskar Wallmark for all help and interesting discussions.

Many thanks to my examiner professor Tore Undeland, for the valuable discussions in our meetings and at other times.

To Mats Hyttinen a special thank is directed for introducing the idea of the series DC wind park to me. I would also like to thank the other members in my reference group, 2001-2003: Peter Christensen from NVE, Kent Sørbrink from Eltra, Christer Liljegren from CLEPS, Pehr Hjalmarsson, Anders Lasson and Jan Svensson from ABB, for the valuable discussions in our meetings and at other times.

Finally, many thanks to all other colleagues at the Division of Electric Power Engineering.

Stefan Lundberg
Göteborg, Sweden
December, 2006

Contents

Abstract	v
Acknowledgements	vii
Contents	ix
1 Introduction	1
1.1 Background	1
1.2 Review of related Research	4
1.3 Purpose of the thesis and Contributions	4
1.4 Publications	5
2 Wind Energy Conversion Systems	7
2.1 Short about aerodynamic energy conversion of wind turbines	7
2.1.1 Wind speed distribution	7
2.1.2 Operating principle of a wind turbine	9
2.1.3 Dynamic aspects of aerodynamic power control	11
2.1.4 Variable speed wind turbines	12
2.2 Fix speed wind turbine	12
2.3 Limited speed range wind turbine	16
2.4 Full range variable speed wind turbines	18
2.4.1 Classical AC output system	18
2.4.2 Variable speed DC wind turbine with IGBT rectifier	21
2.5 Energy efficiency comparison of different wind turbines	23
2.6 Power quality impact of wind turbines and "small" wind parks	24
3 Energy Efficiency of Wind Parks	27
3.1 Wind Farm Layouts	27
3.1.1 AC Systems for Wind Farms	29
3.1.2 Mixed AC and DC Systems for Wind Farms	30
3.1.3 DC Systems for Wind Farms	30
3.2 Energy Production Cost of Different Wind Farms	33

3.2.1	Energy production cost	33
3.2.2	Comparison of Energy Production Costs	35
4	Wind Farm with Series Connected Wind Turbines	39
4.1	System Overview	39
4.1.1	Wind farm layout	39
4.1.2	Steady-state behavior of the series-connection	40
4.1.3	Wind turbine for series-connection	41
4.1.4	Transmission System and Onshore Converter Station	43
4.2	Wind Turbine System	44
4.3	DC/DC Converters	45
4.3.1	Full Bridge Isolated Boost Converter	45
4.3.2	Full Bridge Converter with Phase Shift Control	48
5	Controller Structure and Design	51
5.1	Onshore Converter station Controller	51
5.1.1	Phase-Locked Loop (PLL)	51
5.1.2	DC-transmission controller	53
5.1.3	AC-current controller	54
5.1.4	Modulator for the HVDC	56
5.2	Overview of the Wind Turbine Controller	57
5.2.1	Speed controller	59
5.2.2	DC-link voltage controller	60
5.2.3	Output Voltage controller	62
5.2.4	Mode selector	63
5.2.5	Reference value calculations	64
5.3	Induction machine controller	66
5.3.1	Current model flux estimator	67
5.3.2	Flux controller	68
5.3.3	Current controller	68
5.3.4	Modulator and the three phase converter	70
5.4	Current controller for the FBIB Converter	71
5.5	Controllers for the FBPS Converter	72
5.5.1	Current controller	72
5.5.2	Flux controller	73
6	Park design considerations for the series DC farm	75
6.1	Simulation setup	75
6.1.1	The HVDC-station and the transmission system	76
6.1.2	The wind turbine unit	81
6.2	Analysis of a small wind farm	82

6.3	Energy Capture vs Output Voltage	88
7	Transformer design and measurements	91
7.1	Converter Design for the Series-connection	91
7.1.1	Cooling of the Transformer and the Components	93
7.1.2	Electric Field in the Transformer	93
7.1.3	Full Scale FBPS Converter, 5MW	96
7.2	Down Scaled Converter	97
7.3	Measurements	102
7.3.1	Converter in steady-state	102
7.3.2	Current controller	105
7.3.3	DC/DC transformer flux controller	105
8	Conclusions	107
8.1	Results from present work	107
8.2	Future Research	108
	References	109
A	Data for the implemented models	115
B	Selected Publications	117

Chapter 1

Introduction

1.1 Background

In Europe today (2006) there is a concern about the greenhouse effect and investments are done to decrease it. One part of this is to create a more CO₂ neutral society. For the energy sector this has led to that more investments are done in renewable energy sources, such as wind power, biomass, ... and solar. Wind energy installations have gone from being small units erected one by one to larger units erected in groups. Today wind farms up to a size of 160 MW have been built and several plans of 1000 MW-parks exist [2]. These larger wind parks are mainly considered to be located out in the sea, preferably at such a distance out in the sea that they cannot be observed from the shore [35]. In Fig. 1.1 some plans for offshore wind farms in the baltic sea are shown. Another advantage of selecting an offshore site is that the average wind speed is usually higher than onshore. Drawbacks with offshore sites are that the accessibility to the wind park is lower than onshore, all equipment must be adapted for the offshore environment and the distance from the wind park to the connection point to the grid is usually longer than for an onshore site.

In order for the wind parks to be economically reasonable it is important to keep the energy production cost down. This can be done by having a site with high average wind speed, a wind park layout that fits the site and to keep the number of operation hours high. Another aspect, mainly of importance for smaller wind parks is to not violate any power quality issues at the point of common connection.

For the largest wind parks it is a problem to find a suitable grid connection point, which is strong enough to handle the generated power from the parks. This leads to that, in many cases, the distance between the grid connection point and the wind farm is so long that a DC-transmission may become more favorable than a conventional AC-transmission [3].

Today all offshore wind farms that have been built uses an AC-transmission [3]. The largest so far are the Nysted and Horns Ref offshore wind farms in Denmark. Both of these wind farms use an offshore transformer station to raise the voltage from the wind turbines (33-36 kV) to 132-150 kV for transmission to shore. The proposed layouts for

the electrical system for wind farms in the literature also have such an offshore platform [9, 11, 26]. Offshore transformer stations are rather complex and include large support structures and are thus costly [3]. If the offshore transformer station can be avoided, the cost can accordingly be reduced.

In [34, 58] a solution is proposed which eliminates the offshore platform by connecting wind turbines in series and using DC voltage as the output of the turbines. In this way it is possible to obtain the desired transmission voltage directly without a large centralized DC/DC converter. This solution together with some of the wind farm layouts discussed in for instance [9, 35] are investigated with respect to energy production and energy production cost in [30]. A key result of that study is that a wind farm layout utilizing series-connected wind turbines with a DC voltage output has a very promising energy production cost, if the transmission distance is above 20 km. Although the series-connected DC wind farm is an interesting solution from an economic point of view, it has not been investigated dynamically using transistor/IGBT techniques yet. The system investigated in [58] is based on thyristor technic and in [34] only the layout and the steady-state behavior of the series-connected wind farm are investigated.

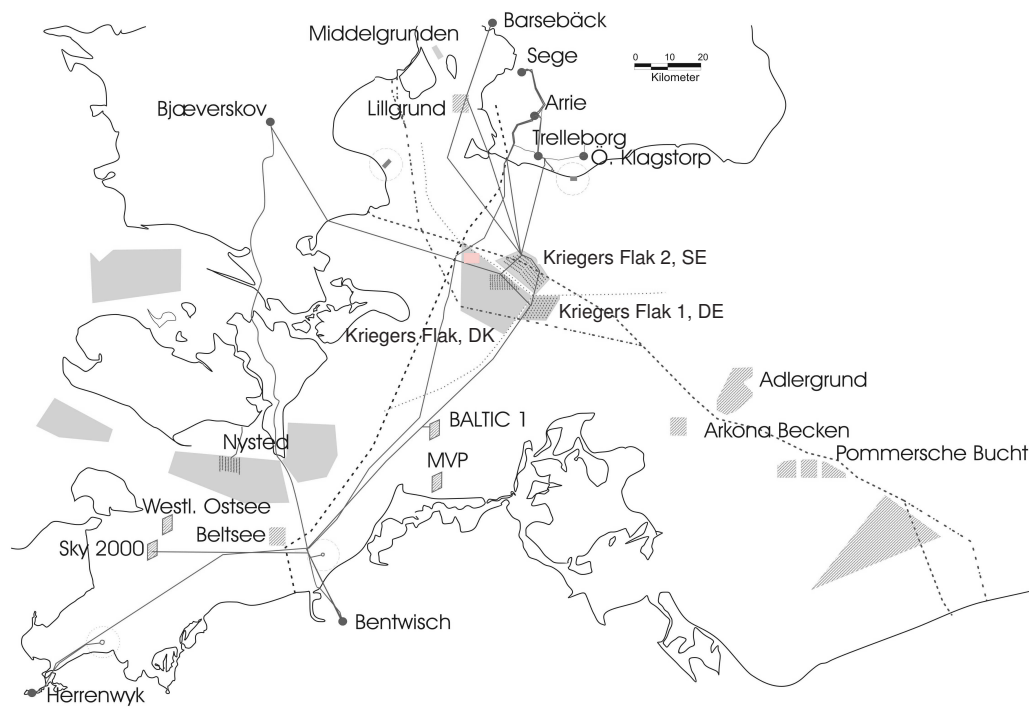


Figure 1.1: Planned offshore wind farms in the Baltic sea. Courtesy of Peter Christensen and Niels Andersen, (NVE, Denmark 2003)

Name	Rated power	Country
Nysted (built)	160 MW	Danmark
Lillgrund	150 MW	Sverige
Kriegers Flak 1	340 MW	Tyskland
Kriegers Flak 2	640 MW	Sverige
Kriegers Flak 3	300 MW	Danmark
Sky 2000	150 MW	Tyskland
Westl.Ostsee	150 MW	Tyskland
Beltsee	415 MW	Tyskland
Pommersche Bucht	1000 MW	Tyskland
Arkona Becken	945 MW	Tyskland
Adlersgrund	790 MW	Tyskland
Baltic 1	50 MW	Tyskland
MVP	40 MW	Tyskland

1.2 Review of related Research

Wind park design studies have been presented in several papers, for instance [3, 24, 26, 35, 45, 47, 49, 61]. The most detailed study was made by Bauer, Haan, Meyl and Pierik [9]. In [34] some interesting DC solutions for offshore wind parks are presented and especially the proposal of a wind park with wind turbines connected in series, is of great interest. The energy production of various wind parks is calculated in [35, 43, 50], and in [24, 35, 48, 50, 53] the estimated cost of the produced electric energy is presented. In [8] the economics of some offshore wind farms that are built and are planned to be built, are presented.

Of importance when determining the energy capture of a wind turbine is to have detailed blade data as well as detailed loss models of components. Relevant blade data is not trivial to obtain, however previous authors have used the following method: By not revealing the origin of the blade description, it is possible to obtain such data. Generator loss models has for instance been presented in [20, 48], gear-box losses have been found in [20]. However, available loss models of existing high power DC/DC-converters are very crude.

Cost data is another large problem area. Here the same principle seems to be dominant: Data can be obtained providing that the sources are not revealed. However, in [12, 36, 42, 50, 53] valuable cost information is given which can be utilized.

Energy capture calculations of wind turbine systems and wind farms is a subject in which it is possible to find much information in the literature. However, detailed comparisons between different electric generating systems for wind turbines are not so common. As a part of the present work, article [40] was published where a detailed comparison between electric generating systems for wind turbines was studied.

Regarding the power quality impact on the grid by wind turbines there exists a large number of papers. Of special interest for this work are [39, 52] where the impact of X/R is discussed and [51, 52] where the summing up of power pulsations was investigated.

Papers investigating DC/DC also for higher powers are starting to emerge. Of special interest for this work are the DC/DC converters studied in [14].

1.3 Purpose of the thesis and Contributions

The main purpose of this thesis is to investigate the wind park with series connected wind turbines with a DC output and to find a possible control scheme. The "core" investigation is made in the end of the thesis, and the contributions from this part are: The dynamic investigation of the system, the requirements on the wind turbine system, the developed control scheme for the wind turbine in normal operation as well as operation using a proposed over voltage limiter.

An additional goal was to investigate the energy production cost of various wind park

layouts, based on energy efficiency calculations and cost estimations. The contributions from these studies are the energy efficiency of different wind turbine systems and of different wind park layouts. Also, from an energy production cost point of view, when the different investigated wind park layouts are to prefer and what parameters that are influencing the energy production cost.

An initial goal, of interest for smaller parks, in particular parks equipped with fixed speed turbines, was to investigate the impact of wind turbine type, number of turbines and properties of the receiving grid on the power quality. The electrical grid limitations have been investigated for different types of fixed speed wind turbines. The contributions from these studies are knowledge about how the flicker emission is depending on the type of wind turbine, the receiving grid and number of turbines, as well as suggesting electrical limiting factors for small wind farms.

1.4 Publications

Apart from the Licentiate thesis [32] and a technical report [33], the publications originating from this project are:

- I A. Petersson, **S. Lundberg** and T. Thiringer, "A DFIG Wind-turbine Ride-Through System Influence on the Energy Production," *Wind Energy*, vol. 8, issue 3, pp. 251-263, July/September 2005.
- II A. Petersson and **S. Lundberg**, "Energy Efficiency Comparison of Electrical Systems for Wind Turbines," *Nordic Workshop on Power and Industrial Electronics (NORpie 2002)*, Stockholm, Sweden, August 12-14, 2002, CD-ROM.
- III **S. Lundberg**, T. Petru and T. Thiringer, "Electrical limiting factors for wind energy installations in weak grids," *International Journal of Renewable Energy Engineering*, vol. 3, no. 2, pp. 305 - 310, August, 2001.
- IV T. Thiringer, T. Petru and **S. Lundberg**, "Flicker Contribution from Wind Turbine Installations," *IEEE Transactions on Energy Conversion*, vol. 19, no. 1, pp. 157-163, March 2004.
- V **S. Lundberg**, "Evaluation of wind farm layouts," *EPE Journal*, vol. 16, no. 1, pp. 14-21, February 2006.
- VI O. Carlsson and **S. Lundberg**, "Integration of Wind Power by DC-Power Systems," *PowerTech Conference*, St. Petersburg, Russia, June 2005, Panel session paper.
- VII L. Max and **S. Lundberg**, "System efficiency of a DC/DC converter based wind turbine grid system," *Nordic Wind Energy Conference*, Espoo, Finland, 22-23 May, 2006.

Paper I-VII are found in Appendix B of this thesis. The conference publications below, (VIII, IX), has after the conference been published in journals, (V, I) respectively, and therefore are they not included in this thesis:

VIII S. Lundberg, “Evaluation of wind farm layouts,” *2004 Nordic Workshop on Power and Industrial Electronics (NORpie 2004)*, Trondheim, Norway, 14-16 June, 2004.

IX A. Petersson, S. Lundberg, T. Thiringer, “A DFIG Wind-turbine Ride-Through System Influence on the Energy Production,” *Nordic Wind Energy Conference*, Göteborg, Sweden, March 1-2, 2004.

Chapter 2

Wind Energy Conversion Systems

(WELS), operational behavior, energy capture and power quality impact

2.1 Short about aerodynamic energy conversion of wind turbines

2.1.1 Wind speed distribution

The wind speed can be treated as a continuous random variable. The probability that a given wind speed shall occur can be described with a density function. There are several density functions that can be used to describe how the wind speed is distributed. The two most common are the Weibull and the Rayleigh functions. The Rayleigh distribution, or chi-2 distribution, is a subset of the Weibull distribution and is described by [25]

$$f(w_s) = \frac{k}{c} \left(\frac{w_s}{c} \right)^{k-1} e^{-(w_s/c)^k} \quad (2.1)$$

where:

- $f(w_s)$ Probability density
- w_s Wind speed > 0 [m/s]
- k Shape parameter > 0
- c Scale parameter > 0

Comparisons with measured wind speeds over the world show that the wind speed can be reasonably well described by the Weibull density function if the time period is not too short. Periods of several weeks to a year or more are usually reasonably well described by the Weibull distribution, but for shorter time periods the agreement is not so good [25]. The mean wind speed can be calculated using the equation for calculating the expectation

value of a continuous random variable, which gives

$$w_{s,\text{mean}} = \int_0^{\infty} w_s f(w_s) dw_s = \frac{c}{k} \Gamma\left(\frac{1}{k}\right) \quad (2.2)$$

where Γ is Euler's gamma function

$$\Gamma(z) = \int_0^{\infty} t^{z-1} e^{-t} dt. \quad (2.3)$$

If the shape parameter, k , is equal to 2 the Weibull distribution is equal to the Rayleigh distribution. The advantage of the Rayleigh function is that it only depends on the scale parameter c , which is dependent only on the mean wind speed. The scale parameter can be calculated for a given mean wind speed as

$$c = \frac{2}{\sqrt{\pi}} w_{s,\text{mean}} \quad \text{for } k = 2, \quad \Gamma\left(\frac{1}{2}\right) = \sqrt{\pi}. \quad (2.4)$$

In Fig. 2.1 the Rayleigh distribution function is shown for different mean wind speeds. Mean wind speeds of 5.4 m/s and 7.2 m/s correspond to a medium and high wind site

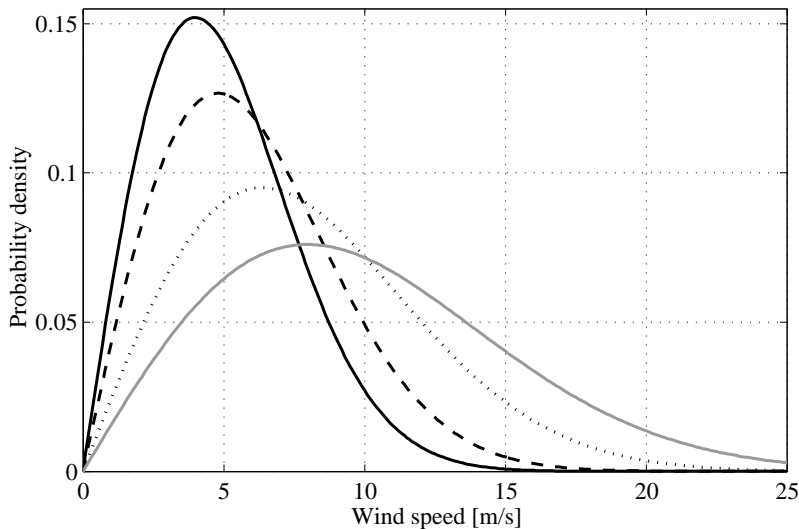


Figure 2.1: Rayleigh distribution function for different mean wind speeds. Solid 5 m/s, dashed 6 m/s, dotted 8 m/s and grey 10 m/s.

in Sweden, according to [55], and an average wind speed of 9.7 m/s is found at Horns Rev [16]. The Rayleigh distribution is used in this work to describe the distribution of the wind speed.

2.1.2 Operating principle of a wind turbine

A wind turbine consists of a tower, a nacelle and a rotor. The rotor converts wind energy to mechanical energy. In the hub, the drive train is located. In the drive train, the mechanical energy is converted into electrical energy. The drive train consists of one or several shafts, generator and usually a gear-box.

A wind turbine has a specific rating at which it reaches its maximum power. Sizes year 2006 are up to 6 MW. The rated power level is reached at a wind speed of 12-15 m/s, and the wind speed when the rated power is reached is referred to as rated wind speed. Below rated wind speed the turbine tries to capture as much energy as possible from the wind. Below 3-4 m/s there is so little energy available in the wind so the turbine stops. At wind speeds above rated, the operation principle is different. The wind turbine rotor must now limit the incoming power to the rated shaft power. This is done by utilizing the blades. Either the blades are turned out of the wind, pitch control, or the blades are designed in such a way that the flow becomes disturbed and the blades lose their efficiency, stall control.

As mentioned before, the rotor blades convert some of the kinetic energy of the wind to mechanical energy which is transmitted to the rotor shaft. The efficiency of this conversion depends on several factors such as blade profiles, pitch angle, tip speed ratio and air density. The pitch angle, β , is the angle of the blades towards the rotational plane. If the pitch angle is low, the blades are almost perpendicular to the wind and if the pitch angle is high (near 90 degrees) the blades are almost in parallel with the hub direction. The tip speed ratio, λ , is the ratio between the tip speed of the blades and the wind speed, (2.6). The conversion from wind speed to mechanical power can in steady state be described by [25]

$$P_{\text{mec}} = \frac{\pi \rho w_s^3 \left(\frac{D_r}{2}\right)^2}{2} C_p(\lambda, \beta) \quad (2.5)$$

$$\lambda = \frac{\omega_t D_r}{2w_s}. \quad (2.6)$$

Where:

D_r	rotor diameter [m]
ω_t	turbine rotor speed [rad/s]
ρ	air density = 1.225 [kg/m ³]
w_s	wind speed [m/s]
λ	tip speed ratio
β	pitch angle
$C_p(\lambda, \beta)$	aerodynamic efficiency

In Fig. 2.2, the mechanical power and the aerodynamic efficiency for the blade profile used in this report are shown for different pitch angles and for a fixed rotor speed.

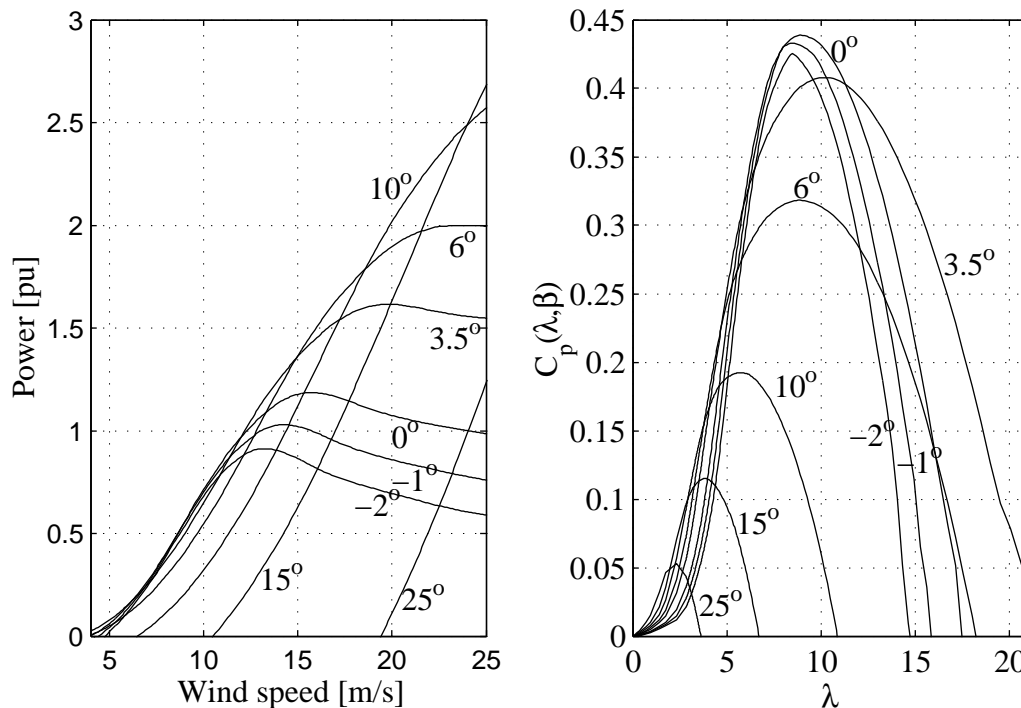


Figure 2.2: The mechanical power as function of wind speed and pitch angle for a fixed rotor speed, left plot, and the aerodynamic efficiency as function of λ and pitch angle, right plot.

Stall control

From Fig. 2.2 it can be noted that if the pitch angle is kept at 0° the turbine automatically limits the output power to a maximum of 1.2 p.u., for -1° the power is limited to a maximum of 1.0 pu using the same rotor speed in the whole wind speed interval. As can be noted, the power reaches a maximum around 15 m/s and then decreases for higher wind speeds.

Stall control in combination with fixed speed was the dominating concept for wind turbines earlier. The reason is, of course, that it is cheaper to have blades that do not need a pitching mechanism. Moreover, power electronic equipment was too expensive earlier and therefore induction generators connected to the grid without power electronic equipment were the preferred choice to be used.

However, for MW size turbines, stall control has been considered to be unfeasible. One important reason is the emergency breaking of the turbine. If the blades can not be turned, the turbine must have a very large brake on the primary shaft. But if turnable blades are used, and in particular if each blade has its own emergency pitching system, this can replace the large main shaft brake. On the other hand, if pitch control is used, it is sufficient to have a much smaller mechanical parking brake, in addition to the breaking

system made up by the pitching of the blades.

Active stall control

If a pitching mechanism is available, a possibility is to slightly modify the pitch angle at high wind speeds also for turbines without a power electronic converter. When the wind speed is 15m/s, a pitch angle of -1° is used, while for 25 m/s the used angle is around 0° . In this way, the power level is kept at the rated value in the whole high wind speed region. In addition, the benefits of using a smaller brake and also a facilitated starting and emergency stopping is obtained.

Pitch control

Another way of obtaining a constant power level at high wind speeds is to turn the blades out of the wind, i.e. to increase the pitch angle. At 12 m/s a pitch angle of 0° is used, at 17 m/s 15° and at 24 m/s and angle of 25° is used, according to Fig. 2.2. The advantage of using pitch control instead of active stall control is that the thrust force (pressure on the turbine disc) is lower.

2.1.3 Dynamic aspects of aerodynamic power control

If fixed rotor speed is used, there is a large drawback with using pitch control: there will be large power variations at high wind speeds. Let us consider the following case: the turbine is operating at 13 m/s with a pitch angle of 6° . The power is now 1 pu. The wind speed increases rapidly to 15 m/s and suddenly the power level is now 1.3 pu. The pitch controller has to increase the pitch angle to 10° and the power error is eliminated. However, if a new wind speed change occurs, a new power pulsation is created. As can be noted from Fig. 2.2, this situation does not occur when using stall control. If we have a pitch angle of -1° , we can note that wind speed changes in the high wind speed area lead to very small power variations. This has led to that fixed-speed turbines are almost all stall-controlled, either passive or active.

However, if the rotor speed can be varied, pitch control becomes much more favorable. In this case the incoming power fluctuations can instead be taken up by changing the amount of energy stored in the rotor, i.e. by adjusting the rotor speed. The wind turbine rotor thus acts as an active low-pass filter for power fluctuations. Variable rotor speed can of course also be used in combination with stall or active stall, but the advantage of using pitch control is, as mentioned, that the thrust force is lowered. This has led to that almost all variable-speed turbines are pitch regulated.

2.1.4 Variable speed wind turbines

As can be noted from Fig. 2.2, right plot, the maximum efficiency of the investigated turbine occurs at λ equal to 9. For the fixed-speed turbine λ is higher than 9 for lower wind speeds and, accordingly, the efficiency of the fixed-speed rotor is lower than optimal at lower wind speeds. For the variable-speed turbine, it is possible to maximize the mechanical power by using a variable rotational speed of the wind turbine. This means that the pitch angle is kept constant at low wind speeds, zero in this case, and the rotational speed of the turbine is adjusted according to the actual wind speed so that λ always equals 9. This means that the turbine will work at the maximum efficiency which gives the maximum mechanical output power of the turbine, in the low wind speed region.

It should be kept in mind that the energy benefit is not the main reason for using variable speed. The main advantage is the reduced stresses on the turbine, due to the variable speed operation. Also the fact that variable-speed turbines are capable of controlling the reactive power is an important reason for selecting a variable-speed turbine.

The upper rotational speed is limited by the mechanical stresses on the blades and the noise level, high speed results in large stresses on the blades and high noise levels [27]. In [44] it is stated that for a 1.5 MW wind turbines the rotor diameter is approximately 64 to 66 m and the rotational speed at rated wind speed is approximately 19 to 23.5 rpm. Corresponding data for a 2 MW wind turbine are: 80 m rotor diameter and max rotor speed 19 rpm. For the 2 MW wind turbines in this work the rotor diameter is set to 80 m and the rotational speed at rated wind speed is set to 19 rpm.

Today, two variable speed systems with different electrical generator systems are common: full range variable speed or limited speed range system. Both systems have the same upper speed limit due to the noise level and mechanical stresses. It should be pointed out that the upper rotor speed limit is an average limit. Shortly the speed is allowed to be above the limit in order to reduce the mechanical stresses due to the power fluctuations originating from the wind speed variations. The full range variable speed system has no lower speed limit, the rotational speed is controlled so that λ equals 9 also at the lowest wind speeds. The purpose is, as mentioned, to have the highest efficiency of the wind turbine in the low wind speed region. In the limited speed range case there is a lower average speed limit apart from the upper one. Normally for the limited speed range systems the speed band is $\pm 30\%$ from synchronous speed [21].

2.2 Fix speed wind turbine

The fix speed wind turbine was earlier the most commonly used wind turbine system. This depends on that it has a very robust design with few components. The system is presented in Fig. 2.3. The weakest component is the gearbox, which has to take up a substantial amount of stress due to torque pulsations. This is due to the fact that the turbine has an

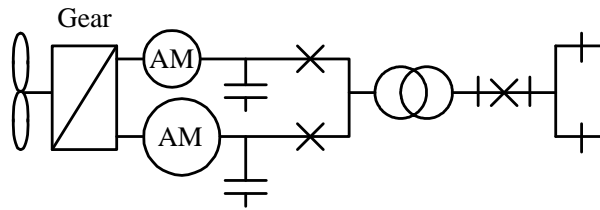


Figure 2.3: Principal scheme of the 2 MW fix speed turbine, with two generators.

almost fixed speed and can store very little energy from the incoming power pulsations. These pulsations are also seen in the output power from a fix speed wind turbine and they cause fast voltage fluctuations on the grid [4, 31, 41].

The efficiency of the fix speed turbine can be increased by having two different generators, denoted AG in the figure above, one larger and one smaller. The small generator has a lower rotational speed and is used at low wind speeds in order to increase the aerodynamical as well as the generator efficiency of the turbine (operation close to the ideal λ at low wind speeds and reduced iron losses). At higher wind speeds, the larger generator is used. In Fig. 2.4 the active and reactive powers for this system are shown, solid and dashed line, respectively. The switch over point between the generators in this work can be noticed in Fig. 2.4 as the knee of the solid line at 6.7 m/s. The dotted line in Fig. 2.4 shows the output power from the wind turbine if the large generator had been used also for low wind speeds. By comparing the dotted line with the solid line for low wind speeds, the increase in efficiency by having two different generators can clearly be noticed. Due to this increase in efficiency, the two generator system is the only one considered in this work.

As mention before, the generator used at low wind speeds has a lower rated power then the generator used for high wind speeds. Due to the lower rated power, the generator no-load losses of the system are lower, and accordingly the total generator losses can be reduced at low wind speeds. This can be noticed in Fig. 2.5 where the losses of the 2 MW fix speed wind turbine is shown. The switch between the different generators can be noticed as the step at 6.7 m/s in the losses for the generator (black dashed line). The dashed grey line shows the generator losses of the large generator, if it would have been used for low wind speeds also. By comparing the grey and the black dashed line for low wind speeds it is noticed that an improvement of the generator efficiency by approximately 0.9 % at low wind speeds is obtained by having two different generators. In addition to the reduced losses at low wind speeds, there is also, as mentioned earlier, a gain in captured energy by the wind turbine rotor.

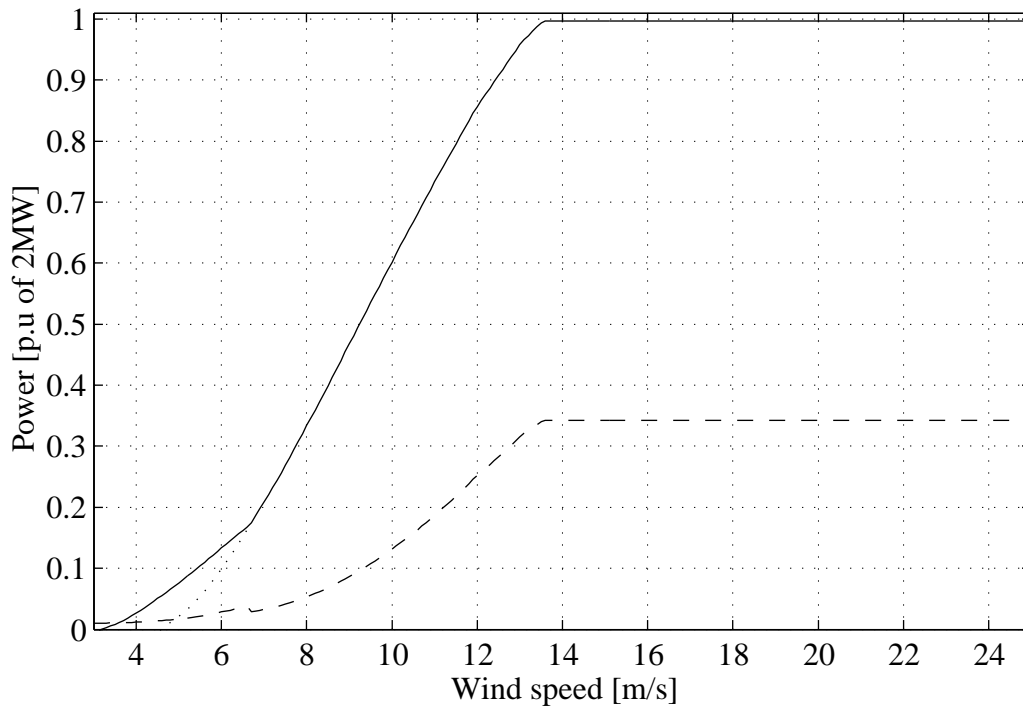


Figure 2.4: The produced active power to the grid is shown (solid) and the reactive power drawn from the grid (dashed) for the 2 MW fix speed turbine. Dotted line shows the output power from the wind turbine if the large generator is used for low wind speed also.

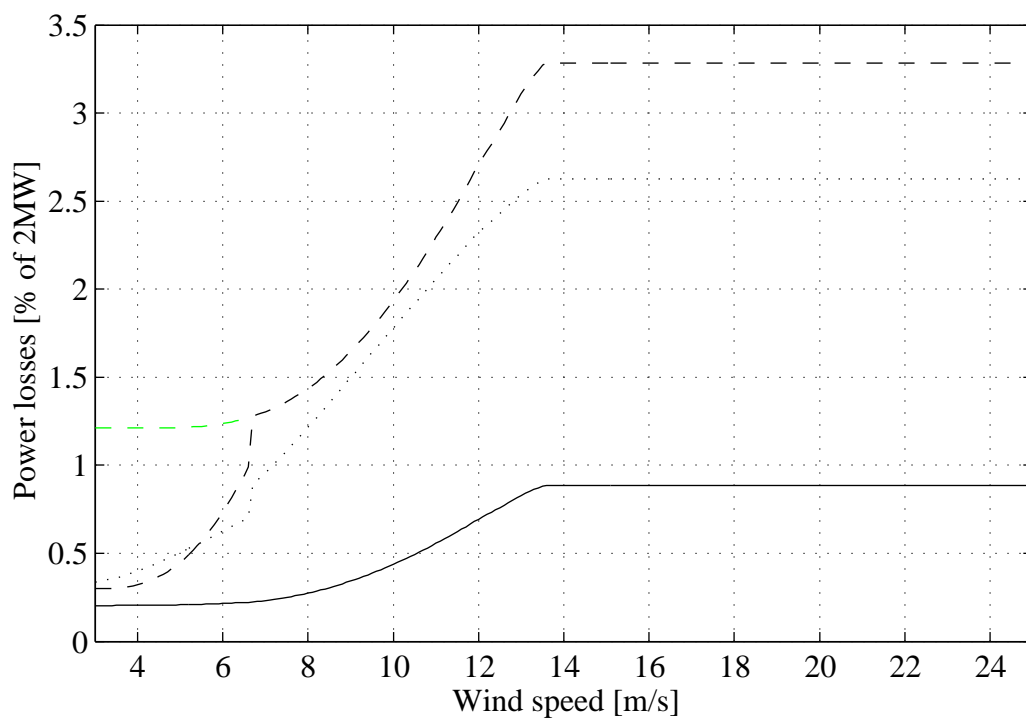


Figure 2.5: The losses for the turbine, solid transformer losses, black dashed generator losses and dotted gearbox losses. Grey dashed line shows the losses of the large generator if it would have been used at low wind speeds also.

2.3 Limited speed range wind turbine

A popular wind turbine system during recent years has been the semi variable speed wind turbine configuration [21]. The key component in this system is an asynchronous generator with a wound rotor and slip rings, also called Doubly-Feed Induction Generator (DFIG). The converter is connected to the rotor circuit via the slip rings and the stator circuit is connected directly to the transformer, as can be seen in Fig. 2.6.

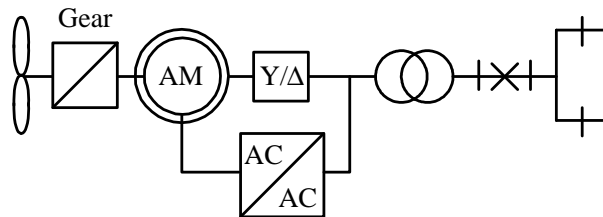


Figure 2.6: Principal scheme of the 2 MW semi variable speed wind turbine.

This system can be optimized to produce maximum energy by choosing the speed range and the stator to rotor winding ratio appropriately [40]. The speed range around synchronous speed is approximately equal to the power through the converter. A common speed range is $\pm 30\%$ from synchronous speed [21], which gives that the maximum power through the converter is 30 % of the rated power [40]. The fact that only a part of the power goes through the converter is the main advantage of this system, which gives a smaller converter (cheaper) and also lower losses.

In [40] it is shown that if the stator of the generator is connected in Y for low wind speeds and in Δ for high wind speeds the energy production can be increased by up to 1.2 %. The Y Δ switch is shown in Fig. 2.6. This way of increasing the energy production of the DFIG system is used in this work as standard for the DFIG system.

In Fig. 2.7 the losses of the semi variable speed wind turbine are shown. The switch from Y to Δ connection of the stator is seen at 8.7 m/s as a step in the losses of the converter (grey line). If only the efficiency of the generator is studied it can be noticed that the losses of the DFIG is lower at rated power compared to the fix speed system in Fig. 2.5. This is mainly due to that the losses in the stator winding is lower, due to that 30 % of the power is taken out through the rotor and therefore the stator current is approximately 30 % lower.

The asynchronous generator can be magnetized through the rotor and in this way there is a possibility, if desired, to only exchange active power between the stator and the grid. In addition, the converter side connected to the transformer can also be used to generate or consume reactive power. This leads to that the semi variable wind turbine can produce power with a power factor equal to one in the whole wind speed region.

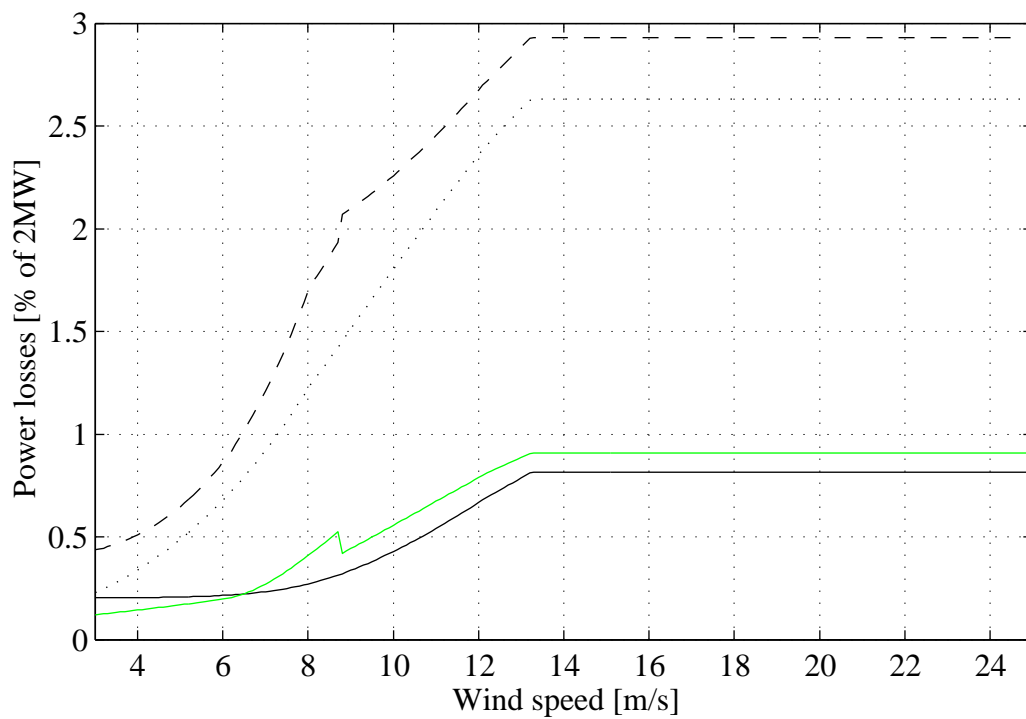


Figure 2.7: The losses of the 2 MW semi variable speed wind turbine. Solid transformer losses, dashed generator losses, dotted gearbox losses and grey converter losses.

2.4 Full range variable speed wind turbines

2.4.1 Classical AC output system

The "full variable speed" wind turbines in this work uses a full power converter connected between the stator of the generator and the wind turbine transformer, as shown in Fig. 2.8. For the full variable speed systems, the reactive power to the grid is fully controllable using the converter.

In this work, two types of generators are used: an asynchronous generator and a low speed multi-pole synchronous generator. Today the system with the low speed synchro-

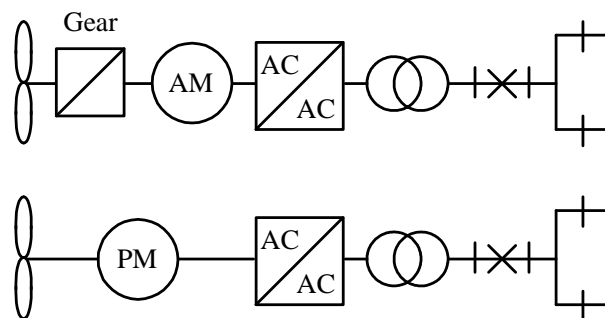


Figure 2.8: Principal schemes of the 2 MW full variable speed turbine, top with asynchronous generator and bottom with permanently magnetized generator.

nous generator is by far the most common one of the two. The reason for this is that this system does not need a gearbox, which is a quite sensitive component, as mention before. If a permanently magnetized directly driven machine is used, a drawback is that this generator requires much more reactive power at rated power then the asynchronous generator. If an electrically magnetized generator is used, the reactive power is not a problem, since it can be produced internally using the field winding.

Accordingly, if the generator is permanently magnetized, the reactive power needed by the generator at high loads (high wind speeds) must be produced externally in order to have a good utilization of the generator [19]. This gives problems if a diode rectifier is connected to the generator. For this case some kind of reactive power compensation must be used: as an example, capacitors on the AC side can be used. In this work it is assumed that the permanently and the electrically magnetized generator performs equally from an energy production point of view, so, only the permanently magnetized generator system is chosen to be investigated in this work.

In Fig. 2.9, the losses of the variable speed wind turbine with an asynchronous generator are shown. If Fig. 2.9 and Fig. 2.5 are compared, it is noticed that the generator losses, at low wind speeds, for the variable speed wind turbine is almost the same as for the small generator used in the fix speed turbine. This is due to that in the full variable speed system, the voltage and the frequency to the generator is fully controllable by the

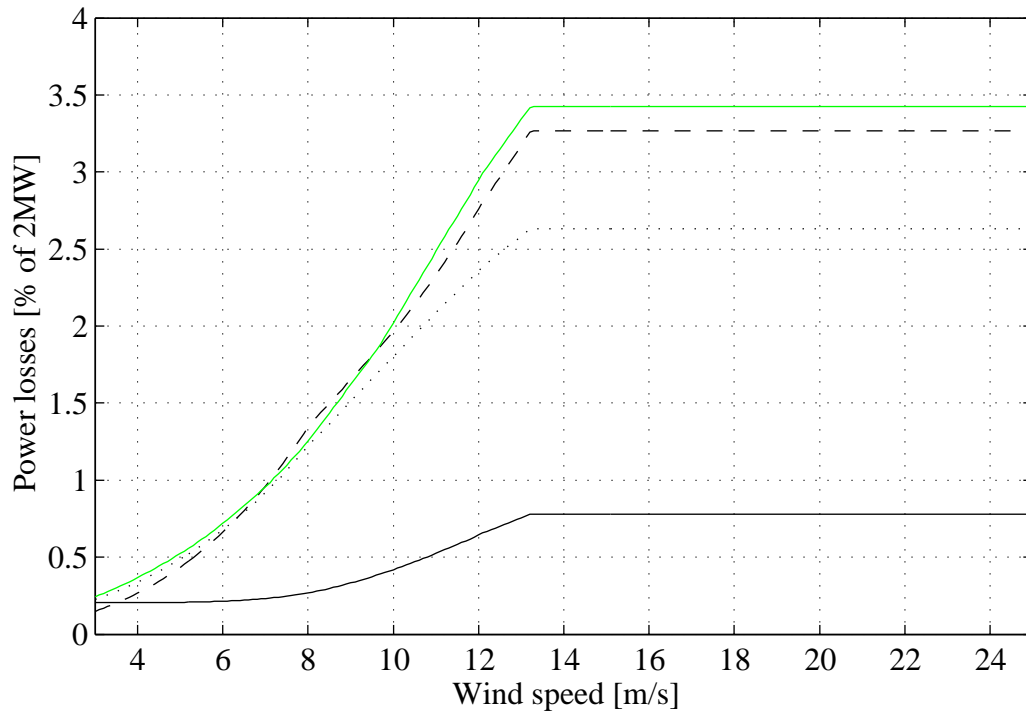


Figure 2.9: The losses of the 2 MW full variable speed turbine equipped with a asynchronous generator. Solid transformer losses, dashed generator losses, dotted gearbox losses and grey converter losses.

converter. At low wind speeds, field weakening of the generator is used in order to reduce the no-load losses. This is done by decreasing the voltage to the generator.

In Fig. 2.10, the losses of the variable speed wind turbine with a permanently magnetized generator and a back to back converter between the stator and the wind turbine transformer are shown. From Fig. 2.10, it is noticed that the losses for the low speed generator are lower then the losses for the system with a gearbox and an asynchronous generator. It shall also be noticed that the converter losses for these two full variable speed systems are much higher then the converter losses in the semi variable system, see Fig. 2.7.

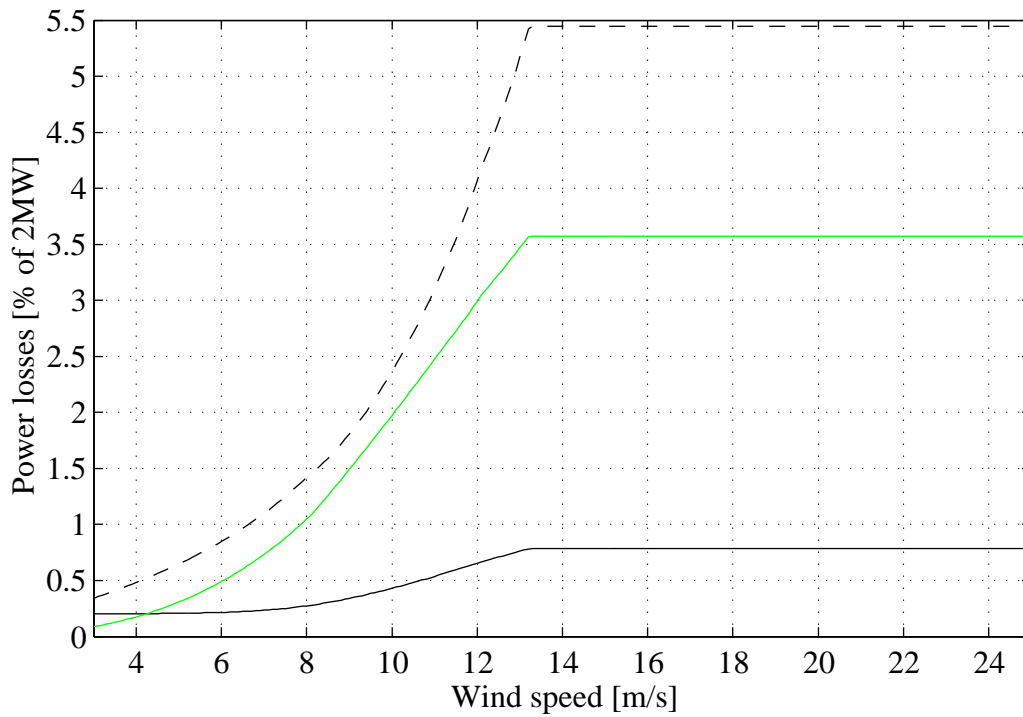


Figure 2.10: The losses of the 2 MW full variable speed turbine equipped with a permanent magnetized generator. Solid transformer losses, dashed generator losses and grey converter losses.

2.4.2 Variable speed DC wind turbine with IGBT rectifier

With variable speed dc wind turbine is meant a turbine that feeds out a high voltage dc, ca 40 kV. This can for instance be achieved by using an IGBT rectifier and a dc/dc converter, as shown in Fig. 2.11. The benefit with the IGBT rectifier is that the torque of the generator

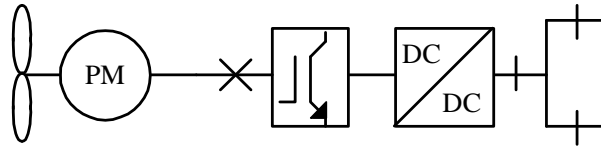


Fig. 2.11 Principal scheme of the 2MW DC wind turbine with full variable speed and IGBT rectifier.

and the reactive power to the generator can be easily controlled. Due to the fact that the reactive power can be controlled, any type of generator can be used.

Another benefit of the IGBT rectifier is that it keeps the input voltage to the DC/DC converter constant. This leads to that the DC/DC converter works at a constant transformation ratio in normal operations. This means that the DC/DC converter can be better optimized, it will work as a constant ratio DC transformer.

In Fig. 2.12 the losses of the variable speed DC wind turbine with an IGBT rectifier and a full bridge converter as DC/DC converter are shown. In this configuration the generator has a rated voltage of 690V and the wind turbine has an output voltage of 40kV.

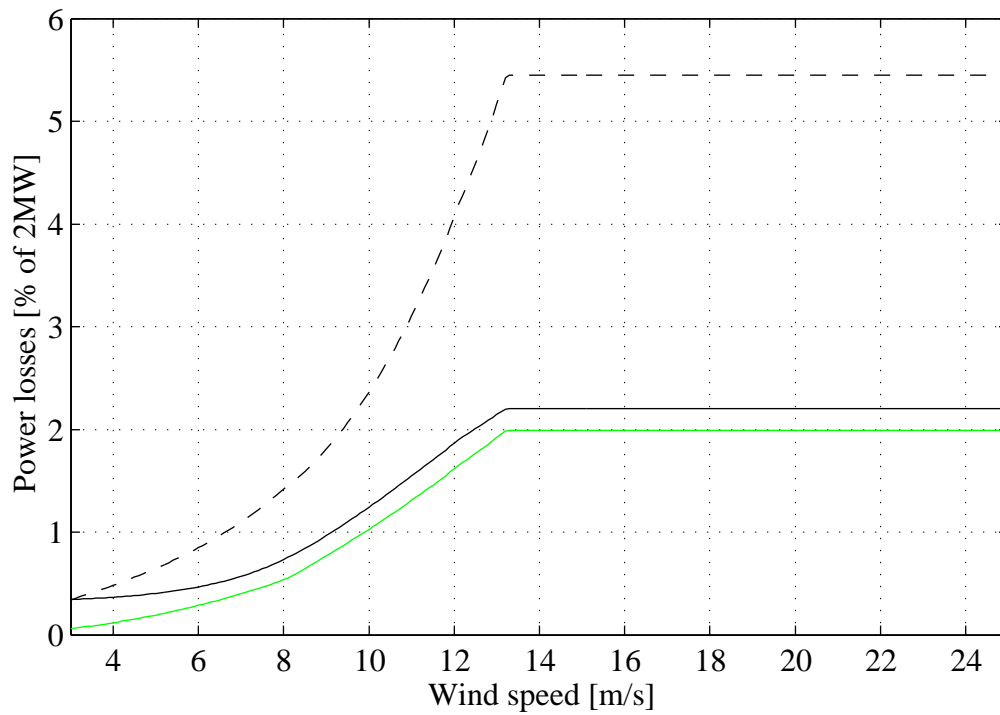


Fig. 2.12 The losses of the 2MW wind turbine equipped with a permanent magnetized generator connected to a IGBT rectifier and a full bridge converter. Dashed generator losses, solid DC/DC converter losses and grey IGBT rectifier losses.

2.5 Energy efficiency comparison of different wind turbines

This section presents a short summary of the results from Papers I, II, , which deals with the energy efficiency determination of various wind turbine systems.

The average power production is calculated by using the wind speed distribution shown in Chapter 2.1. The average power production is calculated in the same way as the mean wind speed, (2.2), ie. the output power is multiplied with the Rayleigh distribution and then integrated from cut in wind speed to cut out wind speed, as can be seen in (2.7). In this work, a cut out wind speed of 25 m/s has been used, which is a suitable value for wind turbines. There is usually no point in using a higher cut out speed, since the contribution to the average power production for wind speeds above 25 m/s is very low, see Fig. 2.1, where the Rayleigh distribution has very low values over 25 m/s. This means that a further mechanical over-dimension in order to allow operation at these high wind speeds does not pay back. The cut in wind speed is set to 3 m/s. The contribution to the average power production from wind speeds lower than 3m/s is quite low. This is due to that the power converted from the wind by the wind turbine is low, see Fig. 2.4, and due to that the distribution decrease rapidly for wind speeds below 3 m/s. The average power production can thus be determined as:

$$P_{\text{out,AVG}} = \int_{w_{\text{cutin}}}^{w_{\text{cutout}}} P_{\text{out}}(w_s) f(w_s) dw_s. \quad (2.7)$$

Where:

$P_{\text{out,AVG}}$	Average power production [kW]
w_{cutin}	Cut in wind speed = 3 [m/s]
w_{cutout}	Cut out wind speed = 25 [m/s]
$P_{\text{out}}(w_s)$	Output power of the wind turbine [kW]
$f(w_s)$	Rayleigh distribution

In Table 2.1, the average power production of some different wind turbines are shown for four different average wind speeds and the power at cut in wind speed and at rated wind speed, in per unit of 2 MW. The four first are wind turbines with 33 kV AC output (AC wind turbines), and the last has a 40 kV DC-voltage as output (DC wind turbine). It shall be remembered that all wind turbines have the same rated shaft power, so the differences in electric power production is only depending on the speed control of the turbine (fix speed, limited speed range or full range variable speed) and the losses in the drive train.

From Table 2.1 it can be observed that the differences in average power production between the different wind turbines for a given mean wind speed is not large, it is maximum around 4-7 %, when all systems as presented in Paper XXX are considered. Note,

Table 2.1: The output power in p.u. of 2 MW for the different wind turbines at cut in wind speed and at rated wind speed and the mean output power in kW for the different wind turbines and for different mean wind speeds.

Type of wind turbine	Power at 3 m/s	Rated power	5 m/s	6 m/s	8 m/s	10 m/s
AM Fix speed	0	0.997	271	434	769	1037
AM, Rotor converter	0.009	0.992	275	437	771	1038
AM, Stator converter	0.011	0.964	270	428	754	1012
PM, Stator converter	0.013	0.967	281	442	769	1027
PM, IGBT, Full bridge	0.012	0.968	281	442	770	1028

that a possibility is to increase the rotor diameter of the turbine at sites with low average wind speeds and in this way it is possible to adjust the turbine to the mean wind speed of the site. In this work, the rotor diameter is the same for all average wind speeds, since the goal here is to compare the energy capture using various electrical systems, so the boundary conditions are set to be as equal as possible in this work.

From this comparison of different wind turbine types, the fix speed AC wind turbine and the rotor converter (limited speed range) AC wind turbine are chosen to be used in the evaluation of the wind parks with AC wind turbines, in the next chapter. For the series connected DC wind park, the DC wind turbine with the full bridge isolated boost converter is chosen.

2.6 Power quality impact of wind turbines and "small" wind parks

When "smaller" wind energy installations are to be connected to the grid, an important issue is the power quality impact that the wind energy installation has on the grid. This issue is of course also of importance for larger wind farms. However, in this case the grid connection can be done in a more designated way compared to when a smaller installation is connected. One issue is the steady-state voltage variation that the wind energy installation causes at the point of common connection, which is fairly easy to determine. The harmonic emission needs some special considerations, which are not dealt with in this thesis. The flicker emission however, is an issue that can be the limiting factor for the installation of a smaller wind farm and this is hard to calculate.

In Fig. 2.13, the limitations from a flicker and steady-state voltage point of view are presented for an installation of one and three stall-regulated turbines. The installations have the same total power rating. To be on the safe side, it is necessary to be above the limiting curves. In the case of a wind park, the total flicker level from the whole wind park should increase with the square-root of the number of turbines [54]. It can be observed that if one turbine is installed, it is the flicker emission that sets the limit, while if three or

more turbines are installed it is the steady-state voltage change that limits the installation.

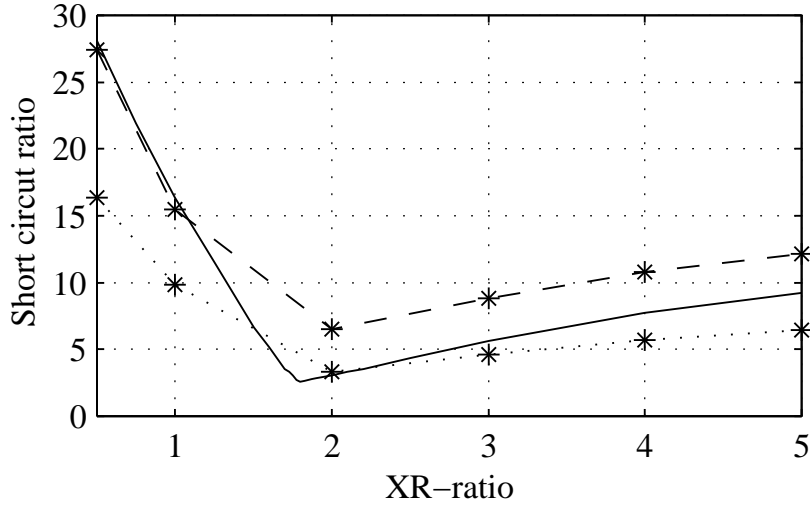


Figure 2.13: Limiting curves for the stall-regulated turbines. The solid curve is for the 2.5 % static voltage level change limit, the dashed curve is for flicker contribution of 0.25 with one turbine and the dotted curve is for flicker contribution of 0.25 with a wind farm consisting of 3 wind turbines.

From these studies, it has been shown that flicker can be a problem if the wind park only consists of a few number of turbines and if the grid is weak. It should be mentioned that fixed-speed turbines with pitch control (and without an external rotor resistance) have an even higher flicker contribution, but this type of turbine is no longer being installed into the grid.

Another important comment deals with the summation of the flicker. In [IEC 61400-21] it is stated that the total flicker contribution from a wind park is determined from the flicker emission of one turbine using the following expression

$$P_{st,tot} = \sqrt{\sum_{i=1}^N P_{st,ind}^2} \quad (2.8)$$

where N = number of turbines, $P_{st,tot}$ is the total flicker contribution from the wind park and $P_{st,ind}$ is the flicker contribution from one individual turbine.

If all turbines are of the same type, (2.8) can be simplified to

$$P_{st,tot} = \sqrt{N} P_{st,ind}. \quad (2.9)$$

Fig. 2.14 presents the discrepancy between two different P_{st} evaluating approaches. The first approach makes use of the flicker values determined from the total active and reactive

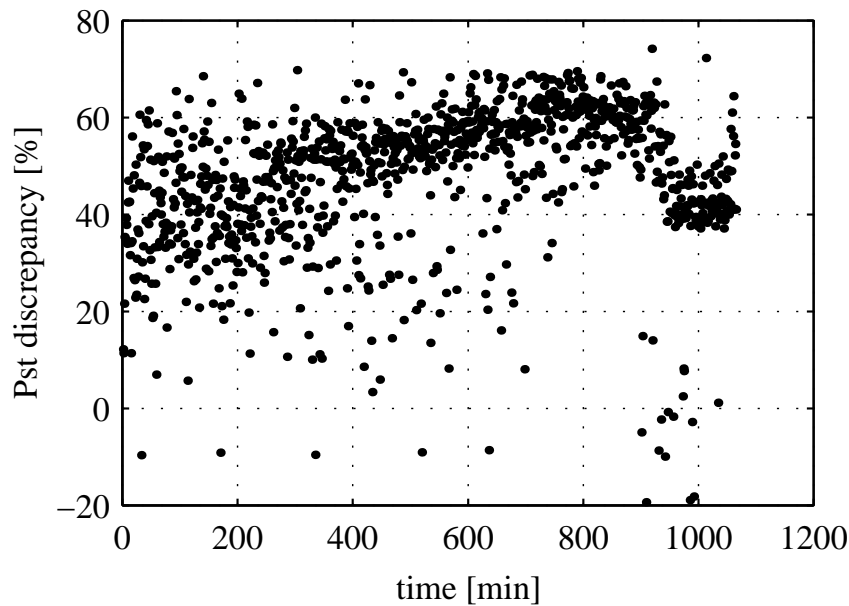


Figure 2.14: Discrepancy between the actual flicker emission and the formula from IEC-61400-21, 70 degrees grid impedance angle.

powers of the wind park. The second approach uses the P_{st} values obtained using the individual P_{st} values and (2.8).

As can be noted from Fig. 2.14, the flicker levels are usually much higher when the total active and reactive powers from the wind park are used. For the 70 degree grid, shown in Fig. 2.14, this method on average gave 48 % higher results, and for a 30 degree grid 20 % higher. In [52], [51] the results found were that there was no detectable differences between these two methods. The reason for the higher flicker values reported here is most likely the voltage fluctuations originating from the grid. This influences all the turbines in the same way, giving rise to fluctuations in the active and reactive powers that are similar from all the turbines, i.e. the sum of the contributions from the wind turbines, not the square root sum. So the result is a mix of these two components. The conclusion that can be made is that when the voltage quality is not very good, caution must be taken when (2.8) and (2.9) are used to determine the flicker emission from a whole wind park.

In [57], the underestimation of the flicker summation for a wind park consisting of seven variable-speed wind turbines is found to be 20 %, i.e. substantially lower.

To sum up, a reasonable approximation is that the limiting factor from an installation of a wind park consisting of 10 or more turbines is the steady-state voltage variation and the current capacity of the receiving network.

Papers III and IV describes the background and intermediate steps for the conclusion drawn in this section.

Chapter 3

Energy Efficiency of Wind Parks

3.1 Wind Farm Layouts

Generally, the wind farms investigated in this work can be represented by the sketch presented in Fig. 3.1. As seen in Fig. 3.1, the wind farm consists of a number of elements:

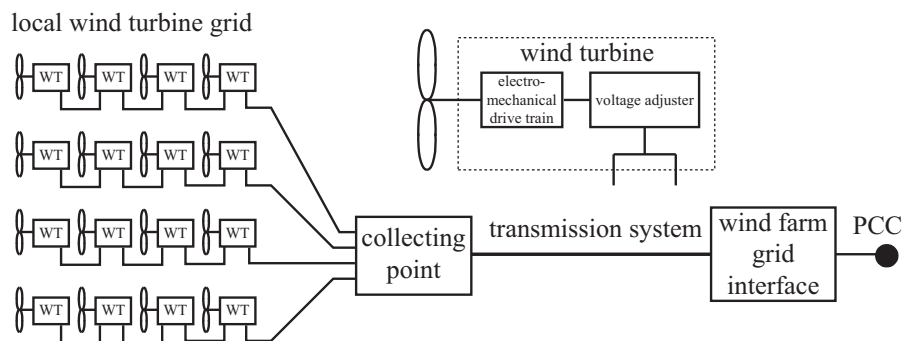


Fig. 3.1 General wind farm layout.

wind turbines (WT), local wind turbine grid, collecting point, transmission system, wind farm interface to the point of common connection (PCC). It shall be noticed that all wind turbines in this work have a voltage adjusting unit (AC or DC transformer) included in the wind turbine unit itself. The local wind turbine grid connects the wind turbine units to the collecting point. The wind turbine units are connected in parallel to radials, unless otherwise is specified in this thesis. In the collecting point, the voltage is increased to a level suitable for transmission. The energy is then transmitted to the wind farm grid interface over the transmission system. The wind farm grid interface adapts the voltage, frequency and the reactive power of the transmission system to the voltage level, frequency and reactive power demand of the grid in the PCC.

In this project, the size of the wind turbines has been selected to 2MW, since these turbines are available for all kinds of wind energy systems today. However, it should be

pointed out that the main results of this study would most likely not be very different if another turbine size would have been selected. Almost all wind turbines considered in this work have a rated generator voltage of 690V. Most likely, the generator voltage will be increased when the rated power of the generator is increased, in order to decrease the losses.

In this chapter, four farm sizes were chosen as templates for the investigations: 60, 100, 160 and 300 MW. Although most wind farms today are much smaller than 60MW, 60MW is used as a small wind farm here. As shown in Section 2.6, there is no need to perform dynamic calculation from a grid connection point of view, and accordingly, only steady-state calculations will be performed. Horns Ref is one example of a 160MW off-shore wind farm 14 – 20km out of the west coast of Denmark [16]. It is today (2006) the largest built so far. No larger wind farms than 300MW is taken under consideration in this work, due to the fact that if a larger wind farm is going to be built it will probably be divided into smaller modules, where a maximum module size of 300MW seems appropriate. Two advantages using modular building of wind farms are that the investment cost of the whole wind farm is spread out over a longer period and that part of the production can start before the whole farm has been built. Another advantage of this division is that if cross connections between the modules are made, the wind farm will be more fault tolerant.

In this work, the wind power plants will be placed in a grid with 7 rotor diameters between the turbines in both directions. This seems to be a commonly used distance and at Horns Rev the distance is 7 rotor diameters [16]. The distance between wind turbines in the wind direction can not be too small. This is due to the fact that when the wind passes through the rotor of the wind turbine, it gets very turbulent and the wind speed is decreased. This means that if the wind turbines are located too close to each other, the wind will be more and more turbulent after it passes each wind turbine. This would lead to that wind turbines downstream in the wind farm, are subjected to strong aerodynamical stresses. This could even lead to that they would have to be shut down, due to that the mechanical loading gets too high during difficult conditions. In addition, the energy losses due to the reduced wind speed will be significant if the wind turbines are put too close to each other. The minimum length to avoid this is approximately 5-7 rotor diameters.

Of course, if the wind is mainly coming from one direction, the wind turbines can be placed closer in the direction perpendicular to the prevailing winds. But for the Nordic countries, wind directions from northwest to south are quite normal, which means that the wind turbines should be placed with an equal distance in all directions.

In this work, it is thus assumed that the wind turbines are put in a grid with 7 rotor diameters between. The distance from the column nearest the collecting point to the collecting point is also 7 rotor diameters, see Fig. 3.1.

Since 7 rotor diameters was used here, it was possible to neglect the wake effects. Anyway, if wake effects were taken into account, it would not affect the comparison

between different wind farm configurations very much. In addition, there is a lack of available, simple and good models for calculating the wake effect in steady-state.

3.1.1 AC Systems for Wind Farms

All wind farms that have been build today have an AC electrical system from the wind turbines to the PCC. In this work, two different AC-systems are investigated, referred to as the small and the large AC wind farm. Three core cables are used for AC transmission throughout this work.

The first configuration to be discussed is the small AC wind farm. The idea with the small AC wind farm, is that it should be suitable for small wind farms with a short transmission distance. In the small AC wind farm, the local wind farm grid is used both for connecting all wind turbines in a radial together and to transmit the generated power to the wind farm grid interface, which is shown in Fig. 3.2. For this system, the cables in

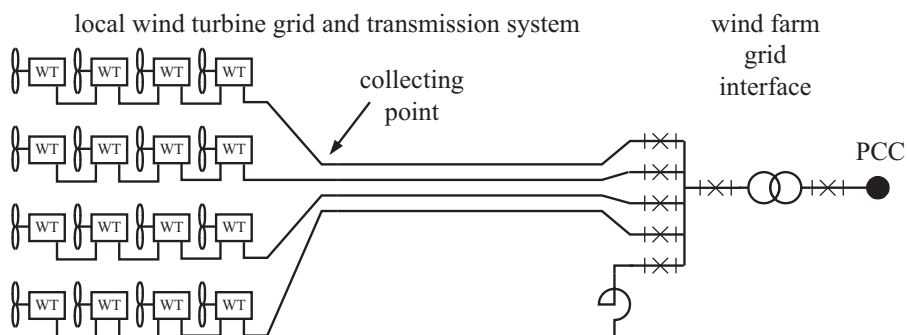


Fig. 3.2 The electrical system for the small AC wind farm.

the local wind farm grid are assumed to be installed one and one from the wind turbines to the collecting point. From the collecting point to the wind farm grid interface all cables are assumed to be installed together. This means that there is one cable installation cost per cable, from the wind turbines to the collecting point, and only one cable installation cost for all cables from the collecting point to the wind farm grid interface.

Let us now study a slightly different configuration, the large AC wind farm. The large AC wind farm system is a more traditional system, based on the general system in Fig. 3.1. This system has a local wind farm grid with a lower voltage level (20-30kV) connected to a transformer and a high voltage transmission system. This system requires an offshore platform for the transformer and switch gear, as can be seen in Fig. 3.3. Horns Rev wind farm is build according to this principle. For this system there is one cable installation cost per cable, due to the fact that all cables have different routes.

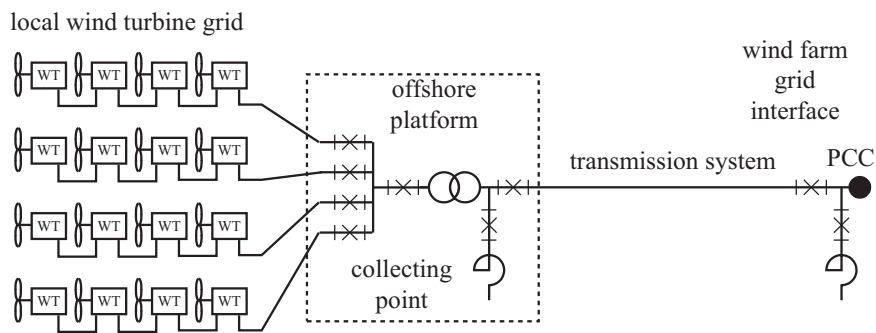


Fig. 3.3 The electrical system for the large AC wind farm.

3.1.2 Mixed AC and DC Systems for Wind Farms

In this system, the AC transmission in Fig. 3.3 has been replaced with a DC transmission. This wind farm will be referred to as the AC/DC wind farm. This type of system does not exist today, but is frequently proposed when the distance to the PCC is long or if the AC grid that the wind farm is connected to is weak. The system is shown in Fig. 3.4. In this system we have an independent local AC system in which both the voltage and the frequency are fully controllable with the offshore converter station. This can be utilized for a collective variable speed system of all wind turbines in the farm. The benefits with this are that the aerodynamic and electrical efficiency can be increased.

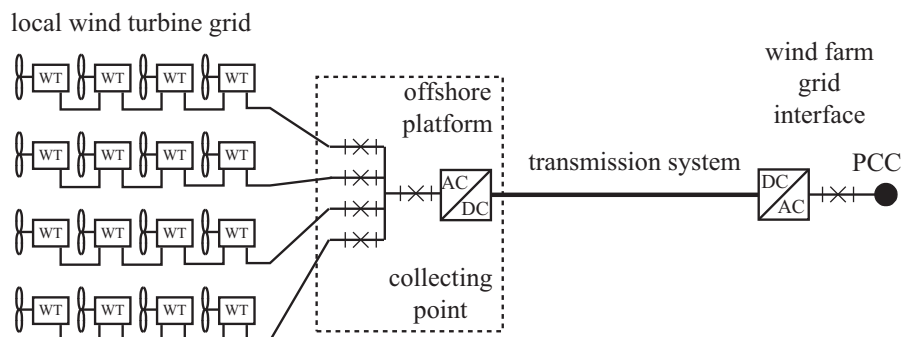


Fig. 3.4 The electrical system for the AC/DC wind farm.

The installation cost of the cables are the same as for the large AC wind farm. The two DC transmission cables, one for the positive pole and one for the negative pole, are assumed to be installed together and therefore there is only one cable installation cost for these two cables.

3.1.3 DC Systems for Wind Farms

For the pure DC wind farm, three different configurations are investigated. Two configurations are based on the two layouts of the AC systems, referred to as the small DC wind

farm and the large DC wind farm, and one configuration with the turbines in series, as shown in [34]. In all DC configurations in this work, the two cables, one for the positive pole and one for the negative pole, are assumed to be installed together and are therefore referred to as one cable.

The electrical system for the small DC wind farm is shown in Fig. 3.5. As can be

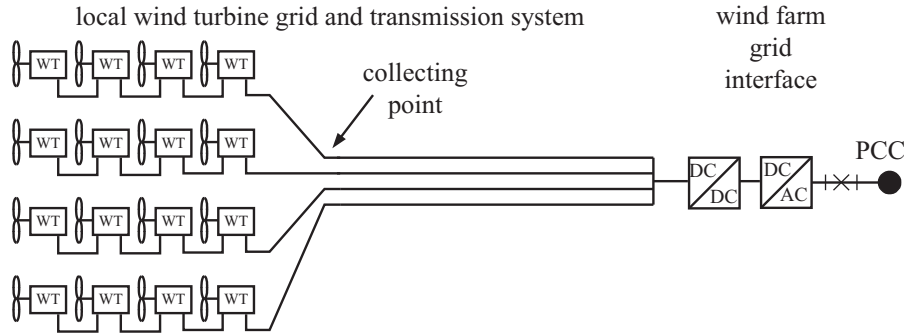


Fig. 3.5 The electrical system for the small DC wind farm.

noticed, the electrical system for the small DC wind farm is identical to the system of the small AC wind farm. The only difference is that the transformer in the wind farm grid interface is replaced with a DC transformer and an inverter. Of course, a rectifier is needed in each wind turbine. The advantage of the small DC farm compared to the large DC farm is, as for the small versus large AC farm, that it does not require an offshore platform. The installation cost of the cables are assumed to be the same as for the small AC wind farm.

The configuration of the electrical system for the large DC wind farm can differ somewhat from the configuration of the large AC wind farm. The difference is if it requires one or two transformation steps to increase the DC voltage from the wind turbines to a level suitable for transmission. It is assumed that if the DC voltage from the wind turbines is high enough (20-40kV), only one transformation step is required. But if the output voltage of the wind turbine is lower (5kV), two steps are required. In Fig. 3.6, this system is presented with two DC transformer steps. For the large DC wind farm with two transformation steps, all wind turbines are divided into smaller clusters. All wind turbines within one cluster are connected one by one to the first transformation step. The high-voltage side of the first DC transformer step are then connected to the second step, as can be noticed in Fig. 3.6. If only one step is used, the wind turbines are connected in radials directly to the second DC transformer step, similarly as for the large AC wind farm in Fig. 3.3. In Paper VII the energy efficiency of various dc/dc converters for such a system is investigated. For this system there is one cable installation cost per cable, due to the fact that all cables have different routes.

In the third DC system, shown in Fig. 3.7, the wind turbines are connected in series, as mention before, in order to obtain a voltage suitable for transmission directly. This system is referred to as the series DC wind farm. The benefit of this system is that in

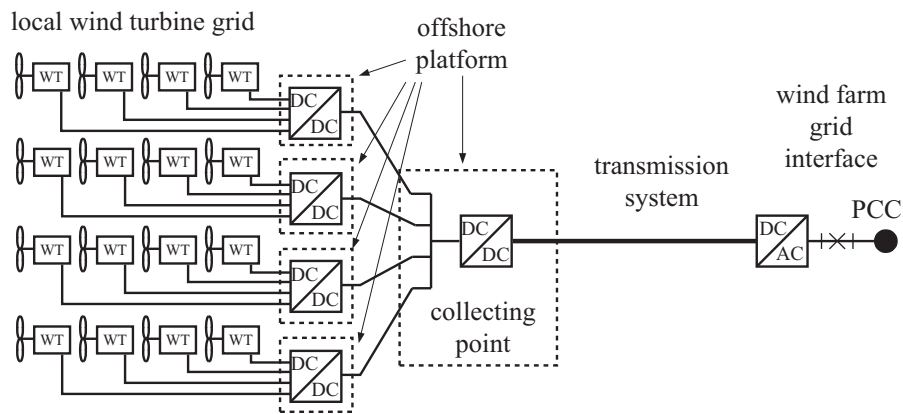


Fig. 3.6 The electrical system for the large DC wind farm with two DC transformer steps.

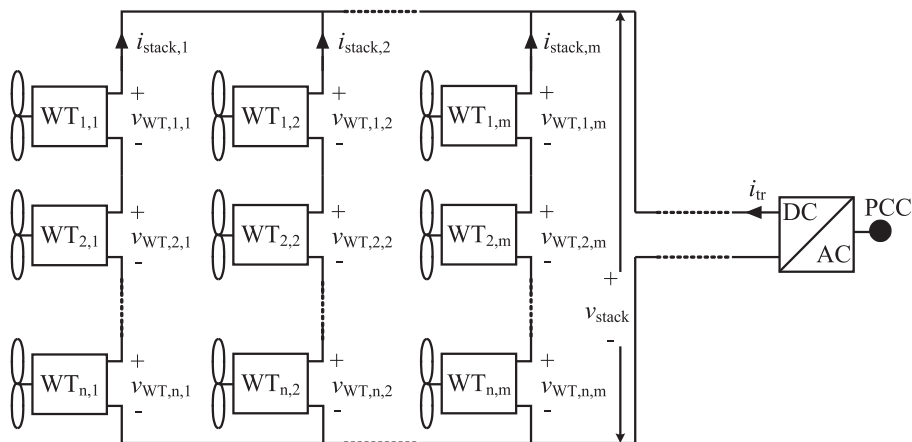


Fig. 3.7 DC electrical system with series connected wind turbines.

spite of a relatively large possible size, it does not require large DC-transformers and offshore platforms. The voltage insulation in the wind turbines is taken by the transformer in the local DC/DC converter. The drawback with this configuration is that the DC/DC converters in the wind turbines must have the capability to operate towards a very high voltage. This is due to the fact that if one wind turbine does not feed out energy and therefore it fails to hold the output voltage, then the other turbines must compensate for this by increasing their output voltage. This system will be described more in detail in the following chapters.

For this system, there is one cable installation cost per cable, due to the fact that all cables have different routes, as can be noticed in Fig. 3.7.

3.2 Energy Production Cost of Different Wind Farms

In this section, the energy production cost for the six different wind farm systems based on the wind turbine systems described in Chapter 2 are compared with each other. All these six types are individually optimized to give the lowest energy production cost. In the second subsection the best configuration of these six types are compared with each other. Furthermore, in the following subsections the individual optimization is described for each of the configurations. The cost and loss models for these calculations are taken from paper V, which means that they originate from 2002-2003.

3.2.1 Energy production cost

The energy production cost is defined as how much it costs to produce and deliver a unit of energy to the grid, i.e to the PCC. This gives that the total investment cost of the wind farm is divided with the total energy delivered to the PCC. The total investment cost is calculated assuming that the whole investment is made in the first year and paid off during the life time of the wind farm. In addition, it is also assumed that some profit shall be made. The total energy that is delivered to the PCC is calculated by multiplying the average power delivered to the PCC with the average number of operational hours during one year multiplied with the lifetime of the wind farm. The average power is calculated with (2.7). With these assumptions, the energy production cost can be calculated as in (3.1).

$$E_{\text{cost}} = \frac{\text{Invest}}{P_{\text{out,AVG}}T} \frac{r(1+r)^N}{(1+r)^N - 1} \frac{100}{100 - PR} = K \frac{\text{Invest}}{P_{\text{out,AVG}}} \quad (3.1)$$

Where:

E_{cost}	Energy production cost [SEK/kWh]
Invest	Investment [SEK]
$P_{\text{out,AVG}}$	Average output power [kW]
T	Average operational hour under one year [h]
r	Interest rate [-]
N	Lifetime of the wind farm [years]
PR	Profit in %
K	Constant

The life time of the wind farm is in this work set to 25 years, the interest rate to 4 %, the profit to 3 % and the average operational hours during one year is set to $365 \cdot 24 = 8760$. This gives that the production cost gets about 65 % higher then without profit and interest rate, i.e. $K = 7.53 \cdot 10^{-6}$ with interest rate and profit and $K = \frac{1}{TN} = 4.57 \cdot 10^{-6}$ without.

As can be seen from (3.1), the losses in the wind farm do not appear explicitly. Indirect they affects the production cost due to that an increase of the losses decreases the average output power. To include the losses more directly in the energy production cost, an input

power must be defined. The input power to the wind farm is defined as the shaft power of a full variable speed wind turbine, described in chapter 2.1.4, multiplied with the number of wind turbines in the wind farm. The cost of the losses in the wind farm is defined as the difference between the energy production cost calculated with (3.1) with the average output power and the energy production cost calculated with (3.1) with the average input power as P_{mean} . With these definitions, the energy production cost can be divided into two parts, as can be seen in (3.2).

$$E_{\text{cost}} = E_{\text{cost,invest}} + E_{\text{cost,loss}} = K \frac{\text{Invest}}{P_{\text{in,AVG}}} + K \frac{\text{Invest}}{P_{\text{in,AVG}}} \frac{P_{\text{loss,AVG}}}{P_{\text{out,AVG}}} \quad (3.2)$$

where:

E_{cost}	Energy production cost [SEK/kWh]
$E_{\text{cost,invest}}$	Energy production cost from the investment [SEK/kWh]
$E_{\text{cost,loss}}$	Energy production cost from the losses [SEK/kWh]
K	Constant, defined in (3.1)
Invest	Investment [SEK]
$P_{\text{in,AVG}}$	Average input power [kW]
$P_{\text{out,AVG}}$	Average output power [kW]
$P_{\text{loss,AVG}}$	Average losses in the wind farm [kW]

From (3.2), the contribution from each component in the wind farm to the energy production cost can be defined. This is due to the fact that the investment, Invest, is the sum of the costs of all components and the mean power loss is the sum of the average power losses in each component. This gives that the contribution to the energy production cost from one component, $c1$, is defined as in (3.3).

$$E_{\text{cost},c1} = E_{\text{cost,invest},c1} + E_{\text{cost,loss},c1} = K \frac{I_{c1}}{P_{\text{in,AVG}}} + K \frac{\text{Invest}}{P_{\text{in,AVG}}} \frac{P_{\text{loss},c1,\text{AVG}}}{P_{\text{out,AVG}}} \quad (3.3)$$

Where:

$E_{\text{cost},c1}$	Contribution to the energy production cost from component $c1$ [SEK/kWh]
$E_{\text{cost,invest},c1}$	Contribution from the cost of component $c1$ [SEK/kWh]
$E_{\text{cost,loss},c1}$	Contribution from the losses in component $c1$ [SEK/kWh]
I_{c1}	Cost of component $c1$ [SEK]
$P_{\text{loss},c1,\text{AVG}}$	Average losses in the component $c1$ [kW]

Equation (3.3) will be used in this work, to divide the energy production cost into two components: the contribution from the investment cost of the component and the component losses.

The energy production cost for the six, in this chapter, investigated types of electrical system are normalized by the energy production cost obtained for the Horns Rev wind farm. According to [16], Horns Rev has a yearly production of 600 000 000 kWh, an average wind speed of 9.7 m/s and a project cost of DKK 2 billion. This gives an energy

production cost of approximately 0.28 SEK/kWh, accordingly to the assumptions in this section.

3.2.2 Comparison of Energy Production Costs

The energy production cost of the best configuration of each of the six wind farm types, small AC, large AC, AC/DC, small DC, large DC and series DC, are compared in this section. The comparison is done for the four selected power levels and the approximations and selections made in Chapters 2 and 3. More analysis of various important aspects as well as investigations of various loss parts can be found in Paper V.

In Fig. 3.8, the energy production cost is shown for the six wind farm configurations for a rated power of the wind farm of 60 MW, and as mention in Section 3.2.1 it is normalized by the production cost for Horns Rev. If the three wind farms with AC are compared,

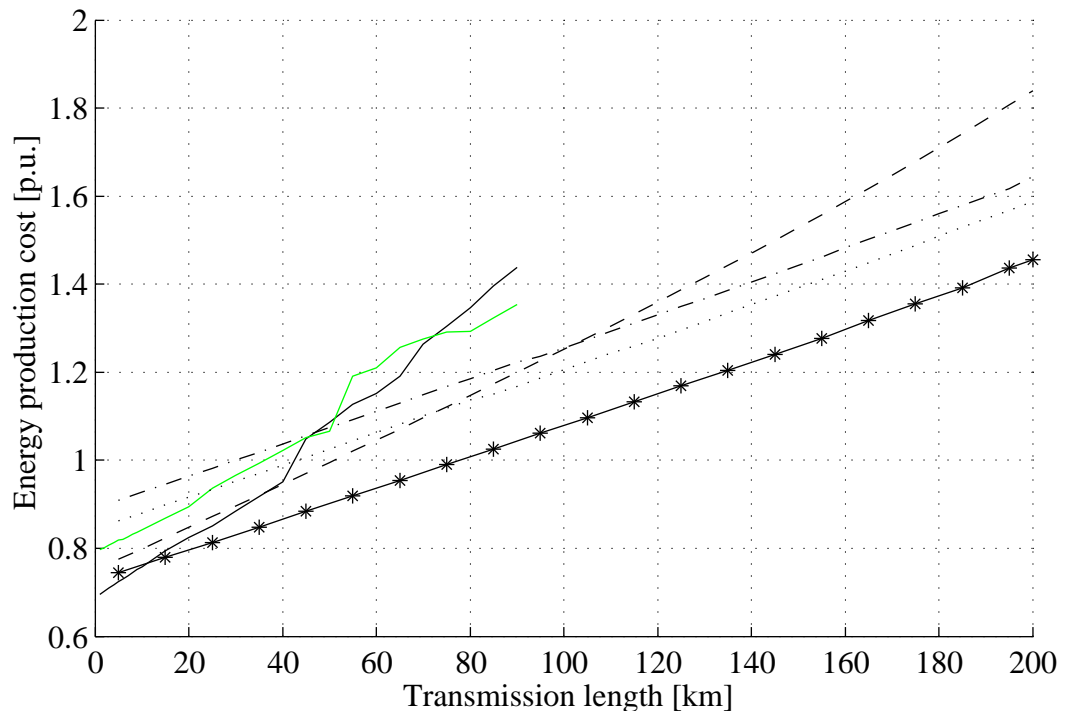


Fig. 3.8 The normalized energy production cost of the different 60 MW wind farms as function of the transmission distance for an average wind speed of 10 m/s. Solid small AC, dashed large AC, dash-dotted AC/DC, grey small DC, dotted large DC and solid with stars series DC.

small AC (solid black), large AC (dashed) and AC/DC (dash-dotted) these results are as expected. The small AC wind farm is the best solution for short distances, the AC/DC is best suitable for long distances and the large AC is best in between. The small AC wind farm is the best for short distances due to that it does not require an offshore platform.

So, the additional cost for many low voltage transmission cables is less than the cost for the platform and the high voltage transmission cable for short distances. The cost for the low voltage transmission increases rapidly when the transmission distance increases. The break even point between the small and large AC system is at a transmission distance of 37 km. The AC/DC system has, due to the expensive converter stations, a high energy production cost for short distances. Due to the fact that the cost for the transmission cables are less for DC than for AC, the AC/DC system gets better than the large AC system for transmission lengths over 100 km.

The large DC system is better than the AC/DC system due to that the losses in the DC wind turbine are lower than in the AC wind turbine. Moreover, the cost for the local DC grid is less than the cost for the local AC grid and the losses in the DC transformer are less than the losses in the offshore converter station. These costs are independent of the transmission length, but since the two systems have the same transmission system (DC cables), the large DC wind farm will for any transmission length be better than the AC/DC wind farm (using the assumptions made in this work).

As could be expected, the small DC wind farm is no good solution. This is due to that it still requires a large DC transformer and a converter station. The gain of cheaper cables and somewhat lower losses is not enough to compensate for the expensive DC transformer and converter station. However, compared to the large DC system, this solution is better for short distances. The reason is that it does not require an offshore platform.

From Fig. 3.8 it can be seen that the best wind farm solution for a transmission length over 11km is the series DC wind farm. This is due to the fact that it does not require an offshore platform, it has a cheaper local wind turbine grid, DC transmission (cheaper than AC) and this system has only one converter station. The uncertainty which is also a great challenge for research in the high voltage field, is how expensive it will be to have the high voltage insulation in each wind turbine.

In Fig. 3.9, the normalized energy production cost are shown for the six systems for a rated power of the wind farm of 160 MW. As can be noticed, the cost found for the large AC farm (The Horns Rev case, totaly 55 km transmission length [17]) is 10 % lower than the "real" case. However, since real price information is hard to obtain and the fact that Horns Rev was the first large offshore wind farm, the results are considered to be surprisingly good. It should be stressed that this work focuses on comparing systems rather than obtaining correct total costs, since this was considered to be out of reach without having access to really good cost data. It can be seen if Figs. 3.8 and 3.9 are compared, that the break even point between the small AC and large AC is decreasing when the wind farm size is increased. This is caused by the fact that the contribution to the energy production cost from the transmission system decreases when the wind farm size is increased. The decrease is larger for the large AC wind farm than for the small AC wind farm. Another observation that can be made is that the energy production cost decreases when the rated power of the wind farm increases.

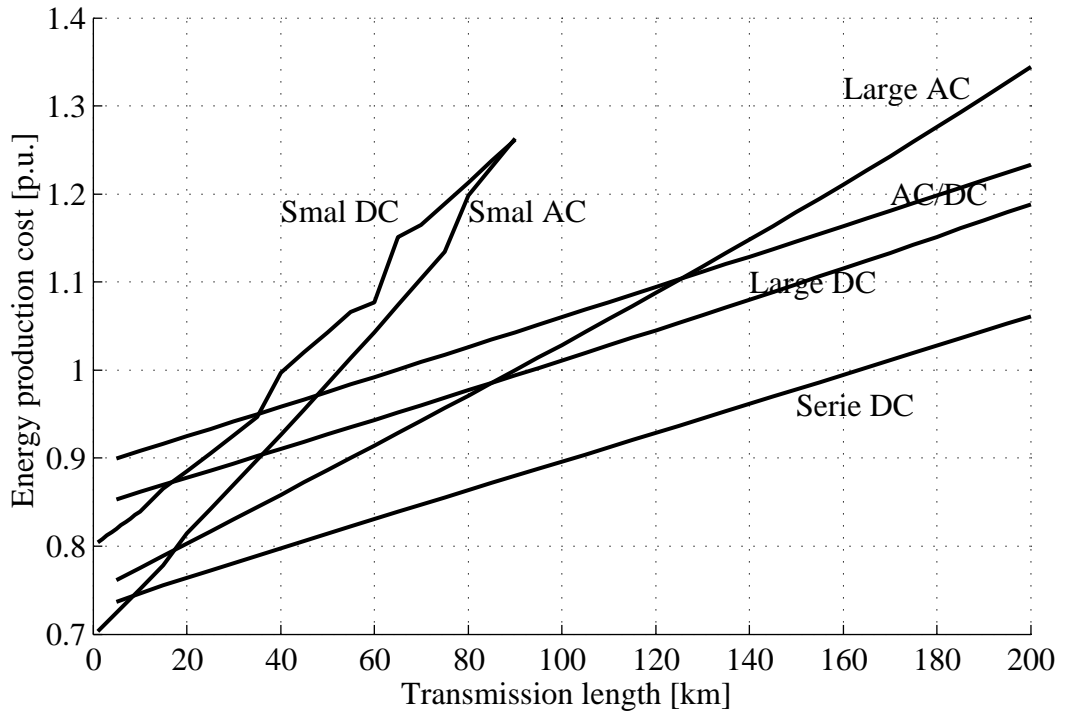


Fig. 3.9 The normalized energy production cost of the different 160 MW wind farms as function of the transmission distance and at a average wind speed of 10 m/s. Solid small AC, dashed large AC, dash-dotted AC/DC, grey small DC, dotted large DC and solid with stars series DC.

In Fig. 3.10 a curve of how the energy production cost varies with the average wind speed is presented. The curve is normalized by the costs at a average wind speed of 10m/s. As can be noticed from the Fig. 3.10 the cost increases rapidly if the average wind speed decreases. At a average wind speed of 6.5 m/s the energy production cost is twice as high as at 10 m/s.

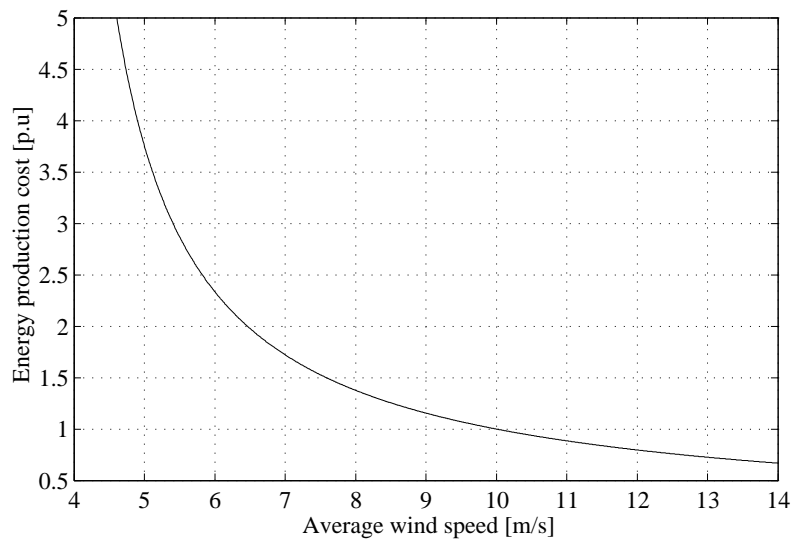


Fig. 3.10 Energy production cost as function of the average wind speed, normalized with the cost at a average wind speed of 10 m/s.

Chapter 4

Wind Farm with Series Connected Wind Turbines

4.1 System Overview

4.1.1 Wind farm layout

Figure 4.1 shows the general layout of the proposed wind farm with series connected wind turbines, the series DC layout. It should be noticed that the wind turbines used in this layout has a DC output voltage. In this wind farm, n wind turbines are series-connected

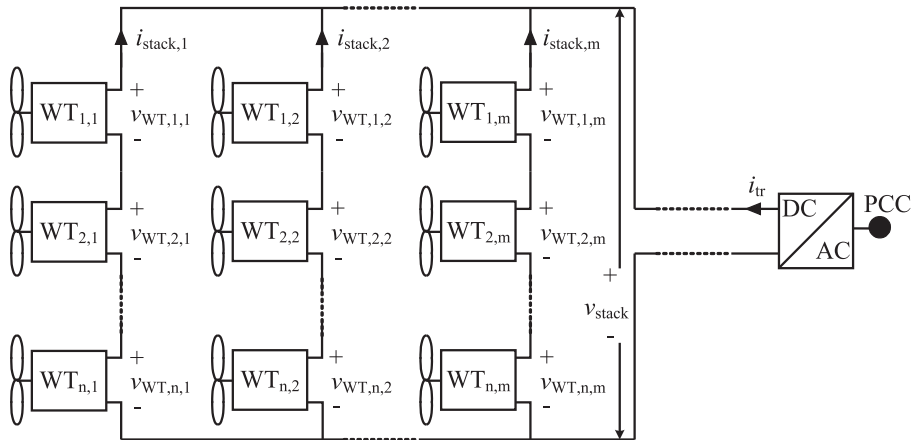


Fig. 4.1 The layout of a wind farm utilizing series-connected wind turbines with a DC output voltage.

to obtain a voltage suitable for transmission and m series-connections are connected in parallel to obtain the desired power level. The n series-connected wind turbines are here called a 'stack'. The suggested wind farm differs in two ways from "traditional" large offshore wind farms: for example the Horns Ref [15] or the Nysted [46] offshore wind

farms: 1) No offshore platform is used and 2) DC voltage is used for bringing the energy to shore.

The fact that no offshore platform with equipment is used, saves almost 20 Million Euros for a 160 MW farm [33], which means 120 kEuro/MW. The long-term cost of the proposed wind turbine electrical system should be in the same range as those used today. In the proposed system, the wind turbine transformer will be smaller and thus possibly cheaper compared to the systems of today, while the cost for the higher isolation at the output of the turbines will be higher. The result is that the proposed electrical systems in the wind turbines will be somewhat higher, but the cost of the total electrical systems will most likely be lower [33]. For a 160 MW wind farm located at 55 km from a suitable grid connection point, the proposed wind farm shows a potential 8 % cost reduction [33].

Reliability is an important subject and it is not possible to come to an accurate conclusion, unless a real wind farm of this type is built. However, by studying existing sea-based wind farms, it can be noted that the majority of problems are related to "traditional" components, such as cables, gear-boxes, local wind turbine 50 Hz-transformers. There are, of course, also problems related to the power electronic equipment, but these are not dominating. The reliability of the equipment of the sea-based platform used in the two Danish 160 MW wind farms of today, seems to be high. It seems therefore logical that the resulting reliability of the proposed wind farm layout should be fairly equal to a "traditional" AC wind farm.

4.1.2 Steady-state behavior of the series-connection

Figure 4.1 shows that the sum of the output voltages, $v_{WT,x,y}$, of the wind turbines equals the voltage across the stacks, v_{stack} , if the voltage drops in the cables between the wind turbines are neglected. From Fig. 4.1, it is also clear that the voltage across each wind turbine cannot be controlled individually by the onshore converter station. The onshore converter station only controls the voltage across the stacks. If the voltage drop in the cables are neglected, the output voltage of a wind turbine, $v_{WT,x,y}$, can be expressed as

$$v_{WT,nom} = \frac{v_{stack}}{n} \quad (4.1)$$

$$P_{s,y} = \frac{1}{n} \sum_{x=1}^n P_{out,x,y} \quad (4.2)$$

$$i_{stack,y} = \frac{\sum_{x=1}^n P_{out,x,y}}{v_{stack}} = \frac{P_{s,y}}{v_{WT,nom}} \quad (4.3)$$

$$v_{WT,x,y} = v_{WT,nom} \frac{P_{out,x,y}}{P_{s,y}} \quad (4.4)$$

where

$$x = 1..n$$

$$y = 1..m$$

$v_{WT,nom}$ Nominal output voltage of the wind turbines [V]

$i_{stack,y}$ Current in stack y [A]

$P_{out,x,y}$ Output power of wind turbine x,y [W]

$P_{s,y}$ Mean power production in stack y [A].

The output voltage across each wind turbine depends on the ratio between the output power from each wind turbine, $P_{out,x,y}$, and the mean power production of the wind turbines in the stack, $P_{s,y}$, see (4.4). This means that wind turbines that have an output power higher than the mean power in the stack, will have a higher output voltage and vice-versa.

The rated output voltage of the wind turbine, i.e. the highest voltage the wind turbine is designed to operate with continuously, is of course limited. If the output voltage exceeds the rated voltage, then the power production must be reduced in order to limit the output voltage to the rated one, see (4.4). Due to this fact, the output power of the wind turbines in one stack will be limited by the wind turbine with the lowest production, if the rated output voltage is selected to be equal to the nominal voltage, see (4.1) and (4.4). This would especially be severe if the production in one wind turbine goes down to zero, because then the production in the whole stack will be lost. In order to avoid this, some voltage overrating must be done, in order to limit the energy production loss in the wind farm due to the uneven power production that naturally occurs. In particular, overrating is needed in order to handle the case that some turbines are out of operation. The selection of a suitable overrating will be investigated in Section 6.3.

4.1.3 Wind turbine for series-connection

Series connection of wind turbines implies that some components in the wind turbine module must have a common mode insulation level high enough to withstand the whole transmission voltage to ground or that all components must be lifted to a high potential. To insulate the wind turbine tower and put the nacelle on high potential does not seem as a good solution. To insulate the generator windings for the common mode voltage and put all components between the generator and the transmission side on high potential is not a practical solution either. There also exists some other ways of solving this potential problem. However, in this study, a solution with an insulated DC/DC converter is the only one considered. A scheme of the electrical system of the wind turbine unit is presented in Fig. 4.2. The figure shows that the high voltage winding of the transformer in the DC/DC converter must be isolated for the transmission voltage to ground. Also all components on the transmission side in Fig. 4.2 must be placed or encapsuled so that they can withstand the transmission voltage to ground. The high insulation level needed for the series connection will most probably mean that the DC/DC converter cannot be easily placed

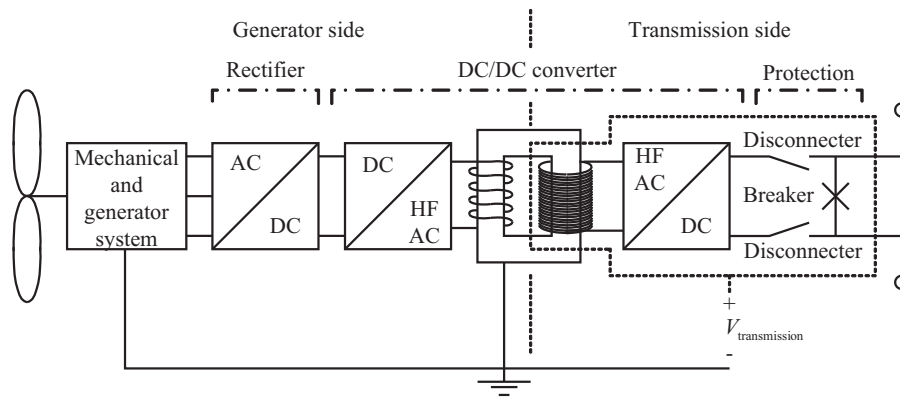


Fig. 4.2 Scheme for a wind turbine electrical system with DC/DC-converter and bypass protection.

inside the turbine. Instead it can be placed in a container outside the wind turbine. The container can be mounted on the wind turbine tower, as done in the small offshore wind farm Utgrunden in the Baltic sea [29].

The series-connected wind turbines must always have a closed path for the current through the stack. A fault that opens this path causes the production in the hole stack to be lost. Due to this factor the protection system of the wind turbine should be designed to short circuit the output of the wind turbine if an internal fault is detected. After this the wind turbine can be disconnected from the stack. In Fig. 4.2 one solution for the protection system is displayed.

There are a large variety of generating and rectifying systems that can be used for this application. The main requirements are that the torque produced by the generator, as well as the output power from the rectifier, should be smooth. For a diode rectifier, a synchronous generator can be used, either electrically or permanently magnetized. The generator can also be either direct driven or of a high speed type. This system requires special attention on the reactive power support to the generator [18] and on the low order harmonics created by the diode rectifier. The low order harmonics can create ripple in both the torque produced by the generator and in the power after the rectifier. One way to reduce the impact of the harmonics is to increase the number of phases in the generator and to place filters between the generator and the rectifier. For the system with a diode rectifier, the torque control of the generator is done with the DC/DC converter, by controlling the DC current from the rectifier. For a transistor rectifier, both the synchronous generator and the induction generator can be good choices, but also other types of generators can be used. For a transistor rectifier system, both the active and reactive power to the generator are fully controllable. In this way, it is no problem to obtain both a smooth torque and desirable flux level in the generator, as well as a good quality of the dc-link voltage.

4.1.4 Transmission System and Onshore Converter Station

Among the possible configurations for the transmission system between the wind farm and the onshore converter station, the two cable configuration has been considered in this work. In Fig. 4.3, a part of the wind farm, the transmission cables, the onshore converter station and the grid to which the wind farm is connected to are shown. The onshore con-

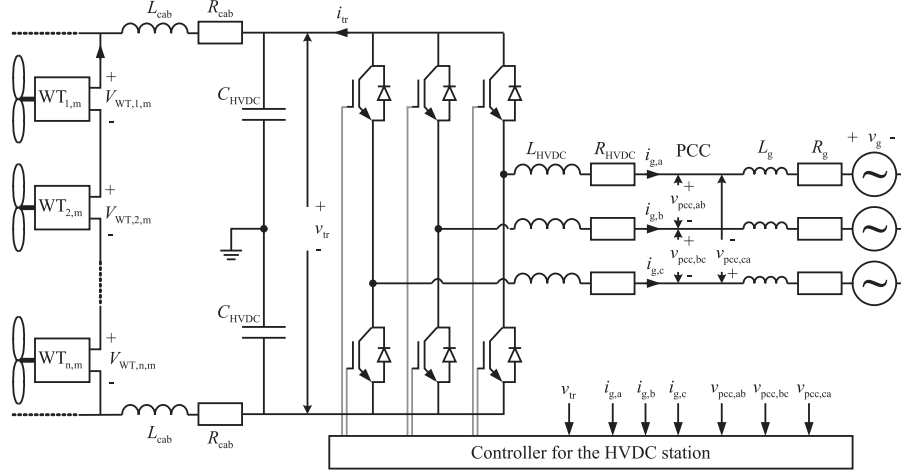


Fig. 4.3 Transmission cables, onshore converter station and the grid the wind farm is connected to.

verter station includes the DC-capacitors, the switches and the AC-side filter. In a actual converter system, the AC-side filters are more complex than the single reactor used in this work. The AC-side usually contains the reactor, shunt capacitors, some notch filters (for the first switching harmonics) and some EMI-filters. However, for simplicity, only a reactor is used as the AC-filter and the other filters should not influence the performance of the converter so much, since they only affects frequencies from the switching frequency and above. In addition, typically a transformer is added between the filtering stage and the PCC. The transformer is used among other things for providing galvanic insulation and for adjusting the grid voltage to a level that is suitable for the converter.

The grid impedance can be calculated as

$$R_g = \frac{v_{g,1-1}^2}{\sqrt{K_{xr}^2 + 1} K_{sc} P_{rated}} \quad (4.5)$$

$$L_g = \frac{K_{xr} R_g}{2\pi f_g} \quad (4.6)$$

where $v_{g,1-1}$ is the line-to-line voltage of the grid, K_{xr} is the XR-ratio of the grid (X_g/R_g) and K_{sc} is the short circuit ratio (the short circuit power of the grid divided with the rated power of the wind farm, P_{rated}). The grid frequency, f_g , is assumed to be 50 Hz. The filter reactor is assumed to be 0.14 p.u., which is in the range of the filter size considered in [1].

It is assumed that all losses in the HVDC station are in the filter reactors and they are assumed to be 2 %. This gives that the reactor can be calculated as

$$L_{\text{HVDC}} = 0.14 \frac{v_{g,l-1}^2}{2\pi f_g P_{\text{rated}}} \quad (4.7)$$

$$R_{\text{HVDC}} = 0.02 \frac{v_{g,l-1}^2}{P_{\text{rated}}} \quad (4.8)$$

The DC-capacitors C_{HVDC} are assumed to be discharged on 2 ms with rated current, yielding

$$C_{\text{HVDC}} = 2 \cdot 10^{-3} \frac{2P_{\text{rated}}}{v_{\text{tr,rated}}^2}. \quad (4.9)$$

The transmission cables are modelled as a resistor and an inductance only, R_{cab} and L_{cab} respectively. The reason for this is that the cable capacitance is smaller than the capacitance in the HVDC-station and in the wind turbines.

4.2 Wind Turbine System

In Fig. 4.4, the selected system for the series-connected wind turbine is shown. From

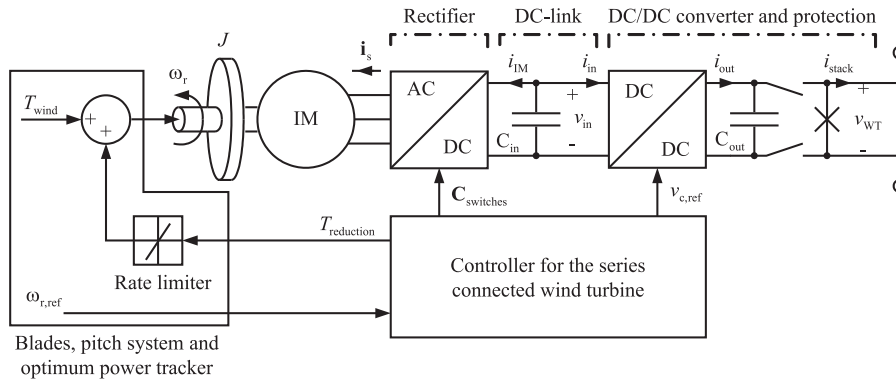


Fig. 4.4 Selected system for the series-connected wind turbine.

the figure it can be seen that an induction machine connected to a transistor rectifier is used. The induction generator is implemented in the stationary reference frame with motor references and the transistor rectifier is implemented as a standard 3-phase converter with IGBT valves.

The mechanical system of the wind turbine, i.e. blades, gearbox and shafts, are modelled as one inertia only. This inertia is added to the inertia of the generator. The conversion from wind to torque is not modelled in the following study of the behavior of an individual wind turbine system. Instead, the behavior of this conversion, the pitch system

and the optimum power tracker for the wind turbine is taken from measurement performed on a variable speed wind turbine. The optimum power tracker operates the blades at maximum efficiency at low wind speeds. This means that the rotational speed of the turbine is proportional to the wind speed and the pitch angle is almost fixed. At wind speeds above the rated wind speed, the optimum power tracker limits the incoming torque to rated torque by utilizing the pitch angle. The rotational speed is in this case equal to the rated speed of the turbine. Information about the generation of the appropriate reference values (pitch angle and speed) can be found in [10, 59]. The inputs to the wind turbine model is the torque, T_{wind} , and the speed reference, $\omega_{r,\text{ref}}$. These signals are taken from the measured torque and speed of a variable speed wind turbine.

The control structure of the series-connected wind turbine during certain operating conditions, that will be described in a later section, needs to decrease the input torque to the generator. In reality, this will be done by changing the pitch angle of the blades. In this section, this is modelled as an addition of the incoming torque, $T_{\text{reduction}}$, which is negative if the torque is reduced by a thought pitch action. To model the speed of the pitch system, a rate limiter is used. Of course, this is a very simplified model of the pitching system, but this is only for the additional reduction of the torque. As mentioned earlier the important behavior is taken from measurements. In Appendix A, the parameters for the induction generator and the mechanical system can be found.

4.3 DC/DC Converters

The DC/DC converter is used, as mention before, to isolate the generator side from the transmission side and as a DC transformer with a variable turns ratio. The DC/DC converter adapts the 'low' DC voltage from the rectifier to the 'high' varying DC output voltage of the wind turbine. In this thesis, two different DC/DC converters are used, the full bridge isolated boost converter (FBIB) and the full bridge converter with phase shift control (FBPS).

4.3.1 Full Bridge Isolated Boost Converter

In Fig. 4.5, the full bridge isolated boost converter (FBIB) with the pulse width modulator is shown. One benefit of the FBIB converter is that it only has few components on the high voltage side of the transformer: the diode rectifier and the output capacitor. This means that only a few components need to be placed or encapsuled so that they can withstand the transmission voltage to ground. It is worth mentioning that the FBIB converter exists today in radar applications where the output voltage is up to 25 kV (of course, the power rating is much lower). In Appendix A the used parameters for the converter are shown.

The operation of the FBIB converter is shown in Fig. 4.6. It can be noted that first all IGBTs are on, to charge the inductor (increasing the input current). The ratio between this

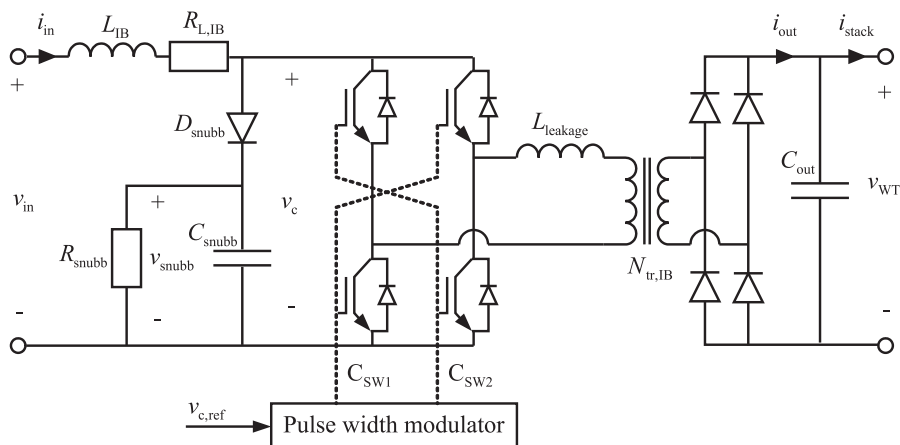


Fig. 4.5 The FBIB converter with snubber circuit and pulse width modulator.

time and the switching period is defined as the duty ratio D , in Fig. 4.6, the duty ratio is approximately 0.3. Then, two are turned off and some of the stored energy is transferred to the load through the transformer. When all switches are on, the output capacitor supplies the load, which can be observed as a decreasing voltage in Fig. 4.6c.

The leakage inductance in the transformer causes difficulties when the two IGBTs are turned off, because then two current stiff components are connected in series (the leakage inductance and the inductor, L). This requires a snubber circuit in order to avoid over-voltages across the IGBTs. In Fig. 4.5, the snubber circuit, consisting of R_{snubb} , C_{snubb} , D_{snubb} , is shown. Fig. 4.6 d) shows the voltage over the IGBTs, v_c , at rated operation of the FBIB converter. It can be noticed that the snubber limits the voltage over the IGBTs to approximate 1.3 times the ideal peak voltage, i.e. $v_{\text{WT,rated}}/N_{\text{tr,IB}}$. Instead of burning the energy (stored in the snubber capacitor at each turnoff) in the snubber resistance, a small DC/DC converter can be used to transfer the energy back to the DC link capacitor. This might increase the efficiency of the converter, but it will also increase the complexity.

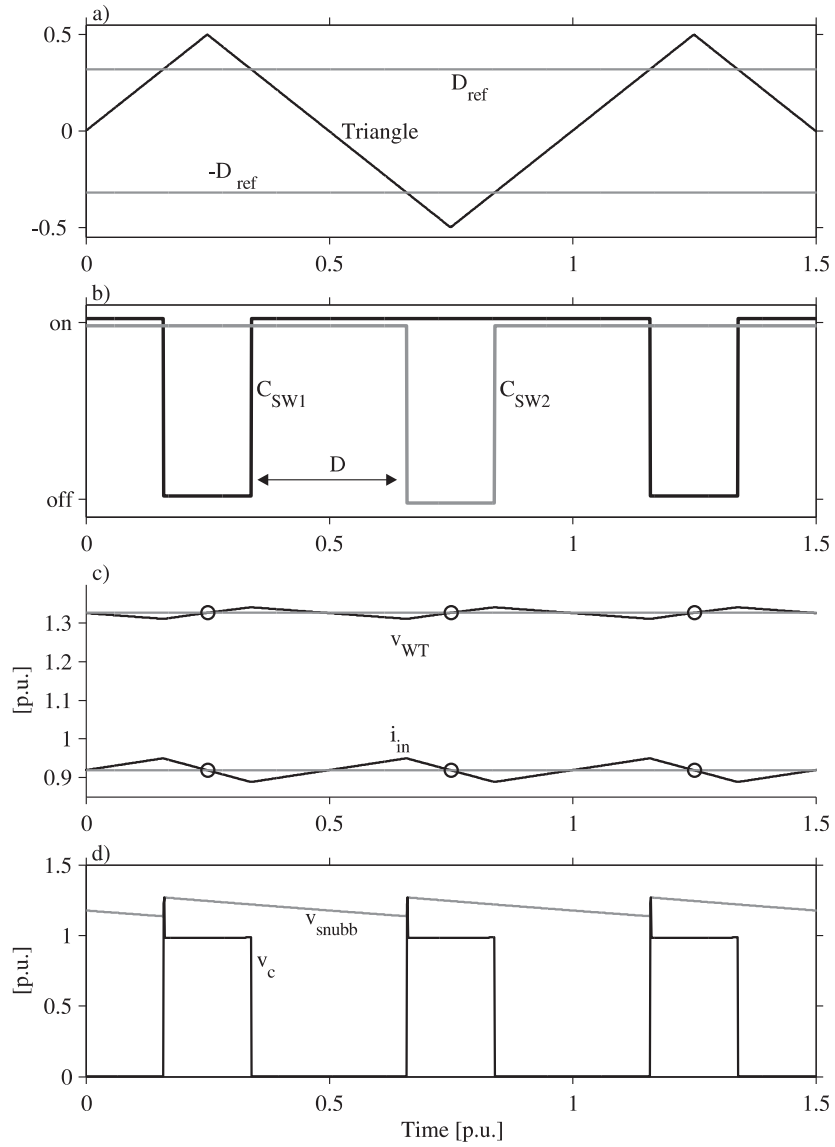


Fig. 4.6 Waveforms of the FBIB converter, the plots are shown with the time in p.u. of the switching period: a) Triangular wave and duty ratio reference. b) Control signals to the valves. c) Input current, in p.u. of rated current, and output voltage, in p.u. of nominal voltage, as black solid lines and the measured quantities as grey lines. The circles indicates the sampling times. d) Voltage over the IGBTs, v_c , and the voltage over the snubber capacitor v_{snubb} in p.u. of $v_{WT,rated}/N_{tr,IB}$.

From Fig. 4.5 it can be seen that the input to the pulse width modulator is the reference for the voltage v_c . For continuous current operation mode, the duty cycle reference can be obtained as

$$D_{\text{ref}} = 0.5 - \frac{N_{\text{tr,IB}}}{2v_{\text{WT}}} v_{c,\text{ref}}. \quad (4.10)$$

To obtain the control signals to the valves (C_{SW1} and C_{SW2}), triangular modulation is used, as shown in Figs. 4.6 a) and 4.6 b). From the figures it can be noticed that the duty ratio is limited between 0 and 0.5. In steady-state the voltage drop over the inductor is zero, which gives that the input voltage, v_{in} , is approximately equal to v_c , a value obtained by neglecting the voltage drop over the resistance. This gives that the lower limit for the output voltage of the wind turbine is approximately $v_{\text{WT}} = N_{\text{tr,IB}} V_{\text{in}}$. The maximum output voltage is limited to the rated output voltage of the converter. This limited output voltage range must be taken into consideration when the controllers for the wind turbine are designed.

4.3.2 Full Bridge Converter with Phase Shift Control

In the full bridge converter there is no inductance on the low-voltage side, so the transistors switch a stiff voltage. On the secondary side there is an inductor that reduces the current ripple on the high voltage side. A drawback with this set-up is the extra cost for having the inductor on the high-voltage side. The full bridge converter is shown in Fig. 4.7.

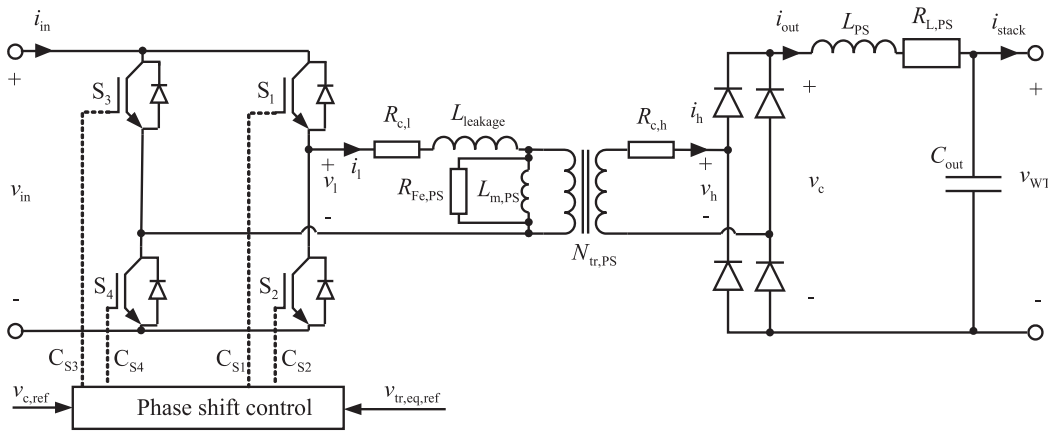


Fig. 4.7 Fullbridge converter.

For the phase-shift control, each leg (IGBT S_1, S_2 and S_3, S_4) in the converter is operated at 50/50. This means that the top switch is on for 50 % of the period and the bottom switch in on for the rest of the period. The output voltage from each leg is a square wave voltage which is equal to the input voltage for 50 % of the period and zero for the

rest. The voltage to the transformer is controlled by changing the phase, ϕ_{PS} between these two voltages. If they are in phase, the voltage to the transformer is zero and if they are 180 degrees out of phase the voltage is equal to the input voltage (v_{in}) for half the period and minus the input voltage ($-v_{in}$) for the rest of the period. The second input signal $v_{tr,eq,ref}$, is the reference for the DC-component of the voltage to the transformer. Ideally this voltage component should be zero. However, it is needed due to the fact that in an actual converter, there will be a DC-component in the applied transformer voltage. The reason for this is that the physical components are not equal and the fact that the on and off times for the legs are not equal. This topic together with a solution will be further discussed in Section 5.5.2.

In Fig. 4.8 the wave-forms for the phase-shift controlled converter is displayed for a phase-shift of approximately 45 degrees. Observe that in the figure also the blanking time for the switches is shown and a small leakage inductance in the transformer is assumed. The blanking time is the time delay between the turn off, of one IGBT in the leg, until the other IGBT can be turned on safely. When the phase shift is increased, the signals for IGBTs 1 and 2 are shifted to the right and for IGBTs 3 and 4 they are shifted to the left, as indicated in the figure. The vertical lines in Fig. 4.8 indicates the sampling instances. Sampling at these instances results in that the average value of the inductor current is obtained, without using low pass filters.

The phase shift is calculated from the reference $v_{c,ref}$ as:

$$\phi_{PS} = \frac{180}{N_{tr,PS}} \frac{v_{c,ref}}{v_{in}}. \quad (4.11)$$

It can be mentioned that it is possible to use "loss-less" snubbers, i.e. capacitors over the switches and diodes. These capacitors take over the task of "shifting/altering" the leg output voltages as a transistor is turned on or off. Without the loss-less snubbers this task is achieved by the transistors, which lead to turn-on and turn-off losses in the transistors. With the assistance of the capacitors, the periods with high current and high voltage in the transistors are in principle eliminated, and accordingly the losses are strongly reduced. The diode turn-off losses (reverse recovery losses) are also reduced since the voltage over the diode now "slowly" becomes negative so that the diode with low losses can move into its blocking status.

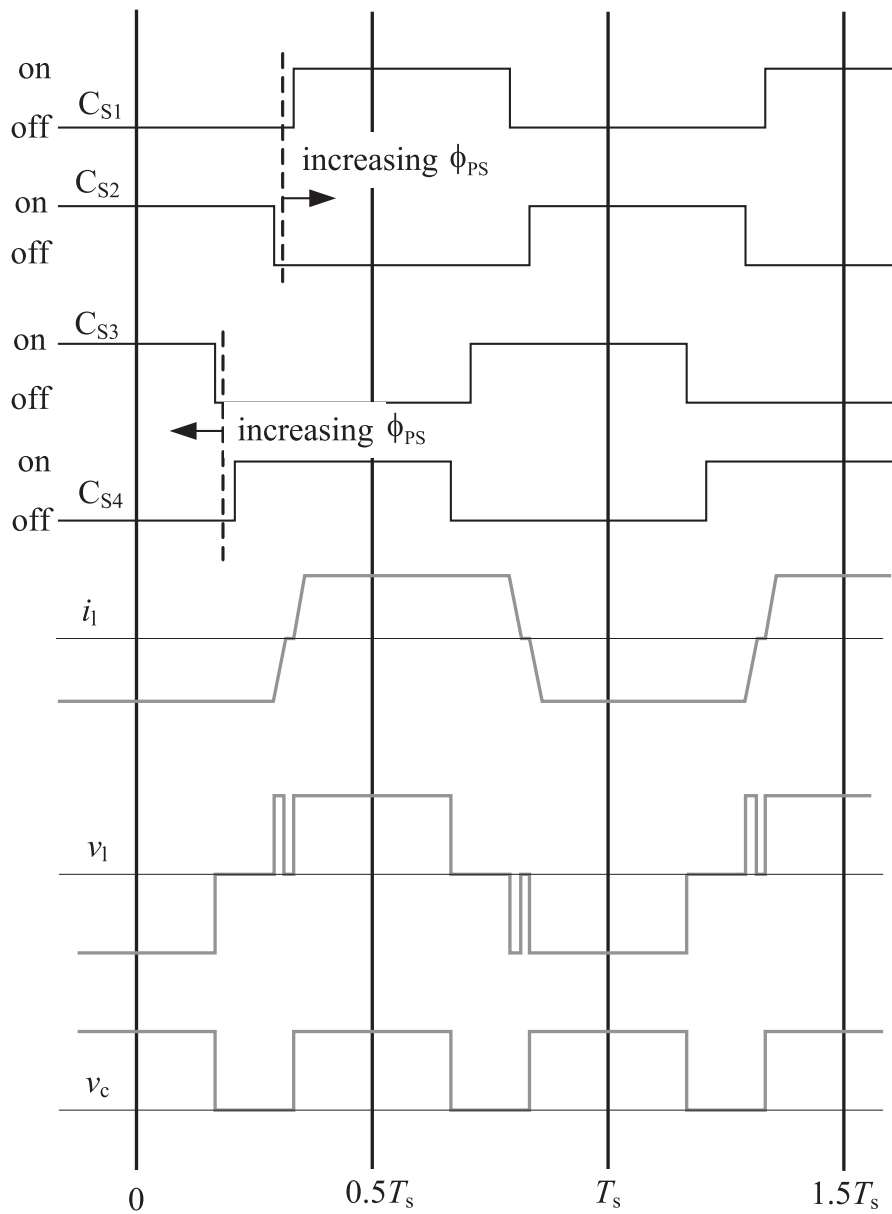


Fig. 4.8 Principal wave forms of the full bridge converter with phase shift control. Observe that the wave forms are drawn assuming a blanking time for the IGBTs and a small leakage inductance in the transformer.

Chapter 5

Controller Structure and Design

5.1 Onshore Converter station Controller

In Fig. 5.1 the controller structure for the onshore HVDC station is shown. From the figure it can be seen that the controller can be divided into four main blocks, phase-locked loop (PLL), DC-transmission controller, AC-current controller and the modulator. The controllers for the AC-side is implemented in a rotating coordinate system. The PLL

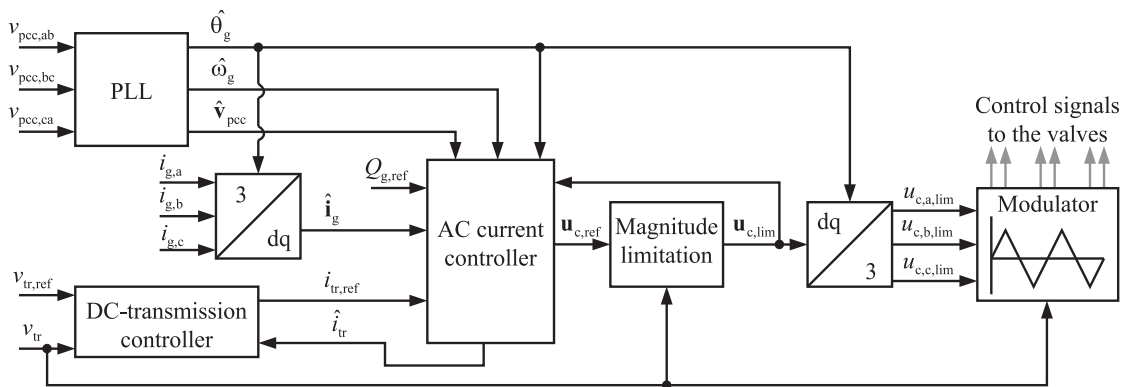


Fig. 5.1 The controller structure for the HVDC station.

tracks the voltage in the PCC so that the voltage vector in the rotating system is on the q -axis in steady-state. The DC-transmission controller, controls the voltage at the HVDC station, v_{tr} in Fig.4.3, this means that the stack voltage out in the wind farm will be somewhat higher due to the cable impedance. The AC-current controller fulfills the active current demand from the DC-transmission controller and the reactive power demand, Q_{ref} .

5.1.1 Phase-Locked Loop (PLL)

Since no capacitors or notch filters are used in the AC-filter to smoothen the voltage in the PCC, the measured voltages needs to be filtered before they are sampled and used in the

PLL. If not, the switching harmonics will be aliased and influence the estimation of the voltage in the PCC. As antialias filter, 8th order butterworth filters with a cut off frequency of half the switching frequency, as can be seen in Fig. 5.2 where the layout of the PLL is shown. It is assumed that the frequency is constant and equal to 50 Hz, therefore, the

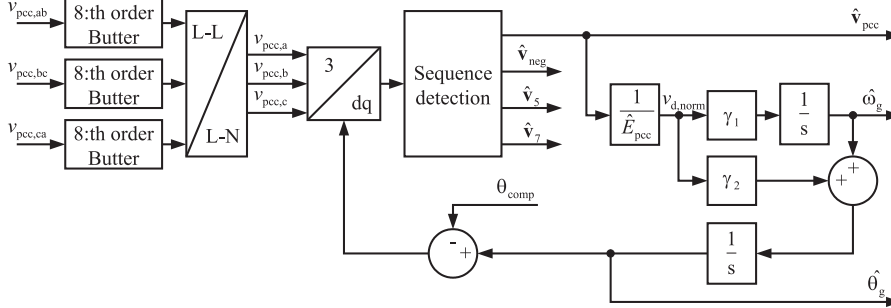


Fig. 5.2 The layout of the PLL used in the controller of the onshore HVDC station.

phase shift introduced by the filters at the grid frequency is compensated for by a constant angle, θ_{comp} , which is set to the phase shift of the filters at 50 Hz. The calculation of the line to neutral voltage from the line-to-line voltage is done by assuming that there is no zero sequence in the grid voltage. The line-to-neutral voltage is calculated as

$$v_{pcc,a} = \frac{v_{pcc,ab} - v_{pcc,ca}}{3} \quad (5.1)$$

$$v_{pcc,b} = \frac{v_{pcc,bc} - v_{pcc,ab}}{3} \quad (5.2)$$

$$v_{pcc,c} = \frac{v_{pcc,ca} - v_{pcc,bc}}{3} \quad (5.3)$$

The phase sequence and harmonic detection can be incorporated in the control as described in [5], however, in this thesis work only the fundamental voltage positive sequence is used.

The input to the PLL is the normalized voltage in the d-direction, $v_{d,norm}$. The voltage is normalized by dividing the voltage in the d-direction by the estimated magnitude of the voltage vector, \hat{E}_{pcc} . In this way the bandwidth of the PLL will be independent of the magnitude of the input signal [38]. The gains in the PLL are set to $\gamma_1 = \alpha_{PLL}^2$ and $\gamma_2 = 2\alpha_{PLL}$ where α_{PLL} is the bandwidth of the PLL. The PLL is transformed from continuous time to discrete time with the method described in [7]. The discrete PLL can be implemented, using the forward Euler method, in fortran as

$$\hat{\theta}_g(k+1) = \hat{\theta}_g(k) + T_s \hat{\omega}_g(k) + T_s \left(\gamma_2 + \frac{\gamma_1 T_s}{2} \right) v_{d,norm} \quad (5.4)$$

$$\hat{\omega}_g(k+1) = \hat{\omega}_g(k) + T_s \gamma_1 v_{d,norm} \quad (5.5)$$

5.1.2 DC-transmission controller

When designing the DC-transmission controller it is assumed that the DC-side is purely capacitive and the wind turbines can be represented as a current source, acting as a disturbance. In Fig. 5.3 the implemented DC-transmission controller and the model of the process used for the controller design are shown. The active damping conductance Y_{aHVDC} is used to add damping to the process $G_{HVDCt}(s)$.

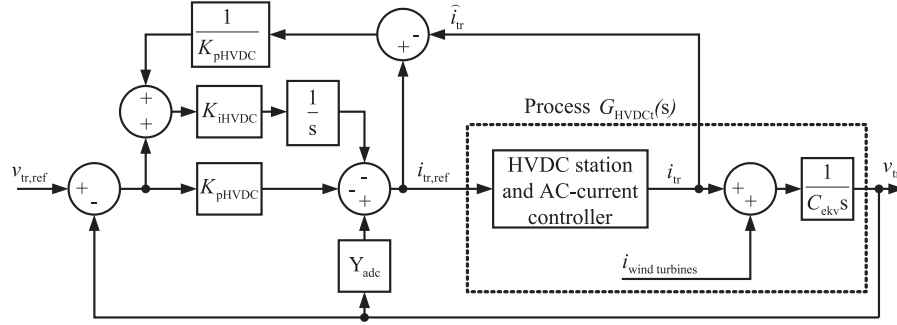


Fig. 5.3 The DC-transmission controller and the model of the process used for the design of the controller.

When designing the DC-transmission controller, the actuator (the HVDC station together with the AC-current controller) is treated as a unity gain. By incorporating the active damping with the process, a new process is obtained

$$G'_{HVDCt}(s) = \frac{1}{C_{ekv}s + Y_{aHVDC}} \quad (5.6)$$

for which the DC-transmission controller is designed. The DC-transmission controller is designed according to the IMC method [22]. In this method a bandwidth for the close loop system, from reference to actual quantity is set. The resulting transfer function will be a first order low pass filter with the selected bandwidth α_{HVDCt} . This method will also be used for the design of the other controllers in this thesis, unless stated otherwise. Accordingly the controller gains should then be selected as $K_{pHVDC} = \alpha_{HVDCt}C_{ekv}$ and $K_{iHVDC} = \alpha_{HVDCt}Y_{aHVDC}$. The active conductance is selected so that the process $G'_{HVDCt}(s)$ has the same bandwidth as the DC-transmission controller. This gives $Y_{aHVDC} = \alpha_{HVDCt}C_{ekv}$. The DC-transmission controller is transformed from a continuous time controller to a discrete time controller. By adding back-calculation [22], integrator windup can be avoided, i.e. an antiwindup function. The controller now becomes:

$$\begin{aligned} i_{tr,ref}(k) &= K_{pHVDC}(v_{tr,ref}(k) - v_{tr}(k)) + S_{HVDCt}(k) - Y_{aHVDC}v_{tr}(k) \quad (5.7) \\ S_{HVDCt}(k+1) &= S_{HVDCt}(k) + \\ &+ K_{iHVDC} \left(v_{tr,ref}(k) - v_{tr}(k) + \frac{\hat{i}_{tr}(k) - i_{tr,ref}(k)}{K_{pHVDC}} \right) T_s \quad (5.8) \end{aligned}$$

where $S_{HVDCt}(k)$ is the integration state.

5.1.3 AC-current controller

From Fig. 5.1 it can be seen that the input to the AC-current controller is the DC-current reference, $i_{tr,ref}$ and the reactive power reference $Q_{g,ref}$. Assuming steady-state conditions and that the grid voltage is in the q -direction only, the active and reactive power produced by the converter can be calculated as

$$\begin{aligned} P_g + jQ_g &= \frac{3}{2K^2}(\mathbf{v}_{pcc}\mathbf{i}_g^*) = \frac{3}{2K^2}(jv_{pcc,q}(i_{g,d} - ji_{g,q})) = \\ &= \frac{3}{2K^2}(v_{pcc,q}i_{g,q} + jv_{pcc,q}i_{g,d}) \end{aligned} \quad (5.9)$$

where $*$ denotes the complex conjugate. This relation is used to calculate the d -current reference as

$$i_{g,d,ref} = \frac{2K^2 Q_{g,ref}}{3 v_{pcc,q}}. \quad (5.10)$$

The q -current reference is calculated from $i_{tr,ref}$ by assuming that the power taken from the DC-side is equal to the power delivered to the AC-side (loss-less converter). This assumption gives

$$i_{g,q,ref} = -\frac{2K^2 i_{tr,ref}v_{tr}}{3 v_{pcc,q}}. \quad (5.11)$$

Before the d - and q -current references are used, they are limited within the ratings of the HVDC converter. First the q -current reference is limited to be within the rating of the converter and then the d -current is limited so that the length of the current vector is within the rating of the converter. This means that the q -current has priority over the d -current. In this way the converter can always produce the maximum power to control the DC-transmission. In Fig. 5.4 these limitations are shown together with the AC-current controller and the model of the filter used for the design of the controller. When calculating the limited DC-current \hat{i}_{tr} used in the antiwindup of the integrator in the DC-transmission controller equation (5.11) and the limited q -current reference are used.

When designing the AC-current controller, only the filter reactor is considered. The voltage at the PCC is assumed to be unaffected by the current and therefore considered as an disturbance in the controller design. In Fig. 5.4, the model of the filter in the rotating coordinate system is shown. To reduce the effects of the cross-coupling between the d - and q -currents and of the voltage at the PCC, a feed forward of estimations of these are used. In this feed forward, an active damping resistor R_{aHVDC} is also added. Assuming perfect feed-forward, the voltage at the PCC and the cross-coupling are cancelled and the process to control becomes

$$\hat{G}'_{filter}(s) = \frac{1}{s\hat{L}_{HVDC} + \hat{R}_{HVDC} + R_{aHVDC}}. \quad (5.12)$$

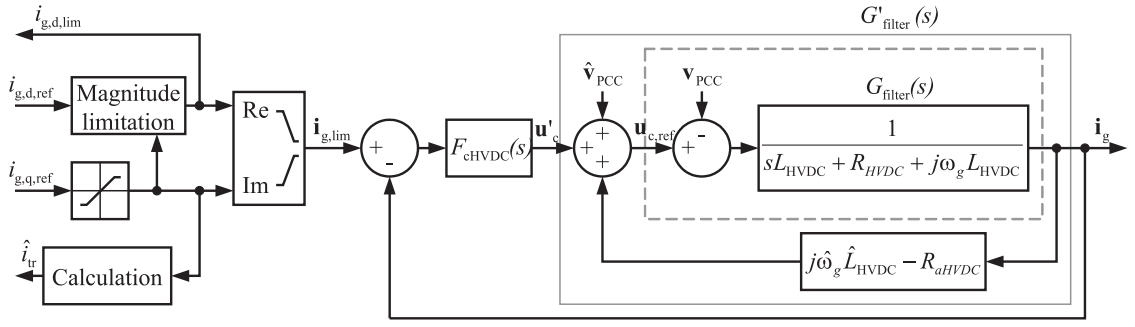


Fig. 5.4 The AC-current controller and the filter model used for the controller design.

For this system the current controller is designed so that the closed loop system becomes a first order low pass filter with a bandwidth α_{cHVDC} . The controller can be calculated as

$$\begin{aligned}
 F_{cHVDC}(s) &= \frac{\alpha_{cHVDC}}{s} \hat{G}'_{filter^{-1}}(s) = \frac{\alpha_{cHVDC}}{s} \left(s\hat{L}_{HVDC} + \hat{R}_{HVDC} + R_{aHVDC} \right) = \\
 &= \alpha_{cHVDC} \hat{L}_{HVDC} + \frac{\alpha_{cHVDC}(\hat{R}_{HVDC} + R_{aHVDC})}{s} \\
 &= K_{pcHVDC} + \frac{K_{icHVDC}}{s}.
 \end{aligned} \tag{5.13}$$

Separating the controller into its d - and q -components, adding antiwindup of the integrator and transforming it into discrete time, the controller can be implemented as

$$\begin{aligned}
 u_{c,d,ref}(k) &= K_{pcHVDC}(i_{g,d,lim}(k) - \hat{i}_{g,d}(k)) + S_{dHVDC}(k) - R_{aHVDC}\hat{i}_{g,d}(k) + \\
 &\quad - \hat{\omega}_g \hat{L}_{HVDC} \hat{i}_{g,q}(k) + \hat{v}_{pcc,d}
 \end{aligned} \tag{5.14}$$

$$\begin{aligned}
 u_{c,q,ref}(k) &= K_{pcHVDC}(i_{g,q,lim}(k) - \hat{i}_{g,q}(k)) + S_{qHVDC}(k) - R_{aHVDC}\hat{i}_{g,q}(k) + \\
 &\quad + \hat{\omega}_g \hat{L}_{HVDC} \hat{i}_{g,d}(k) + \hat{v}_{pcc,q}
 \end{aligned} \tag{5.15}$$

$$\begin{aligned}
 S_{dHVDC}(k+1) &= S_{dHVDC}(k) + \\
 &\quad + K_{icHVDC} \left(i_{g,d,lim}(k) - \hat{i}_{g,d}(k) + \frac{u_{c,d,lim} - u_{c,d,ref}}{K_{pcHVDC}} \right) T_s
 \end{aligned} \tag{5.16}$$

$$\begin{aligned}
 S_{qHVDC}(k+1) &= S_{qHVDC}(k) + \\
 &\quad + K_{icHVDC} \left(i_{g,q,lim}(k) - \hat{i}_{g,q}(k) + \frac{u_{c,q,lim} - u_{c,q,ref}}{K_{pcHVDC}} \right) T_s
 \end{aligned} \tag{5.17}$$

where $u_{c,d,lim}$ and $u_{c,q,lim}$ are the limited voltage references. The active damping is selected so that the process $\hat{G}'_{filter}(s)$ has the same bandwidth as the AC-current controller α_{cHVDC} . The active damping can be calculated as [23]

$$R_{aHVDC} = \alpha_{cHVDC} \hat{L}_{HVDC} - \hat{R}_{HVDC}. \tag{5.18}$$

5.1.4 Modulator for the HVDC

The level is depending on the rating of the transmission voltage. The peak voltage that can be produced at the output of the switches is half of the transmission voltage. This gives that, if only the fundamental is used when controlling the switches the maximum peak value of the phase voltage will then be equal to the half of the transmission voltage. If a zero-sequence voltage is subtracted from the fundamental before the control signals fo

The line-to-line RMS grid voltage is selected as

$$V_{g,l-l} = \frac{V_{tr, rated}}{\sqrt{2}} 0.8 \quad (5.19)$$

where $V_{tr, rated}$ is the rated transmission voltage and 0.8 is the factor between the rated line-to-line voltage and the maximum voltage that the converter can produce.

The voltage reference from the current controller should be realized by the converter. This is done by switching the valves on and off and thereby producing the right average voltage to the filter. The on and off signals to the valves are obtained by triangle wave modulation, the duty cycle for each phase is compared with a triangular wave and if the duty cycle reference is greater, then the top switch is on, otherwise the bottom switch is on. The modulator is shown in Fig. 5.5

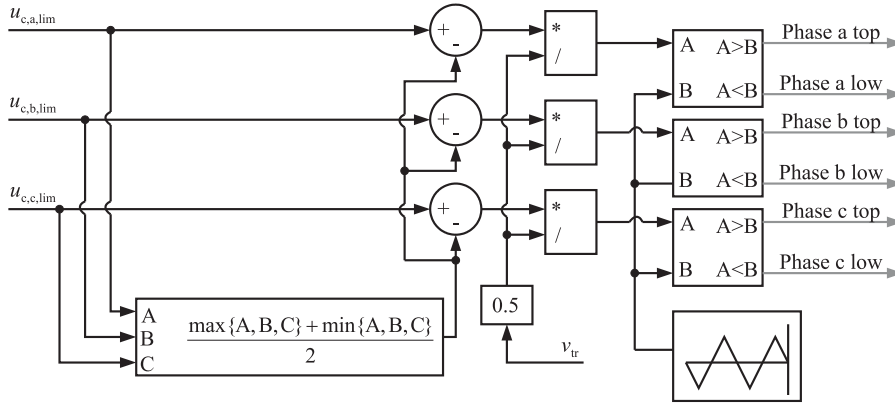


Fig. 5.5 The modulator used for the HVDC controller.

The zero-sequence voltage Δ is subtracted from the phase voltage in order to utilize the converter better. In this way the converter can produce approximately 15 % more voltage than compared to the case without the zero-sequence voltage for the same DC-voltage. With the zero-sequence voltage addition, the maximum voltage the converter can produce is that the peak value of the line-to-line voltage is equal to the DC-voltage. Accordingly, the maximum length of the voltage vector the converter can produce is

$$\max\{|\mathbf{u}_c|\} = \frac{K v_{tr}}{\sqrt{3}} \quad (5.20)$$

and it is to this value the length is limited to in the "Magnitude limitation" block in Fig. 5.1.

5.2 Overview of the Wind Turbine Controller

The controller structure for the series-connected wind turbine have two different modes of operation, normal (N) mode and voltage limitation mode (VL). When the output voltage of a wind turbine unit is within the unlimited operation region of the DC/DC converter, the controller is in N-mode and when the output voltage is close to the limit, the controller is in VL-mode. In Fig. 5.6 the principal operation of the series connected wind turbine is shown for the case when the input power to the wind turbine varies but is constant for the other turbines in the stack. The figure shows the case when a FBIB converter is used in

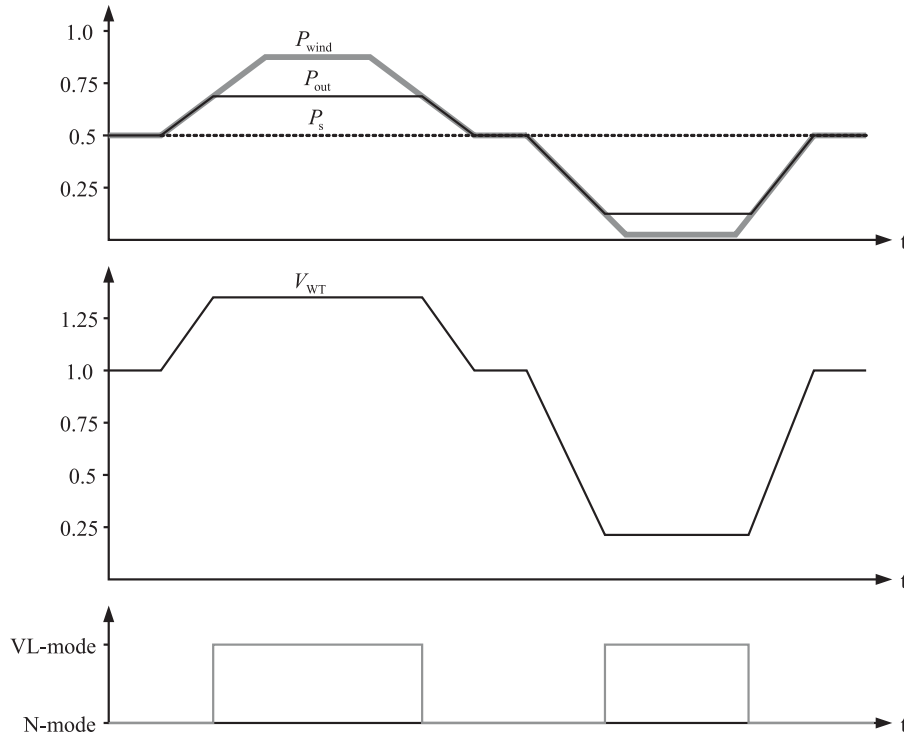


Fig. 5.6 The principal operation of the series connected wind turbine when the input power to the wind turbine varies but is constant for the other turbines in the stack. P_{out} is the real output, while P_{wind} is the power that could have been extracted from the wind.

the wind turbine, i.e. there is a lower limit of 0.2 p.u. and the rated voltage is 1.35 p.u. of the nominal output voltage.

In Fig. 5.7 a principle controller structure of the series-connected wind turbine is shown. This structure is schematic, and it has as a main purpose to serve as a description of the differences in the control signal flow for the N and VL mode operation. The overall wind turbine control strategy is assumed to be equal to a standard pitch regulated variable speed turbine and is not dealt with more in this thesis. For the induction machine controller and for the DC/DC converter current controller the inputs marked with N are used in normal operation and the inputs marked with VL are used in voltage limitation

ually. The only signal used in the controllers that contains information about the other wind turbines is the stack current and this can be measured in each wind turbine. The stack current holds information about the average power production in the stack (4.3).

5.2.1 Speed controller

The speed controller used is a PI controller implemented using a velocity algorithm [6], is shown in Fig. 5.8. The velocity algorithm is used due to that in voltage limitation mode the pitch system is used as actuator for the speed controller. The simplified pitch system used in this work has a rate limiter, i.e. the magnitude of the derivative of $T_{\text{reduction}}$ is limited. To avoid integrator windup due to this limitation, the magnitude of the derivative of output of the speed controller is limited by the saturation block Sat 2. The saturation is set to be equal or less than the rate limitation, in this case it is set to be equal in voltage limitation mode and 50 times higher in normal mode. This is due to the fact that there is no rate limitation since the current controller for the induction machine is used as an actuator in normal operation mode. Another advantage of the used velocity algorithm is that no antiwindup function needs to be implemented due to saturation in the actuator. When the maximum or minimum output level of the speed controller is reached the integration is stopped at this level, this is shown in Fig. 5.8 as an integrator with saturation. One drawback with the speed form is that the proportional parts of the controller needs to be derived, which can cause problems if the signals are noisy. This problem is reduced by the fact that the derivative action is limited to frequencies up to $k_{\omega}\alpha_{\omega}$, where α_{ω} is the selected bandwidth of the speed controller and $k_{\omega} = 90$. A factor of 90 is used to be sure that this will not influence the performance of the speed controller. But if the measured speed signal is noisy then this factor probably needs to be reduced.

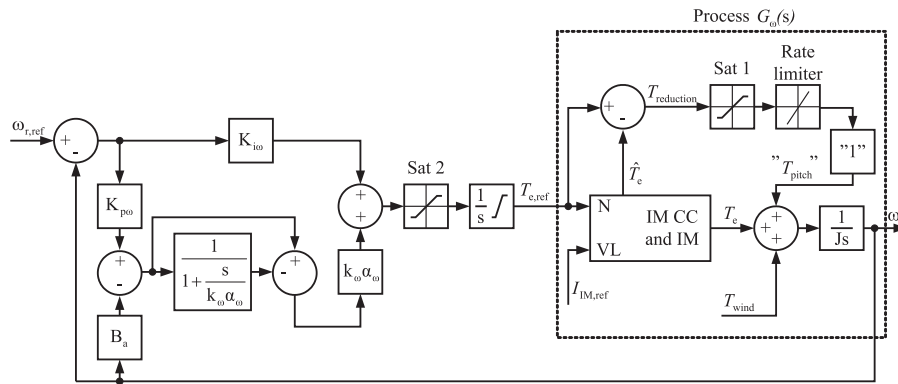


Fig. 5.8 The speed controller and the model of the process used for the design of the speed controller.

In Fig. 5.8 both the speed controller and the process that it controls are shown. When designing the controller parameters it is assumed that the controller is a normal PI controller and that the process has a unity gain from the reference to the actual value (for

the time-scale that the speed controller operates in). From the figure it can be noticed that active damping, B_a , is used to add some additional damping to the process $G_\omega(s)$. By incorporating this with the process and treating the torque from the wind as a disturbance a new process is given,

$$G'_\omega(s) = \frac{1}{J_s + B_a} \quad (5.21)$$

for which the speed controller is designed. The speed controller is designed so that the closed loop system becomes a first order low pass filter with unity gain and with a bandwidth α_ω . The controller gains can then be selected as $K_{pw} = \alpha_\omega J$ and $K_{iw} = \alpha_\omega B_a$. The active damping is selected so that the process $G'_\omega(s)$ has the same bandwidth as the speed controller. This gives $B_a = \alpha_\omega J$. The speed controller is transformed from a continuous time controller to a discrete time controller and the result can be implemented in fortran as

$$T_{e,\text{ref}}(k+1) = T_{e,\text{ref}}(k) + \text{Sat}_2\{K_{iw}(\omega_{r,\text{ref}}(k) - \omega_r(k)) + k_\omega \alpha_\omega (K_{pw}(\omega_{r,\text{ref}}(k) - \omega_r(k)) - B_a \omega_r(k) - S_\omega(k))\} T_s \quad (5.22)$$

$$T_{e,\text{ref}}(k+1) = \text{Sat}_3\{T_{e,\text{ref}}(k+1)\} \quad (5.23)$$

$$S_\omega(k+1) = e^{-k_\omega \alpha_\omega T_s} S_\omega(k) + (1 - e^{-k_\omega \alpha_\omega T_s})(K_{pw}(\omega_{r,\text{ref}}(k) - \omega_r(k)) - B_a \omega_r(k)) \quad (5.24)$$

$$\text{Sat}_n\{x\} = \begin{cases} \max_n & \text{if } x > \max_n \\ x & \text{if } \min_n \leq x \leq \max_n \\ \min_n & \text{if } x < \min_n \end{cases} \quad (5.25)$$

where T_s is the sampling period and Sat_3 is the limitation in the integration block of the speed controller.

5.2.2 DC-link voltage controller

For the DC-link voltage controller a PI controller with active damping and antiwindup of the integrator is used. In Fig. 5.9 the implemented DC-link voltage controller and the model of the process used for the controller design are shown. The active damping conductance Y_{adc} is used to add damping to the process $G_{\text{vdc}}(s)$.

When designing the DC-link voltage controller, the actuator (the IM system or the DC/DC system) is treated as a unity gain. By incorporate the active damping with the process and treat the current $i_{\text{disturbance}}$ as a disturbance, a new transfer function for the process is found,

$$G'_{\text{vdc}}(s) = \frac{1}{C_{\text{in}}s + Y_{\text{adc}}} \quad (5.26)$$

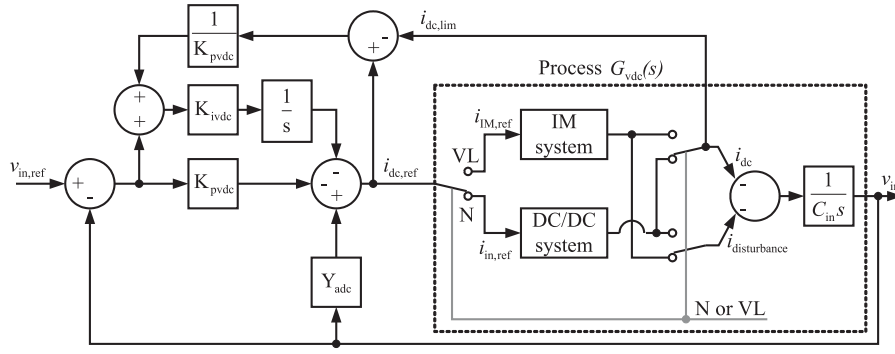


Fig. 5.9 The DC-link voltage controller and the model of the process used for the design of the DC-link voltage controller.

for which the DC-link voltage controller is designed. The DC-link voltage controller is designed with a closed loop system bandwidth α_{vdc} . The controller gains are selected as $K_{pvdc} = \alpha_{vdc} C_{in}$ and $K_{ivdc} = \alpha_{vdc} Y_{adc}$. The active conductance is selected so that the process $G'_{vdc}(s)$ has the same bandwidth as the DC-link voltage controller. This gives $Y_{adc} = \alpha_{vdc} C_{in}$. The bandwidth of the DC-link voltage controller, α_{vdc} , is selected to 150 rad/s. The discrete DC-link voltage controller can be implemented as

$$i_{dc,ref}(k) = Y_{adc}v_{in}(k) - K_{pvdc}(v_{in,ref}(k) - v_{in}(k)) - S_{vdc}(k) \quad (5.27)$$

$$S_{vdc}(k+1) = S_{vdc}(k) + K_{ivdc} \left(v_{in,ref}(k) - v_{in}(k) + \frac{i_{dc,ref}(k) - i_{dc,lim}(k)}{K_{pvdc}} \right) T_s \quad (5.28)$$

where $S_{vdc}(k)$ is the integration state.

In N-mode the actuator is the DC/DC system and in voltage limitation mode the actuator is the IM system. One problem that occurs when the wind turbine controller changes mode is that the output from the DC-link voltage controller must change sign. In order for the wind turbine to produce power, the current reference for the IM system should be negative and for the DC/DC system positive. To solve this problem the value of the integrator is changed when the mode is changed. The integrator is changed so that the current before the change is the same as after the change. This means that when changing to voltage limitation mode the integrator is set to

$$S_{vdc}(k) = Y_{adc}v_{in}(k) - K_{pvdc}(v_{in,ref}(k) - v_{in}(k)) - i_{IM}(k) \quad (5.29)$$

and when changing to normal mode it is set to

$$S_{vdc}(k) = Y_{adc}v_{in}(k) - K_{pvdc}(v_{in,ref}(k) - v_{in}(k)) - i_{in}(k). \quad (5.30)$$

This prevents large transients in the generator torque and in the output voltage when changing mode. But it gives a transient in the DC-link voltage, since the losses in the systems are not taken into account when recalculating the integrator.

5.2.3 Output Voltage controller

For the wind turbine output voltage controller a PI controller is used as shown in Fig. 5.10. In the figure also the process model used for the design of the controller is shown. From the figure it can also be seen that an active damping conductance Y_{awt} and anti wind up of the integrator are used. When designing the controller the DC/DC system is treated as a unity gain, i.e. the dynamics of the DC/DC converter and the DC/DC current controller are neglected.

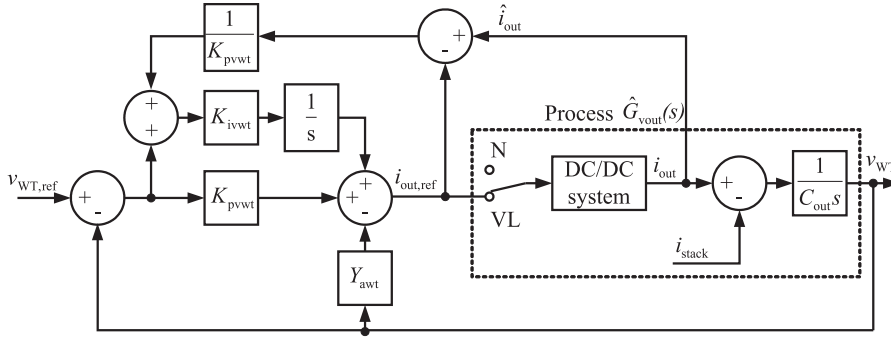


Fig. 5.10 The output voltage controller for the wind turbine and a part of the process model.

Incorporating the active damping conductance in the process model gives the following process model

$$\hat{G}'_{vout}(s) = \frac{1}{\hat{C}_{out}s + Y_{awt}} \quad (5.31)$$

for which the PI controller is designed for. The design is done so that the closed loop system becomes a first order low pass filter with unity gain and with a bandwidth α_{vwt} . The controller gain should then be selected as $K_{pvwt} = \alpha_{vwt}\hat{C}_{out}$ and $K_{ivwt} = \alpha_{vwt}Y_{awt}$. \hat{C}_{out} is the estimation of the output capacitance.

From Fig. 5.10 it can be noticed that in N-mode, the input to the DC/DC system is taken from another signal than the output from the output voltage controller. In this mode the system shown in the figure has three inputs, i_{out} , i_{stack} and $v_{WT,ref}$ and one output $i_{out,ref}$. It is here assumed that the estimated current \hat{i}_{out} is equal to the actual current i_{out} . The output current can be determined as

$$i_{out,ref} = K_{pvwt}(v_{WT,ref} - v_{WT}) - \frac{\alpha_{vwt} \left(1 - \frac{C_{out}}{\hat{C}_{out}}\right)}{s + \alpha_{vwt}} i_{out} + \frac{\hat{C}_{out}}{C_{out}} \frac{\alpha_{vwt}}{s + \alpha_{vwt}} i_{stack} \quad (5.32)$$

and with perfect parameters, $\hat{C}_{out} = C_{out}$, the expression becomes

$$i_{out,ref} = K_{pvwt}(v_{WT,ref} - v_{WT}) + \frac{\alpha_{vwt}}{s + \alpha_{vwt}} i_{stack}. \quad (5.33)$$

This is the controller structure obtained if no active damping is used and the closed loop system is designed as a first order low pass filter with bandwidth α_{vwt} . To decrease the influence of the stack current in this P-controller a low pass filtered stack current is used as a feed forward.

Transforming the controller to discrete time gives the following implementation

$$i_{\text{out,ref}}(k) = K_{\text{pvwt}}(v_{\text{WT,ref}}(k) - v_{\text{WT}}(k)) + S_{\text{vwt}}(k) - Y_{\text{awt}}v_{\text{WT}}(k) \quad (5.34)$$

$$\begin{aligned} S_{\text{vwt}}(k+1) &= S_{\text{vwt}}(k) + \\ &+ K_{\text{ivwt}} \left(v_{\text{WT,ref}}(k) - v_{\text{WT}}(k) + \frac{\hat{i}_{\text{out}}(k) - i_{\text{out,ref}}(k)}{K_{\text{pvwt}}} \right) T_s \end{aligned} \quad (5.35)$$

where $S_{\text{vwt}}(k)$ is the integration state.

5.2.4 Mode selector

The mode selector decide which mode the wind turbine should be operated in, normal (N) or voltage limitation (VL) mode. If the DC/DC converter used has an under voltage limit, then the VL-mode is divided into under voltage limitation and over voltage limitation. If the DC/DC converter can operate at zero output voltage then the VL-mode only consists of over voltage limitation. In the following, the conditions for a switch over from N-mode to VL-mode and the opposite will be treated. The description starts with the over voltage mode since this is always used and then the under voltage mode which also is needed if the DC/DC converter has an under voltage limit.

VL-mode due to over voltage

To decide when to change from N-mode to VL-mode the output voltage controller is used. It shall be remembered that the output voltage controller is still active in N-mode even if it's output is not connected. The current reference from the output voltage controller is equal to the current needed to bring the output voltage to the reference, see (5.33). The reference voltage in this case is the rated voltage of the turbine. The mode changes to VL-mode when the current reference from the output voltage controller, $i_{\text{out,ref}}$, is less then the current i_{out} . This is used as a criterion since the current i_{out} is higher then the current needed for bringing the output voltage to the reference. So if the mode is not changed this would probably lead to an output voltage higher then the reference, at least if the estimated current from the output voltage controller is correct.

When the wind turbine is in voltage limitation mode due to over voltage, it limits the power transfer, as discussed before. This means that the pitch has to reduce the incoming torque from the wind. This means that $T_{\text{reduction}}$ is less then zero, since the induction machine and the IM controllers are in motor references. The switch back from VL-mode to N-mode is done when the torque reference from the speed controller is greater then 99

% of the torque produced by the IM. This means that the power production ordered by the speed controller is less than the power production in VL-mode. A switch back will result in a decreasing output voltage, which is desired. The 99 % is introduced to obtain a suitable hysteresis, to prevent a direct switch back to VL-mode.

When the wind turbine changes mode, the controller structure of the turbine is changed in a step and this results in transients. To prevent that these transients result in that the mode is directly changed back and an oscillation between the modes start, a time delay is used that prevent the mode selector to change back the mode directly after the mode is changed. The time delay should be set so that the transients from the mode change have time to die out.

VL-mode due to under voltage

When there is an under voltage limit, as in the case with the FBIB converter, a second output voltage controller is used, which has the under voltage limit as reference. The change from N-mode to VL-mode due to under voltage is done when the current reference from the output voltage controller, $i_{out,ref}$, is greater than the current i_{out} . This is used as a criterion since the current i_{out} is lower than the current needed for bringing the output voltage to the reference. So if the mode is not changed this would probably lead to an output voltage lower than the reference, at least if the estimated current from the output voltage controller is correct. It should be remembered that to keep the output voltage up, the power transfer needs to be increased.

The increased power transfer means that the extra power needed will be taken from the kinetic energy of the turbine. This means that if the incoming power from the wind does not increase, or that the power production in the stack decreases or the voltage reference to the output voltage controller can be reduced, the turbine will decelerate and finally come to a full stop. The switch back from VL-mode to N-mode is done when the torque reference from the speed controller is less than 101 % of the torque produced by the IM. This means that the power production desired by the speed controller is greater than the power production in VL-mode. A switch back will result in an increasing output voltage, which is desired. The 101 % is again introduced to give an appropriate hysteresis, to prevent a direct switch back to VL-mode. Also here a time delay is used to prevent that the mode selector starts to jump between the modes due to the transients introduced by the change of mode.

5.2.5 Reference value calculations

In the case when the FBIB converter is used, there is a problem with that the lowest output voltage of the converter is the input voltage times the transformer turns ratio. This means that when the produced power of the wind turbine starts to decrease compared to the total production in the stack, it would be an advantage to decrease the input voltage to the FBIB

converter in order to decrease the under voltage limit of the converter. But due to the fact that the three phase converter for the IM is connected to the input of the DC/DC converter care must be taken so that the DC-link voltage is not reduced below the back-emf of the IM. If the DC-link voltage reference is put below the peak value of the line-to-line voltage of the back-emf, then the three phase converter will act as a three phase diode rectifier and the control of the IM is lost.

To prevent this, first the desired DC-link voltage, $v_{in,desired}$, is calculated. From this the flux reference is calculated so that the peak of the line-to-line stator voltage is less than the desired DC-link voltage. The DC-link voltage reference, $v_{in,ref}$, is then calculated from the estimated flux magnitude, $\hat{\psi}_R$. The voltage reference for the output voltage controller used for under voltage limitation is set to $v_{WT,ref} = v_{in,ref} N_{tr,IB} 1.2$, where $N_{tr,IB}$ is the turns ratio of the transformer and the value 1.2 is used to give a safety margin. The desired input voltage is calculated by assuming that the estimated input power times the estimated efficiency of the system is equal to the output power and that the output voltage is equal to the wanted DC-link voltage times $N_{tr,IB} 1.2$. This gives

$$v_{in,desired} = LP \left\{ \frac{\omega_r \hat{T}_{wind} \eta_{tot}}{n_p i_{stack} N_{tr,IB} 1.2} \right\} \quad (5.36)$$

where η_{tot} is the estimated efficiency and \hat{T}_{wind} is the estimated torque produced by the wind. The calculated value is low pass filtered with a bandwidth $\alpha_{v,desired}$. The desired input voltage is limited between 0 and 1 of the rated input voltage. The torque from the wind is estimated as shown in Fig. 5.11. From the figure it can be seen that the estimation

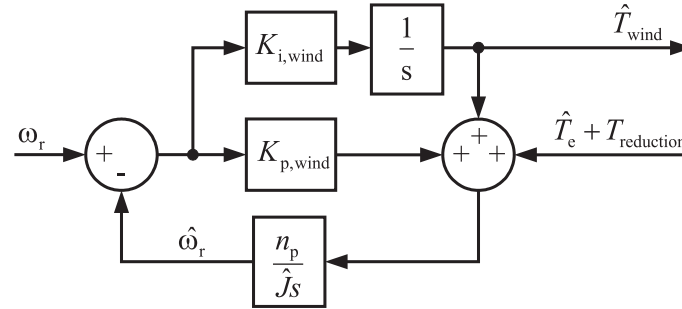


Fig. 5.11 The estimation of the torque produced by the wind.

is based on a model of the mechanical system and a speed controller. Here the disturbance for the mechanical system is the estimated breaking torque from the IM and $T_{reduction}$, and the output from the speed controller is the driving torque produced by the wind. The gains for the estimation speed controller is selected so that a double pole at α_{wind} is obtained

for the system from ω_r to $\hat{\omega}_r$. This gives that the gains should be selected as

$$K_{p,\text{wind}} = \frac{2\hat{J}\alpha_{\text{wind}}}{n_p} \quad (5.37)$$

$$K_{i,\text{wind}} = \frac{2\hat{J}\alpha_{\text{wind}}^2}{n_p}. \quad (5.38)$$

The implementation of this estimator can be done as

$$\begin{aligned} \hat{\omega}_r(k+1) &= (1 - \alpha_{\text{wind}}T_s)e^{-\alpha_{\text{wind}}T_s}\hat{\omega}_r(k) + \frac{n_p}{\hat{J}}T_se^{-\alpha_{\text{wind}}T_s}\hat{T}_{\text{wind}}(k) + \\ &+ ((\alpha_{\text{wind}}T_s - 1)e^{-\alpha_{\text{wind}}T_s} + 1)\omega_r(k) + \\ &+ \frac{n_p}{\hat{J}}T_se^{-\alpha_{\text{wind}}T_s}(\hat{T}_e(k) + T_{\text{reduction}}(k)) \end{aligned} \quad (5.39)$$

$$\begin{aligned} \hat{T}_{\text{wind}}(k+1) &= -K_{i,\text{wind}}T_se^{-\alpha_{\text{wind}}T_s}\hat{\omega}_r(k) + (1 + \alpha_{\text{wind}}T_s)e^{-\alpha_{\text{wind}}T_s}\hat{T}_{\text{wind}}(k) + \\ &+ K_{i,\text{wind}}T_se^{-\alpha_{\text{wind}}T_s}\omega_r(k) + \\ &+ ((\alpha_{\text{wind}}T_s + 1)e^{-\alpha_{\text{wind}}T_s} - 1)(\hat{T}_e(k) + T_{\text{reduction}}(k)). \end{aligned} \quad (5.40)$$

The maximum stator voltage for a given flux is approximated by $|\mathbf{v}_s|_{\text{max}} \approx \hat{\omega}_1(L_\sigma i_{s,\text{rated}} + \hat{\psi}_R)$, where the stator resistance is neglected and it is assumed that the rated current is applied in the d-direction. This gives an over estimation of the stator voltage magnitude, within the normal speed operation region of the wind turbine. From this equation the input voltage reference can be calculated as

$$v_{\text{in,ref}} = \frac{\sqrt{3}}{K}\hat{\omega}_1(L_\sigma i_{s,\text{rated}} + \hat{\psi}_R)C_{\text{pwm}} \quad (5.41)$$

where $C_{\text{pwm}} > 1$ is to add margin and to adjust the DC-link voltage reference so that rated operation of the IM gives the rated DC-link voltage. The inverse of (5.41) is used to calculate the reference flux from the desired DC-link voltage. The flux reference is limited between 1 and 0.2 of the rated flux.

5.3 Induction machine controller

The induction machine controller has the rotor flux reference $\Psi_{R,\text{ref}}$, the torque reference $T_{e,\text{ref}}$ and the converter DC current reference $i_{\text{IM,ref}}$ as inputs and the control signals to the valves C_{switches} , the estimated rotor flux $\hat{\Psi}_R$ and the estimated torque \hat{T}_e as outputs. In Fig. 5.12 the induction machine controller, the induction machine and the transistor rectifier are shown. The induction machine current controller is implemented in the rotating reference frame, orientated with the rotor flux on the d -axis. The input to the current controller is the torque reference, $T_{e,\text{ref}}$ and the rotor flux reference, $\Psi_{R,\text{ref}}$. The outputs from the current controller is the phase voltage references and the estimated torque, \hat{T}_e ,

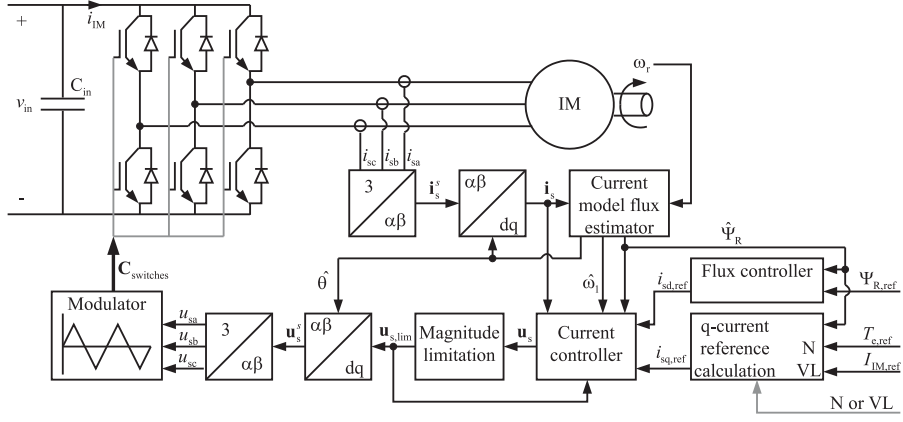


Fig. 5.12 The induction machine controller together with the induction machine system.

produced by the induction machine. To align the dq -system of the controller in the rotor flux linkage direction, a current model flux estimator is used. In [23] the design of the current controller and the current model flux estimator can be found.

For the design of the induction machine controller, the Γ -equivalent model of the induction machine is used [23]. In the rotating dq -coordinate system and with stator current \mathbf{i}_s and rotor flux Ψ_R as state variables the Γ -equivalent model can be expressed as:

$$L_\sigma \frac{d\mathbf{i}_s}{dt} = \mathbf{v}_s - (R_s + R_R + j\omega_1 L_\sigma) \mathbf{i}_s + \left(\frac{R_R}{L_M} - j\omega_r \right) \Psi_R \quad (5.42)$$

$$\frac{d\Psi_R}{dt} = R_R \mathbf{i}_s - \left(\frac{R_R}{L_M} + j\omega_2 \right) \Psi_R \quad (5.43)$$

$$\omega_2 = \omega_1 - \omega_r \quad (5.44)$$

$$T_e = \frac{3n_p}{2K^2} \text{Im}\{\Psi_R^* \mathbf{i}_s\} \quad (5.45)$$

where n_p is the pole pair number and K is the transformation constant, here $K = 1$ is used which gives amplitude invariant transformation.

5.3.1 Current model flux estimator

When deriving the current model flux estimator the rotor flux equation, (5.43), is used. It is assumed that the flux is orientated in the d -direction only and then the equation is divided into the real and imaginary as:

$$\frac{d\hat{\Psi}_R}{dt} = \hat{R}_R i_{sd} - \frac{\hat{R}_R}{\hat{L}_M} \hat{\Psi}_R \quad (5.46)$$

$$0 = \hat{R}_R i_{sq} - \hat{\omega}_2 \hat{\Psi}_R \Rightarrow \omega_1 = \omega_r + \frac{\hat{R}_R i_{sq}}{\hat{\Psi}_R} \quad (5.47)$$

$$\frac{d\theta_R}{dt} = \omega_1. \quad (5.48)$$

The flux estimator is transformed from continuous time to discrete time and the result is

$$\omega_1(k) = \omega_r(k) + \frac{\hat{R}_R i_{sq}(k)}{\hat{\Psi}_R(k)} \quad (5.49)$$

$$\theta_R(k+1) = \theta_R(k) + \omega_1(k)T_s \quad (5.50)$$

$$\hat{\Psi}_R(k+1) = \hat{\Psi}_R(k)e^{-\frac{\hat{R}_R T_s}{\hat{L}_M}} + \hat{L}_M \left(1 - e^{-\frac{\hat{R}_R T_s}{\hat{L}_M}}\right) i_{sd}(k). \quad (5.51)$$

5.3.2 Flux controller

The use of a flux controller is usually not needed in an induction motor drive. However, in this application, it is used in order to have a faster response of the rotor flux. The controller only controls the flux magnitude, since the flux is orientated in the d -axis direction. When designing the flux controller, (5.46) is used to describe the process model. The current controller is assumed to be ideal, i.e. the system from reference current to actual current is treated as a unity gain. The closed loop system from reference to actual is designed to be a first order low pass filter. This gives the following controller

$$F_\Psi(s) = \frac{\alpha_\Psi}{s} \hat{G}_\Psi^{-1}(s) = \frac{\alpha_\Psi}{s} \frac{s + \frac{\hat{R}_R}{\hat{L}_M}}{\hat{R}_R} = \frac{\alpha_\Psi}{\hat{R}_R} + \frac{\alpha_\Psi}{\hat{L}_M} \frac{1}{s} = K_{p\Psi} + K_{i\Psi} \frac{1}{s} \quad (5.52)$$

where α_Ψ is the bandwidth of the flux controller. Transforming the controller to discrete time and adding anti windup of the integrator gives the following implementation expressions,

$$i_{sd,ref}(k) = K_{p\Psi}(\Psi_{R,ref}(k) - \hat{\Psi}_R(k)) + S_\Psi(k) \quad (5.53)$$

$$S_\Psi(k+1) = S_\Psi(k) + K_{i\Psi} \left(\Psi_{R,ref}(k) - \hat{\Psi}_R(k) + \frac{i_{sd,lim} - i_{sd,ref}}{K_{p\Psi}} \right) T_s. \quad (5.54)$$

where $i_{sd,lim}$ is the limited d -current.

5.3.3 Current controller

From Fig. 5.12 it can be seen that the input to the current controller is the reference currents in d - and q -direction. The d -current reference comes from the flux controller and the q -current reference is either calculated from the torque reference originating from the speed controller or coming from the reference obtained by the DC-link voltage controller. This depends on which mode the wind turbine is operated in. In normal operation the q -current reference can be calculated from the torque reference with (5.45). Assuming that the flux is only directed in the d -direction the torque equation becomes

$$T_e = \frac{3n_p}{2K^2} \text{Im}\{\Psi_R \mathbf{i}_s\} \Rightarrow i_{sq,ref} = \frac{2K^2 T_{e,ref}}{3n_p \hat{\Psi}_R}. \quad (5.55)$$

In voltage limitation mode the q -current reference is calculated from $i_{IM,ref}$ by assuming that the power taken from the DC-link is equal to the mechanical power produced by the induction machine. This assumption gives

$$T_e \omega_r = \frac{3n_p}{2K^2} \text{Im}\{\Psi_R \mathbf{i}_s\} \omega_r = i_{IM} v_{in} \Rightarrow i_{sq,ref} = \frac{2K^2}{3n_p} \frac{i_{IM,ref} v_{in}}{\hat{\Psi}_R \omega_r}. \quad (5.56)$$

Before the d - and q -current references are used, they are limited to be within the ratings of the induction machine and the converter. This is done in two steps, first the magnitude of the two components are limited and then the magnitude of the current vector is limited to the rating of the machine and converter. The magnitude is limited by reducing the d -component if it is too high. In this way the generator can always produce the maximum power and the space that is left can be used to change the flux in the induction generator. It is the limited current references that are used for the antiwindup in the controllers that are in the outer control loop. In Fig. 5.13 these limitations are shown together with the current controller and the model of the induction machine used for the design of the controller. When calculating the limited dc-current $I_{IM,lim}$ from the limited q -current (5.56) is used.

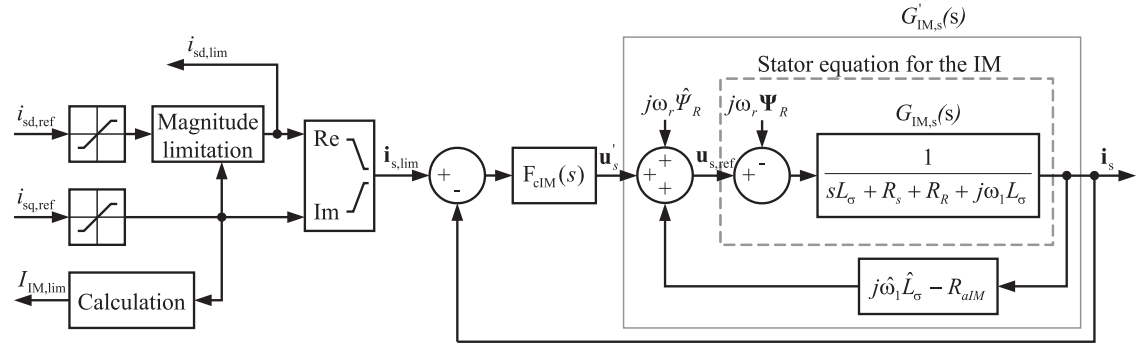


Fig. 5.13 The current controller for the induction machine and the induction machine model used for the controller design.

When designing the current controller, the stator equation of the induction machine (5.42) is used. In this equation, the term R_R/L_M is neglected, since it in this wind turbine application is much smaller than ω_r . The resulting process model $G_{IM,s}(s)$ from stator voltage to stator current is shown in Fig. 5.13. To reduce the effects of the cross coupling between the d and q currents and of the back-emf, a feed forward of estimations of these are used. In this feed forward an active damping resistor R_{aIM} is also added. The stator voltage reference $\mathbf{u}_{s,ref}$ is calculated as the output voltage from the current controller, \mathbf{u}'_s , plus the feed forward term,

$$\mathbf{u}_{s,ref} = \mathbf{u}'_s + (j\hat{\omega}_1 \hat{L}_\sigma + R_{aIM}) \mathbf{i}_s + j\omega_r \hat{\Psi}_R. \quad (5.57)$$

where \hat{x} is the estimation of the quantity x . If it is assumed that the feed forward is perfect the back-emf and the cross coupling is cancelled and the process to control becomes

$$G'_{\text{IM},s}(s) = \frac{1}{sL_\sigma + R_R + R_s + R_{\text{aIM}}}. \quad (5.58)$$

For this system the current controller is designed so that the closed loop system becomes a first order low pass filter with a bandwidth α_{cIM} . The controller can be calculated as

$$\begin{aligned} F_{\text{cIM}}(s) &= \frac{\alpha_{\text{cIM}}}{s} G'_{\text{IM},s}{}^{-1}(s) = \frac{\alpha_{\text{cIM}}}{s} (sL_\sigma + R_R + R_s + R_{\text{aIM}}) = \\ &= \alpha_{\text{cIM}}L_\sigma + \frac{\alpha_{\text{cIM}}(R_R + R_s + R_{\text{aIM}})}{s} = K_{\text{pcIM}} + \frac{K_{\text{icIM}}}{s}. \end{aligned} \quad (5.59)$$

Separating the controller into the d - and q -components, adding antiwindup of the integrator and transform it into discrete time the controller can be implemented as

$$\begin{aligned} u_{\text{sd,ref}}(k) &= K_{\text{pcIM}}(i_{\text{sd,ref}}(k) - i_{\text{sd}}(k)) + S_{\text{dIM}}(k) - R_{\text{aIM}}i_{\text{sd}}(k) + \\ &\quad - \hat{\omega}_1 \hat{L}_\sigma i_{\text{sq}}(k) \end{aligned} \quad (5.60)$$

$$\begin{aligned} u_{\text{sq,ref}}(k) &= K_{\text{pcIM}}(i_{\text{sq,ref}}(k) - i_{\text{sq}}(k)) + S_{\text{qIM}}(k) - R_{\text{aIM}}i_{\text{sq}}(k) + \\ &\quad + \hat{\omega}_1 \hat{L}_\sigma i_{\text{sd}}(k) + \omega_r \hat{\Psi}_R \end{aligned} \quad (5.61)$$

$$\begin{aligned} S_{\text{dIM}}(k+1) &= S_{\text{dIM}}(k) + \\ &\quad + K_{\text{icIM}} \left(i_{\text{sd,ref}}(k) - i_{\text{sd}}(k) + \frac{u_{\text{sd,ref}} - u_{\text{sd,lim}}}{K_{\text{pcIM}}} \right) T_s \end{aligned} \quad (5.62)$$

$$\begin{aligned} S_{\text{qIM}}(k+1) &= S_{\text{qIM}}(k) + \\ &\quad + K_{\text{icIM}} \left(i_{\text{sq,ref}}(k) - i_{\text{sq}}(k) + \frac{u_{\text{sq,ref}} - u_{\text{sq,lim}}}{K_{\text{pcIM}}} \right) T_s \end{aligned} \quad (5.63)$$

where $u_{\text{sd,lim}}$ and $u_{\text{sq,lim}}$ are the limited voltage references. The active damping is selected so that the process $G'_{\text{IM},s}(s)$ has the same bandwidth as the current controller α_{cIM} . The active damping can be calculated as

$$R_{\text{aIM}} = \alpha_{\text{cIM}}L_\sigma - R_R - R_s. \quad (5.64)$$

5.3.4 Modulator and the three phase converter

The voltage reference from the current controller should be realized by the converter. This is done by switching the valves on and off and thereby producing the right average voltage to the machine. The on and off signals to the valves are obtained by triangle wave modulation. The duty cycle for each phase is compared with a triangular wave. If the reference value is greater then the carrier wave the top switch is on, otherwise the lower

switch is on. The duty cycles for the phases are calculated as

$$\Delta = \frac{\max\{u_{sa}, u_{sb}, u_{sc}\} + \min\{u_{sa}, u_{sb}, u_{sc}\}}{2} \quad (5.65)$$

$$D_{sa} = \frac{2(u_{sa} - \Delta)}{V_{in}} \quad (5.66)$$

$$D_{sb} = \frac{2(u_{sb} - \Delta)}{V_{in}} \quad (5.67)$$

$$D_{sc} = \frac{2(u_{sc} - \Delta)}{V_{in}} \quad (5.68)$$

$$(5.69)$$

where Δ is a zero-sequence voltage subtracted from the phase voltage in order to utilize the converter better. In this way the converter can produce approximately 15 % more voltage than compared to the case without the zero-sequence voltage for the same DC-voltage. In the case with zero-sequence voltage addition, the maximum voltage the converter can produce is that the peak value of the line-to-line voltage is equal to the DC-voltage. This gives that the maximum length of the voltage vector the converter can produce is

$$\max\{|\mathbf{u}_s|\} = \frac{KV_{in}}{\sqrt{3}} \quad (5.70)$$

and it is to this value the length is limited to in the "Magnitude limitation" block in Fig. 5.12.

5.4 Current controller for the FBIB Converter

The current controller for the FBIB converter is a PI controller with antiwindup of the integrator and it is implemented as shown in Fig. 5.14. In the figure, the model of the process used for the controller design is also shown. When designing the current con-

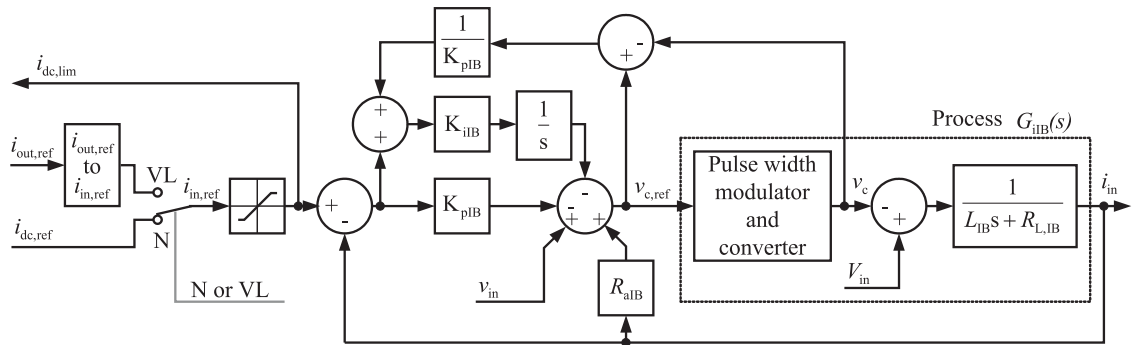


Fig. 5.14 The FBIB converter current controller and the model of the process used for the design of the current controller.

troller, the pulse width modulator and the converter are together treated as a unity gain. The input voltage to the FBIB converter is treated as a slowly varying disturbance, which is compensated for through feed forwarding of the measured voltage. The current controller is designed so that the closed loop system becomes a first order low pass filter with unity gain and with a bandwidth α_{iIB} . The controller gains should then be selected as $K_{pIB} = \alpha_{iIB}L_{IB}$ and $K_{iIB} = \alpha_{iIB}R_{L,IB}$. The active damping resistance is selected so that the process $G'_{iIB}(s) = 1/(L_{IB}s + R_{L,IB} + R_{aIB})$ has the same bandwidth as the current controller. The active damping resistance can be calculated as:

$$R_{aIB} = \alpha_{iIB}L_{IB} - R_{L,IB}. \quad (5.71)$$

Transforming the controller to discrete time gives the following implementation of the current controller for the FBIB converter

$$v_{c,ref}(k) = v_{in}(k) + R_{aIB}i_{in}(k) - K_{pIB}(i_{in,ref}(k) - i_{in}(k)) - S_{IB}(k) \quad (5.72)$$

$$S_{IB}(k+1) = S_{IB}(k) + K_{iIB} \left(i_{in,ref}(k) - i_{in}(k) + \frac{v_{c,ref}(k) - v_c(k)}{K_{pIB}} \right) T_s. \quad (5.73)$$

The calculation of the input current reference from the output voltage reference is done by assuming a lossless converter and then setting the input power equal to the output power. By this the following relation can be obtained,

$$i_{in,ref} = \frac{v_{WT}}{v_{in}} i_{out,ref}. \quad (5.74)$$

5.5 Controllers for the FBPS Converter

5.5.1 Current controller

The current controller for the FBPS converter is a PI controller with antiwindup of the integrator and it is implemented as shown in Fig. 5.15. In the figure the model of the process used for the controller design is also shown. When designing the current controller, the pulse width modulator and the converter are together treated as a unity gain. The output voltage of the FBPS converter is treated as a slowly varying disturbance, which is compensated for through feed forwarding of the measured voltage. The current controller is designed so that the closed loop system becomes a first order low pass filter with unity gain and with a bandwidth α_{iPS} . The controller gains should then be selected as $K_{pPS} = \alpha_{iPS}L_{PS}$ and $K_{iPS} = \alpha_{iPS}R_{L,PS}$. The active damping resistance is selected so that the process $G'_{iPS}(s) = 1/(L_{PS}s + R_{L,PS} + R_{aPS})$ has the same bandwidth as the current controller. The active damping resistance can be calculated as:

$$R_{aPS} = \alpha_{iPS}L_{PS} - R_{L,PS}. \quad (5.75)$$

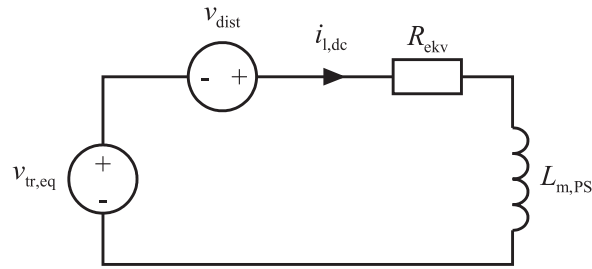


Fig. 5.16 Simple equivalent circuit for the transformer DC-current with additives.

The unbalance current can be found as

$$i_{1,\text{dc}} = \text{LP} \left\{ \frac{i_1(k) + i_1(k-1)}{2} \right\}. \quad (5.79)$$

It is now possible to formulate a regulator for $i_{1,\text{dc}}$ using the same regulator design method previously used in this chapter, with a desired bandwidth, $\alpha_{\text{tr,eq}}$.

To avoid that steps in $v_{c,\text{ref}}$ also creates a DC-offset in the transformer flux, the technique described in [13] can be used. This is based on that when a change in the voltage reference comes, first only half of the change is made and then during the next half period, the last half of the change is made. This method is implemented in the test set-up and the results can be observed in the measurement section. Assuming that the converter is operating in steady-state and the flux is centered around zero, then a voltage reference step is made. The first half period after the step the voltage reference is increased by the half of the change in voltage reference. This means that the flux peak value is changed from the steady-state value to the new peak value. The next half period the last half of the change is added and the flux goes between plus and minus the new peak value.

An alternative solution for the removal of the dc-component is to place a capacitor between one leg and the transformer.

Chapter 6

Park design considerations for the series DC farm

6.1 Simulation setup

The performance of the wind farm, wind turbines and the controllers has been evaluated using the simulation program PSCAD/EMTDC [62]. The test scheme used for the evaluation of the series DC wind farm system and the wind turbine for series-connection is shown in Fig. 6.1. As can be noted in the figure, only three wind turbines are connected

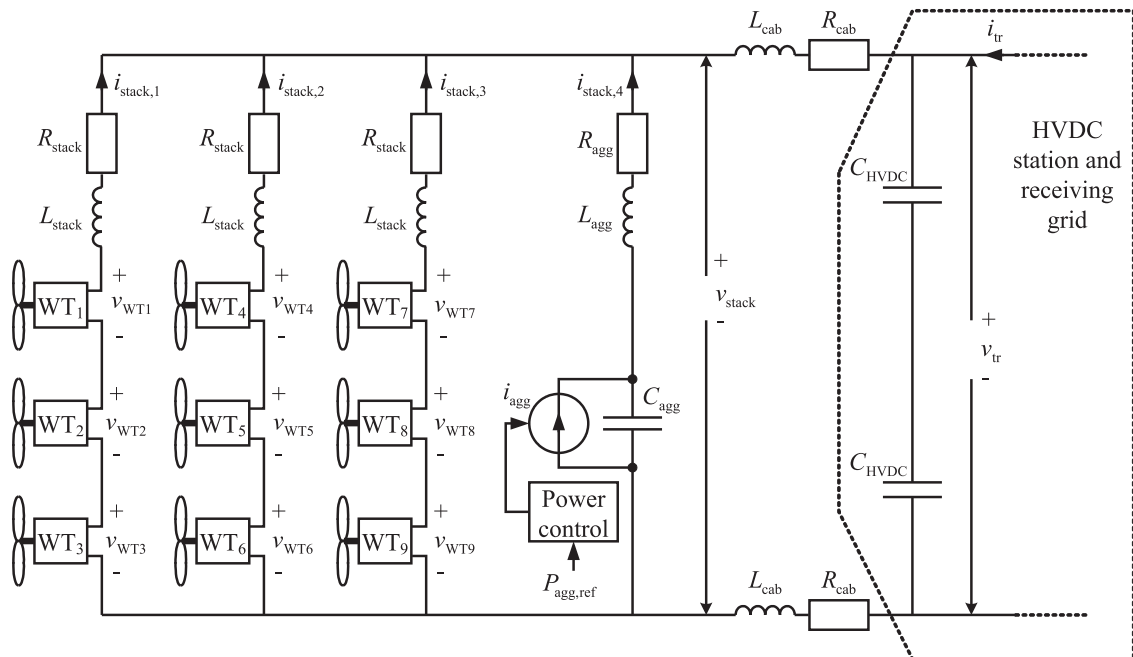


Fig. 6.1 Test scheme for evaluation of the performance of the series DC wind farm system and the wind turbine for series-connection.

in series and three stacks of turbines are in parallel. The low number of wind turbines in series is chosen to enable a clearer presentation of the results, although three turbines are far too few for a practical installation.

For this case study, the rated power of the turbines is selected to be 2 MW and the rated power of the wind farm is 36 MW. The current source i_{agg} together with C_{agg} , L_{agg} and R_{agg} represents an aggregated model of three stacks with three series connected wind turbines. The current source is controlled to produce the aggregated power of these 9 turbines. The current is limited to be maximum 3 times the rated output current of the wind turbine. The parameters of this aggregated model are selected as

$$C_{agg} = C_{out} \quad (6.1)$$

$$L_{agg} = \frac{L_{stack}}{3} \quad (6.2)$$

$$R_{agg} = \frac{R_{stack}}{3}. \quad (6.3)$$

The transmission voltage is selected to be 45 kV, which gives a nominal output voltage of 15 kV for the wind turbines and a rated current of 133 A. This gives a rated transmission current of 800 A. Therefore, a transmission cable with a cross section area of 500 mm² is selected. The resistance of this cable is approximately 0.044 Ω/km (per cable). It is assumed that these cables are put besides each other, which results in an inductance of approximately 0.34 mH/km (per cable). As mention before, the cable capacitance is here not considered, since the capacitance in the HVDC station and in the wind turbines are larger. In this case study the transmission distance is selected to be 20 km and this results in

$$L_{cab} = 0.34 \cdot 10^{-3} \cdot 20 = 6.8 \text{ mH} \quad (6.4)$$

$$R_{cab} = 0.044 \cdot 20 = 0.88 \text{ } \Omega. \quad (6.5)$$

For the cables connecting the wind turbines to the transmission cable, a cross section of 70 mm² is used. The impedance of the stack depends on the cable routes and on the stray inductances and resistances in the wind turbines. The parameters of the stack impedance has been estimated to $L_{stack} = 2 \text{ mH}$ and $R_{stack} = 0.7\Omega$, based on the length of the stack cable.

6.1.1 The HVDC-station and the transmission system

For the parameters of the HVDC-station, it is assumed that the grid has a short circuit power equal to 10 times the rated power of the wind farm, which gives $K_{sc} = 10$. It is also assumed that the XR-ratio, K_{xr} , of the grid is 5. With a rated power of 36 MW and a DC-transmission voltage of 45 kV, the system parameters for the HVDC-station and the

grid can be calculated as

$$v_{g,l-1} = \frac{v_{tr,rated}}{\sqrt{2}} 0.8 = 26 \text{ kV} \quad (6.6)$$

$$R_g = \frac{v_{g,l-1}^2}{\sqrt{K_{xr}^2 + 1} K_{sc} P_{rated}} = 0.37 \ \Omega \quad (6.7)$$

$$L_g = \frac{K_{xr} R_g}{2\pi 50} = 5.9 \text{ mH} \quad (6.8)$$

$$L_{HVDC} = 0.14 \frac{v_{g,l-1}^2}{2\pi 50 P_{rated}} = 8.4 \text{ mH} \quad (6.9)$$

$$R_{HVDC} = 0.02 \frac{v_{g,l-1}^2}{P_{rated}} = 0.38 \ \Omega \quad (6.10)$$

$$C_{HVDC} = 2 \cdot 10^{-3} \frac{2P_{rated}}{v_{tr,rated}^2} = 71 \ \mu\text{F}. \quad (6.11)$$

The switching frequency for the HVDC-station is selected to 2 kHz [60] and the sampling frequency to 4 kHz. The bandwidth of the PLL in the HVDC-station is set to $\alpha_{PLL} = 2\pi \text{ rad/s}$. This choice was made in order to obtain a good suppression of disturbances; as an example, this gives an attenuation in the angle estimation of 34 dB for the negative sequence voltage [38].

When selecting the bandwidth of the controllers for the HVDC-station, the DC-transmission system needs to be considered. This necessity occurs since the cable inductance, together with the capacitances of the station and the wind turbines, forms a resonance circuit. The controllers must be designed so that this resonance will not be triggered. Furthermore, the controllers can be used to provide additional damping at these frequencies. Assuming that all stacks can be modelled as a single equivalent one and modelling the HVDC-station as a capacitor and a current source, the system can be simplified down to the system shown in Fig.6.2. The equivalent parameters of this model are, $C_1 = C_{HVDC}/2 = 35.5 \ \mu\text{F}$, $C_2 = C_{out}9/3 = 210 \ \mu\text{F}$, $R_{tot} = 2R_{cab} + R_{stack}/9 = 1.84 \ \Omega$ and $L_{tot} = 2L_{cab} + L_{stack}/9 = 13.8 \text{ mH}$. The transfer function from the two currents to

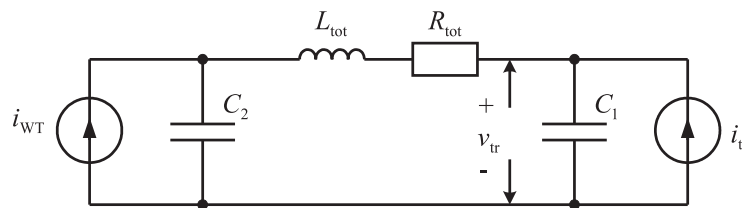


Fig. 6.2 The simplified system of the wind turbines, the transmission cables and the HVDC-station.

the transmission voltage can be expressed as

$$v_{tr}(s) = \frac{\left(L_{tot}s^2 + R_{tot}s + \frac{1}{C_2}\right) i_{tr}(s) + \frac{1}{C_2} i_{WT}(s)}{C_1s \left(L_{tot}s^2 + R_{tot}s + \frac{1}{C_p}\right)} \quad (6.12)$$

$$C_p = \frac{C_1C_2}{C_1 + C_2}. \quad (6.13)$$

From (6.12) it can be seen that there is a resonance at $f = 1/(2\pi\sqrt{C_pL_{tot}}) = 246$ Hz. Due to this resonance, the bandwidth of the AC-current controller is selected to be $\alpha_{cHVDC} = 2\pi 800 = 5000$ rad/s. The selection is such that it can act reasonable at the resonance frequency. The DC-transmission controller is in cascade with the current controller and for a cascade system the rule of thumb is that the outer controller should be a decade slower than the inner one [23]. For this case, this means that the controller bandwidth should be selected to 80 Hz. But this is too close to the resonance, the DC-transmission controller will see the resonance and act on it. To prevent this, the DC-transmission controller bandwidth is selected to a decade below the resonance, $\alpha_{vdc} = 150$ rad/s. Due to this, the influence of the cable impedance can be neglected when calculating the DC-transmission controller. This gives that the capacitance used when calculating of the controller gains is $C_1 + C_2 = C_{ekv}$.

In Fig. 6.3, the overall performance of the HVDC-station is shown. For this simulation, the 9 wind turbines are operated with a constant input torque of half the rated torque and the speed reference is equal to rated speed. This gives that the wind turbines are producing half of rated power. At 0.2 s, a step up to 5 MVar in the reference reactive power is made and this is kept for the rest of the simulation. At 0.25 s, the reference DC-transmission voltage is stepped up from 45 kV to 50 kV and at 0.35 s it is stepped down again. At 0.45 s, the aggregated power reference is stepped from zero to 18 MW and at 0.55 s it is stepped down to 9 MW. The grid frequency is set to be constant at 50 Hz throughout the simulation. From the figure it can be seen that the overall performance of the HVDC-station is good. In Fig. 6.3 it can be seen that a step of half the rated power results in a 9 % overshoot in the transmission voltage, while a step decrease of a fourth of the rated power results in a undershoot of 4 %. It is important to stress, that in an actual wind farm such power variations occur in a time scale of tens of seconds (except for an emergency case). Accordingly, the dc-voltage control will work completely satisfactory in a standard, normal operation case. The step functions used here, have been used in order to "heavily" test the dynamic performance of the system. From the figure it can also be noticed that the stack voltage is slightly higher than the transmission voltage at the station. This is due to the voltage drop over the transmission cables.

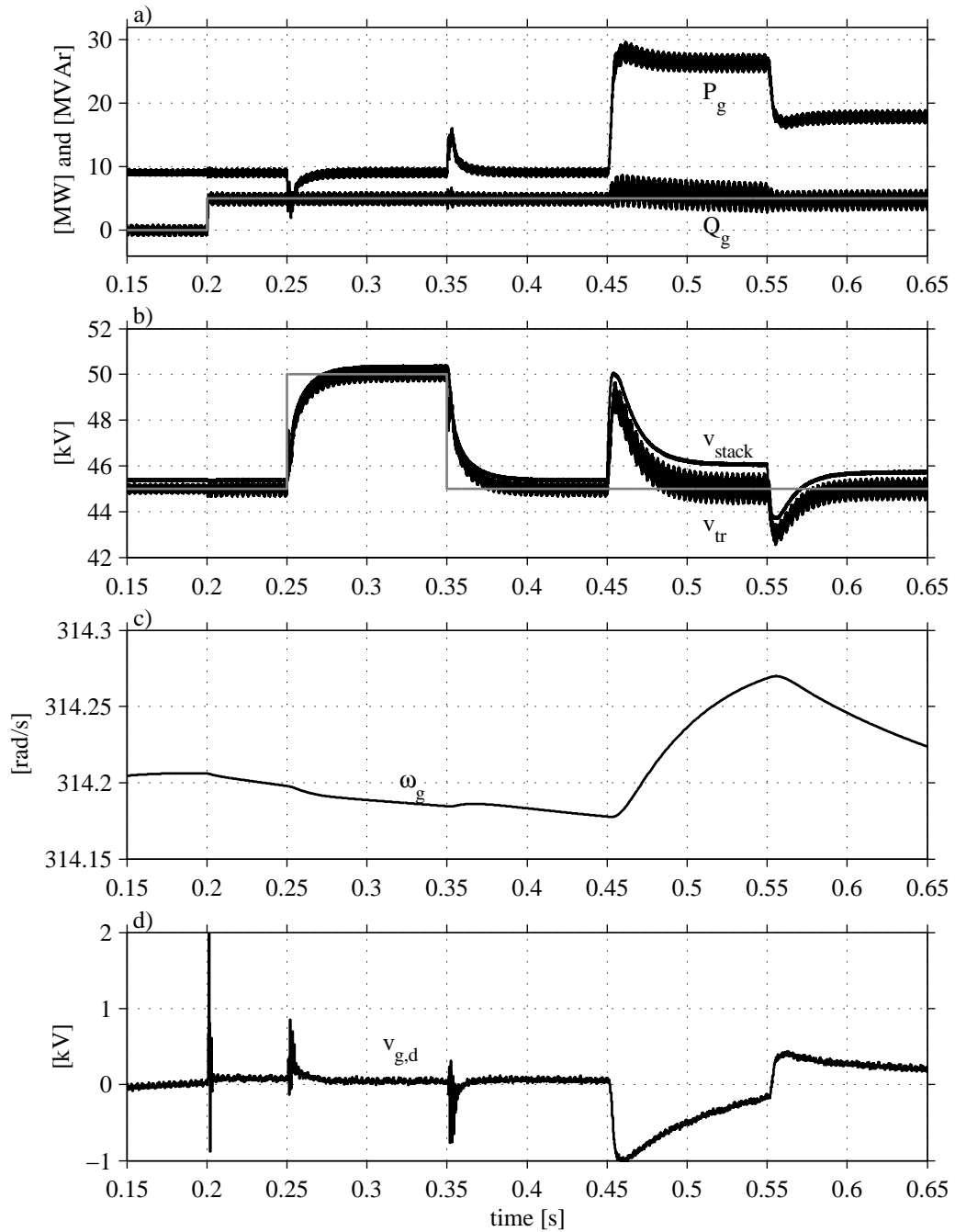


Fig. 6.3 The overall performance of the HVDC-station. a) The active, reactive power and reactive power reference as grey. b) The transmission voltage, stack voltage and the transmission voltage reference as grey. c) The estimated grid frequency. d) The estimated grid voltage in d-direction.

The impact of the slow PLL can be seen in Fig. 6.3 d) at the aggregated power steps. The change of power production affects the angle of the voltage in the PCC and due to the slow PLL it takes some time to track the new angle. The error in the estimated angle can also be seen in the reactive power production at 0.45 s. Since the reactive power production is done in an open loop manner, the estimation error results in a reactive power production that is different than the reference. However, as a conclusion regarding the bandwidth of the PLL, it was found that also using this slow PLL, the performance was found to be satisfactory.

In Fig. 6.4, the performance of the AC-current controller for the HVDC-station when stepping the reactive power, is shown. From plot a) it can be seen that the current has a rise time around what can be expected for a controller with this bandwidth and there is a damped oscillation. The oscillation is due to the fact that the current step affects the voltage in the PCC, which in turn affects the current. In plot b) it can be seen that the estimated voltage in the PCC is affected by the current step.

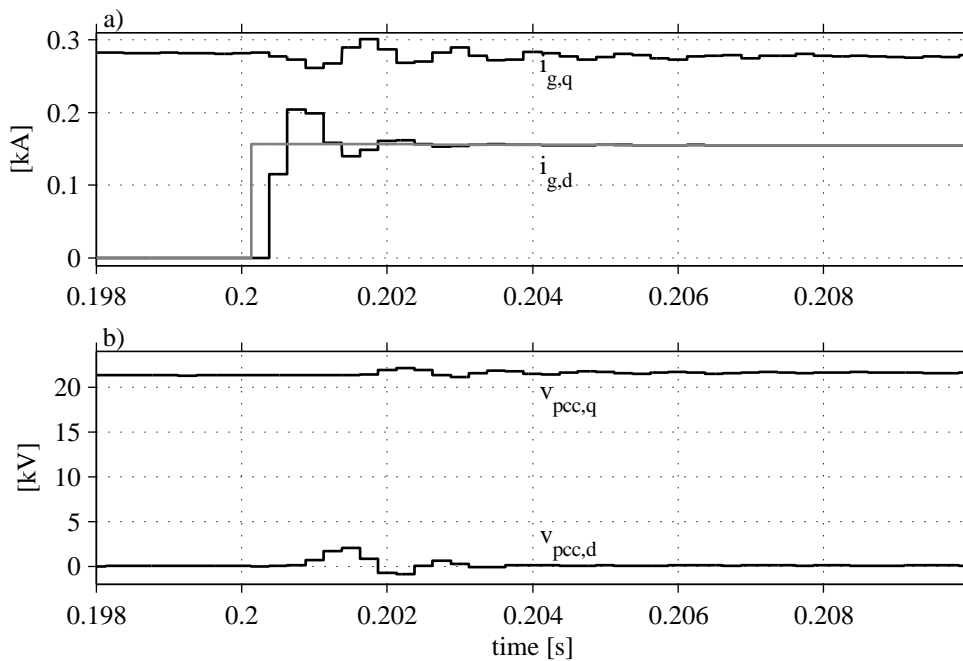


Fig. 6.4 The performance of the AC-current controller for the HVDC-station, shown for the step in reactive power. a) The d -current, q -current and the d -current reference as grey. b) The estimated grid voltage components in PCC.

In Fig. 6.5, the performance of the DC-transmission controller is demonstrated for an applied reference voltage step, (plots a) and b)) and for the case when a step in the aggregated power is applied (plots c) and d)). This step correspond to an increase in wind for other turbines in the park. From plot b) it can be noticed that when the step in the reference voltage is applied, there is a transient in the q -current reference. The reason for this transient is that when the q -current step comes, this current only charges the

HVDC-station capacitor and therefore the voltage at the station, v_{tr} , increases rapidly. The DC-transmission controller reacts to this rapid change and decreases the current reference again. At this point, the voltage at the station is greater than the stack voltage, which results in a decrease of the cable current and the capacitors in the wind turbines are charged, which leads to that the stack voltage starts to increase. The same response is obtained when the DC-transmission voltage reference is stepped down.

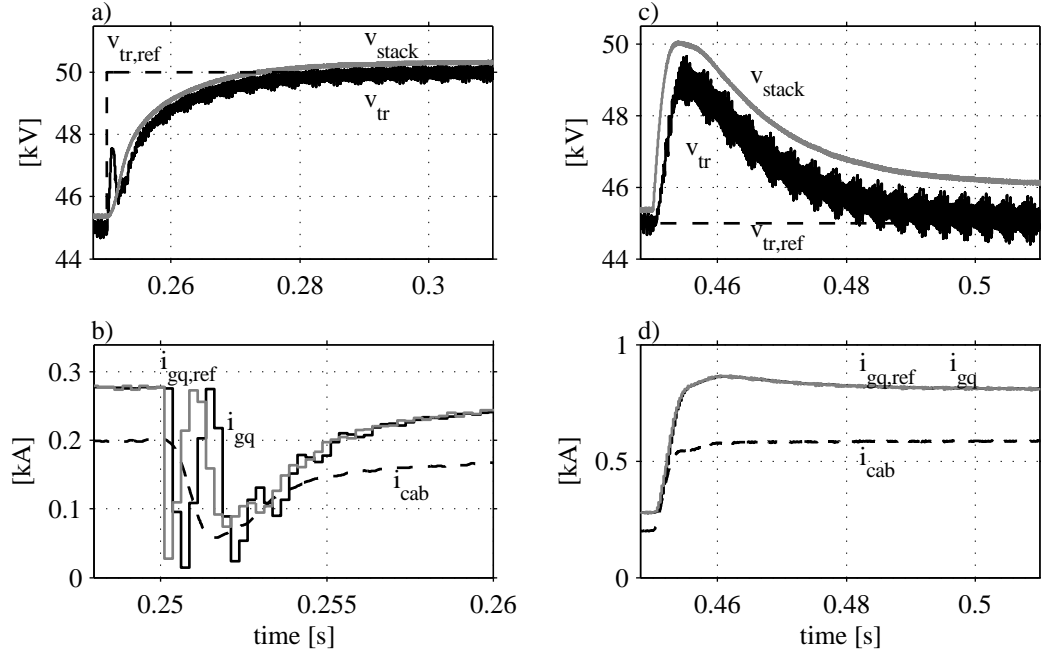


Fig. 6.5 The performance of the DC-transmission controller for the HVDC-station, a) and b) shown for the step in DC-transmission voltage reference and c) and d) for the step in aggregated power reference. a) and c) The DC-transmission voltage (black), stack voltage (grey) and the DC-transmission voltage reference (black dashed). b) and d) The q-current (black), cable current (black dashed) and q-current reference (grey).

When the step in the aggregated power reference is done, Figs. 6.5 c) and d), it can be seen that the response of the current is much smoother compared to the case with the reference voltage step.

6.1.2 The wind turbine unit

The selection of the controller bandwidths of the wind turbine is much more straightforward than for the HVDC-station. This means that no pure step response curves for the various controllers will be shown here. The switching frequency of the three phase rectifier and of the DC/DC converter is selected to be 5 kHz and the sampling frequency to 10 kHz. The bandwidths of the current controllers, α_{cIM} , α_{iIB} and α_{iPS} , are selected to be 3000 rad/s, approximately a decade lower than the switching frequency. The voltage

controller (DC-link and output) bandwidths, α_{vdc} and α_{vwt} , are selected to be equal to the DC-transmission controller bandwidth, 150 rad/s. This is 20 times lower than for the current controllers and in this way the current controller dynamics can be neglected when designing the voltage controllers, as has been done in this thesis.

The bandwidth of the speed controller, α_{ω} , is selected to 1.5 rad/s. The selection of 1.5 rad/s is quicker than the values suggested in [56]. However, in order to be on the "safe side", in this investigation a quicker value was chosen. The bandwidth of the estimation of the torque from the wind is set to 20 rad/s and the bandwidth of the low-pass filter for the desired input voltage for the DC/DC converter, $\alpha_{v,desired}$, is set to the same bandwidth. The flux controller bandwidth, α_{ψ} , is set to 100 rad/s, in order for the flux to be able to track the desired input voltage.

The parameters of the wind turbine unit can be found in Appendix A. For these data and with the controller settings discussed in this chapter, the controllers were tested with steps and ramps and the performances were close to ideal.

As mentioned before, the pitch system and the overall control of the wind turbine is not implemented in the simulation model. With overall control means the optimum power tracker that provides the pitch and speed reference. Instead of modelling these systems and modelling the wind, measurements from a variable speed wind turbine are used. The inputs T_{wind} and $\omega_{r,ref}$, to the wind turbines are taken from the measurements. The data series used are shown in Fig. 6.6. The last minutes of the measurements are slightly modified in order to obtain a fit between the last data point and the first, so that a circular data series is achieved. In this way, different starting times can be used to create different input signals to the wind turbines, and still a one hour simulation can be performed.

6.2 Analysis of a small wind farm

For this simulation, the measurements presented in Fig. 6.6, are used as inputs to the wind turbines. The rated voltage of the turbines is set to 1.41 of the nominal voltage, i.e. to 21.1 kV. The starting times were selected randomly for wind turbines 1 to 6. For stack 2, all wind turbines are operated within the limits. For stack 3, the idea was that in the beginning of the simulation, wind turbines 7 and 9 should be in overvoltage limitation mode and wind turbine 8 in undervoltage limitation mode. For the inputs of wind turbine 8, this could be achieved by selecting the starting time with the lowest wind torque and subtracting 0.15 p.u. from the wind torque and adding 0.08 p.u. to the speed reference. For wind turbines 7 and 9, starting times resulting in rated operation were selected. In the simulation, the aggregated power source is at 9 s ramped up to full power in 1 s and at 15.5 s it is ramped down to zero in 1 s. The reason for this selection is to give a more realistic disturbance than the steps used previously. However, these disturbances are still very quick for a normal operating situation. In Fig. 6.7, the output voltage for wind turbines 7, 8 and 9 for the one hour simulation, are shown. All voltages are expressed in

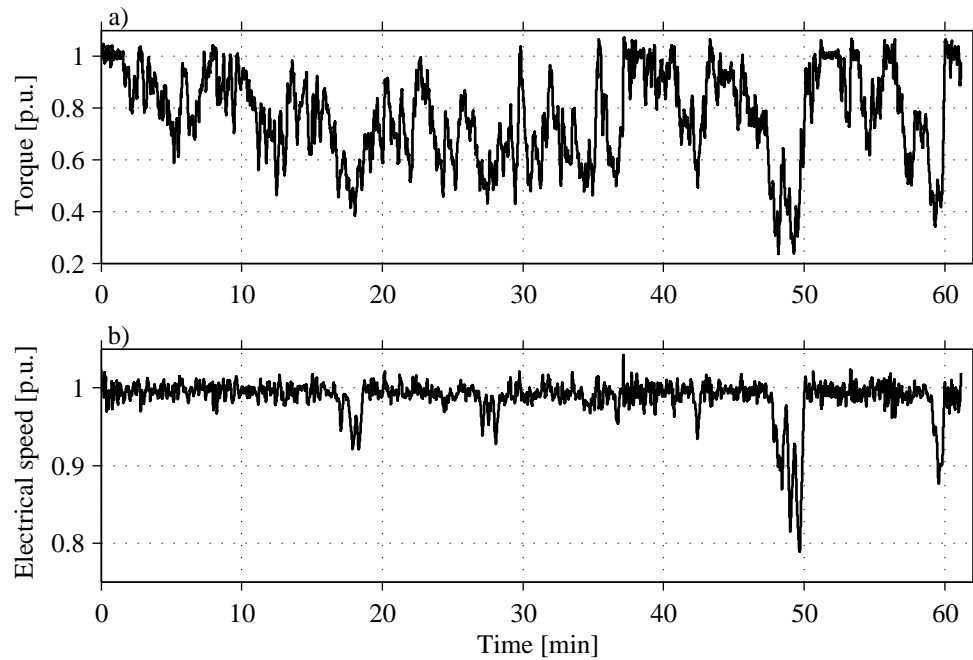


Fig. 6.6 a) Measured torque used as the torque produced by the wind in the simulations. The torque is in p.u. of rated torque. b) Measured speed of the wind turbine, used as the speed reference in the simulations. The speed is shown in p.u. of rated speed.

p.u. of the nominal voltage i.e. 15 kV. In the figure, the output voltage reference is also shown as a grey line when the wind turbine is in VL-mode. When the wind turbine is in N-mode the reference is not shown. From the figure it can be noticed that the turbines more often switch to VL-mode due to overvoltage than due to undervoltage. The case with VL-mode due to undervoltage is more severe for the wind turbine system than the case due to overvoltage. This is the case since the undervoltage case arises from a too low input power, and the extra power needed is taken from the kinetic energy of the rotor. In this case, the rotor starts to decelerate and this leads to a full stop of the turbine, if the input power does not increase or the flux in the machine can be reduced further. The VL-mode due to overvoltage arises from a too high input power, which can be decreased by the pitch system. Thus, from the wind turbine point of view, it does not matter so much that it is operated in VL-mode due to overvoltage more frequently than due to undervoltage. But from the wind farm point of view, the VL-mode due to overvoltage means that the energy production is decreased.

In Fig. 6.8, the first 18 s of the simulation in Fig. 6.7 is shown, for a more detailed view of the performance of the series-connected wind turbines. Moreover, Fig. 6.9 shows the stack voltage, stack currents as well as the total power for the same occasion. From Fig. 6.8 it can be seen that wind turbine 7 is in VL-mode between 3 and 10 s, approximately. Wind turbine 8 is in VL-mode between 3 and 9 s, approximately. Wind turbine 9 is in VL-mode two times, between 1.5 and 8.5 s and between 10.5 and 15 s, approximately. From Fig. 6.8

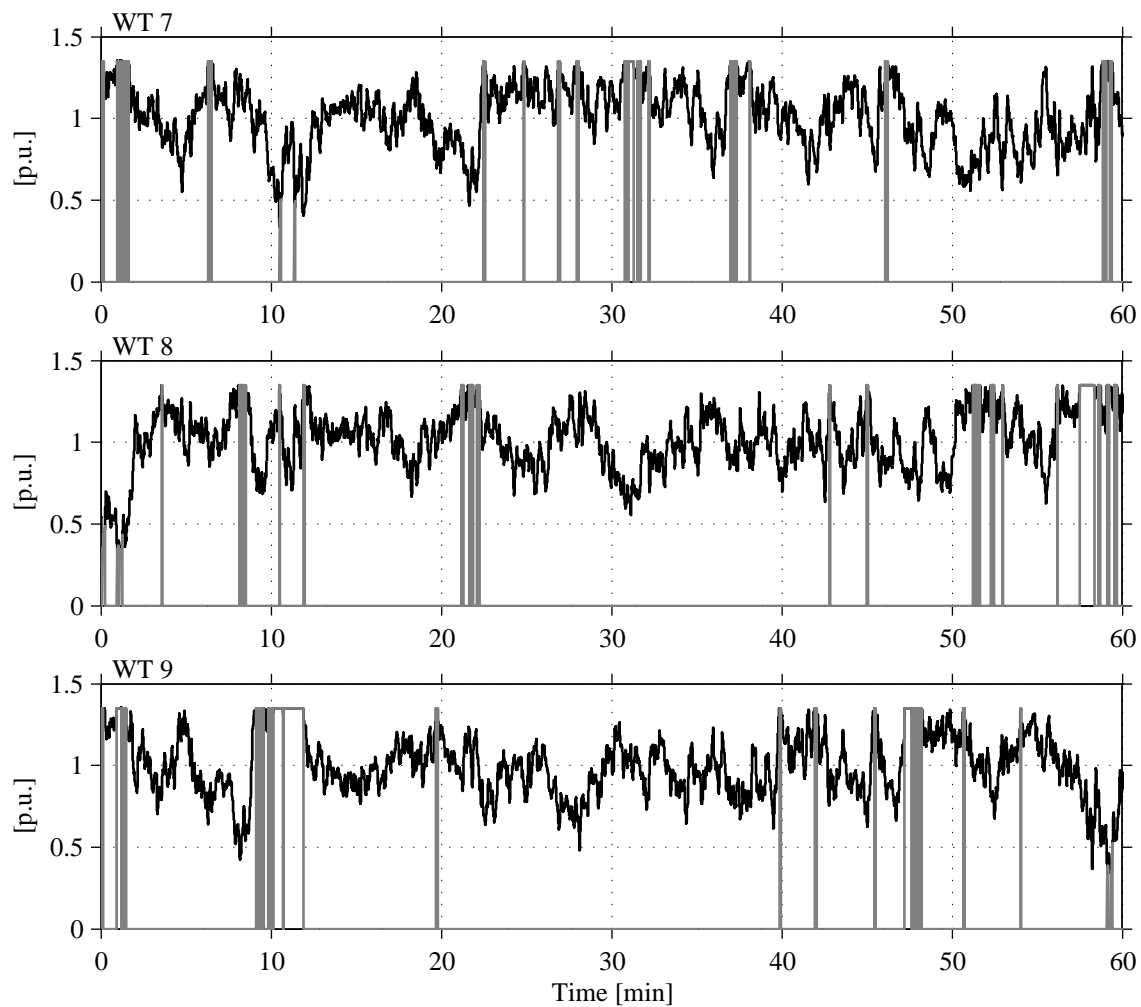


Fig. 6.7 The output voltage of wind turbines 7, 8 and 9 in p.u. of the nominal voltage of the wind turbine for the one hour simulation. The output voltage reference is shown as a grey line when the wind turbine is in voltage limitation mode, when the wind turbine is in normal operation the reference is not shown.

it can be seen that the output voltage controllers manage to keep the references, except for wind turbine 9, where the output voltage is below the reference between 6 and 8 s. This is due to the fact that all wind turbines are in VL-mode and wind turbine 8 increases its output voltage. The stack voltage is constant, as can be seen in Fig. 6.9 a). Therefore, if one voltage increases at least one must decrease. From Fig. 6.9 b) it can be seen that the stack current, for the investigated stack, increases during this time, due to the fact that the integrator in the output voltage controller of wind turbine 9 is increasing due to the voltage error. During this time, the output voltage controllers are fighting with each other and the result is an increasing stack current. But this higher stack current results in that wind turbine 9 changes to N-mode and the fight is over.

The switching between the modes can be seen as small transients in the stack current

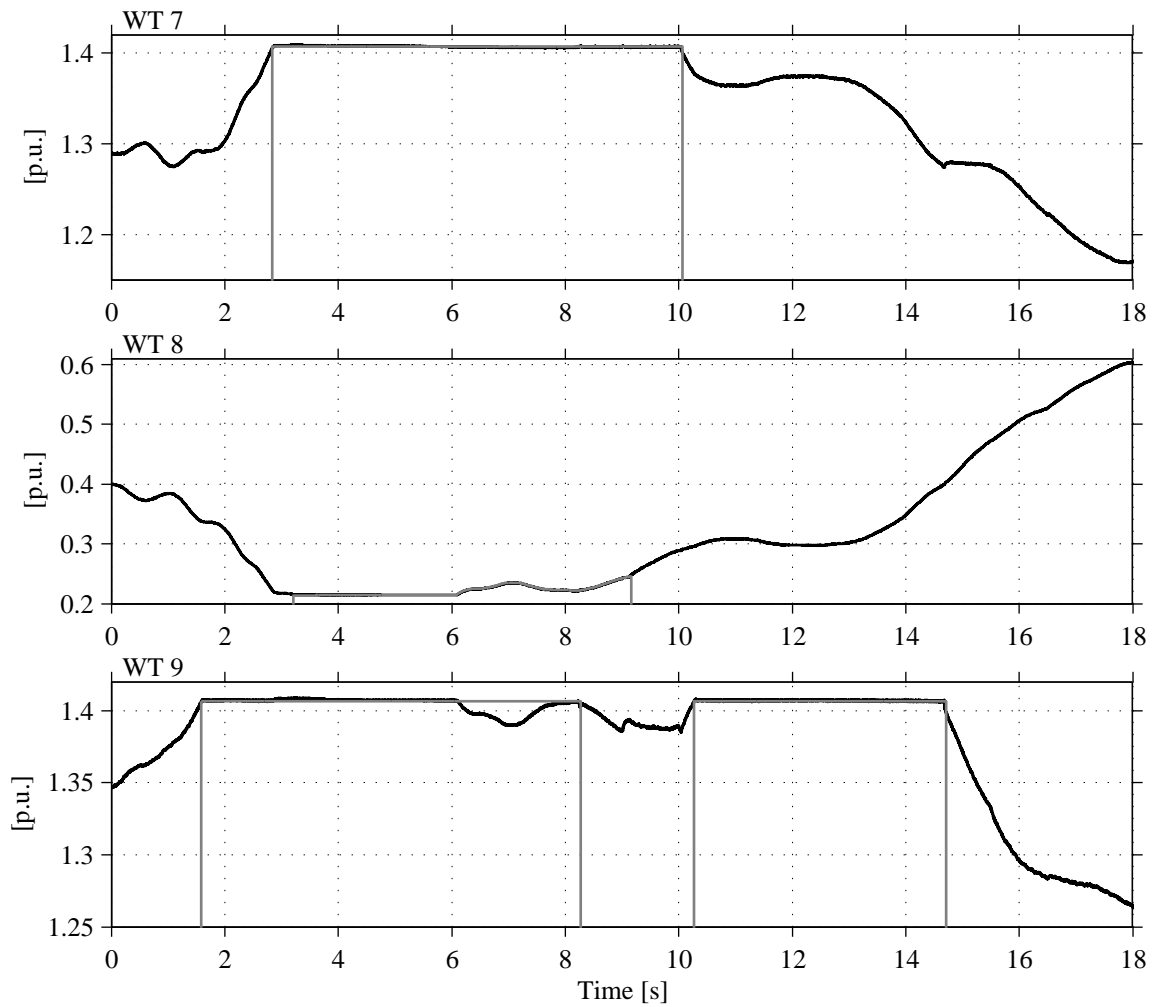


Fig. 6.8 The output voltage of wind turbines 7, 8 and 9 for the first 18 s of the simulation shown in Fig. 6.7.

for the stack in which the turbine is located. But the other stack currents and the stack voltage are unaffected by these, see Fig. 6.9. The changes in the current for stack 3 between 3 and 8 s does not seem to affect the stack voltage either. Accordingly, from this observation it can be concluded that the stacks can operate independently of each other. Not even the ramp disturbance of 0.5 p.u., applied by the aggregated power source, is a problem for the operation of the wind farm or affects the stacks noticeable.

In Fig. 6.9 c) it can be noticed that the power production of the wind farm is smooth, except for the occasions when the ramp disturbances are applied. From plot a) it can be seen that the DC-transmission controller keeps the transmission voltage to the reference also when the disturbances are present. It should be stressed that these more realistic power ramps (although very quick) gives a much smaller disturbance as compared with the steps made in Fig. 6.3.

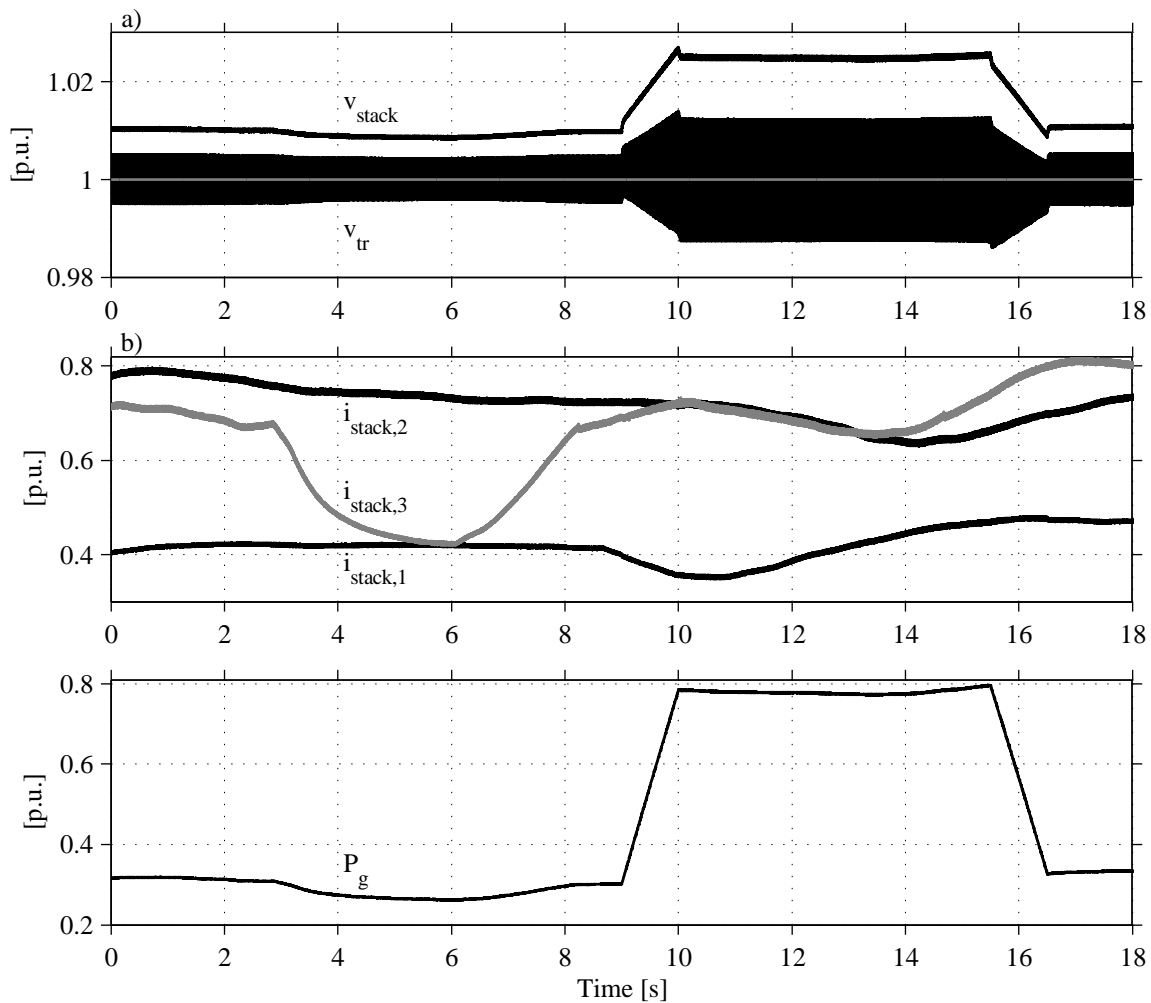


Fig. 6.9 The behavior of the wind park for the first 18 s of the simulation. a) transmission voltage, stack voltage and transmission voltage as grey in p.u. of rated transmission voltage. b) stack currents in p.u. of rated output current of the wind turbine. c) power produced by the wind farm in p.u. of the rated power of the wind farm.

In Figs. 6.10 and 6.11, the operation of the wind turbines 8 and 9 are shown in detail. An overall comment from these figures is that the tracking performance of the controllers is satisfactory. The important discrepancies can be found for the rotor speed, which will be discussed shortly, caused by the switching to VL-mode.

Let us now look more into detail of the operation of wind turbine 8 and start with the situation when wind turbine 8 goes into VL-mode due to under voltage between 3 and 9 s, as is indicated in Fig. 6.10 d). In this figure, the output voltage reference can be observed when the turbine is in VL-mode. In the beginning of this simulation the turbine is in N-mode, but the torque from the wind is decreasing. This results in a decreasing desired DC-link voltage and thereby a decreasing flux and DC-link voltage. The decreasing torque from the wind, together with the decreasing speed reference, results in a decreasing power

production, and this in turn results in a decreasing output voltage. In Fig. 6.10 f), the input current and the input current reference are shown. In the plot also the reference from the output voltage controller, recalculated from an output current reference to an input current reference (therefore denoted $i'_{\text{out,ref}}$) is shown. The transformation from the output current reference to an input current reference is done by (5.74). From the plot it can be seen that when the input current reference command is lower than $i'_{\text{out,ref}}$, the turbine switch to VL-mode due to the under voltage operation mode constraints. Now, i'_{out} is used as the input current reference for the DC/DC converter and thereby the output voltage controller is activated. The output voltage controller keeps the output voltage to the reference in the undervoltage limitation mode by increasing the power transfer. This increase can be noticed between 3 and 5 s in Fig. 6.10 a), where the breaking torque from the IM, as a consequence, is higher than the torque from the wind, even though the speed error is such that it should be lower. At 5 s, the torque from the wind starts to increase, which eventually results in a decreasing speed error and at approximately 9 s the torque reference from the speed controller becomes higher than the breaking torque of the IM and the wind turbine switch back to N-mode. It should be pointed out that without this wind increase, the turbine would shortly come to a stop. And, as pointed out before, in the beginning of this section, the speed is here deliberately chosen too high and the torque too low, in order to provoke an under voltage situation.

In Fig. 6.11 the operation of wind turbine 9 for these first 18 s of the simulation is shown. From plot d) it can be seen that the turbine is in VL-mode due to overvoltage at two times, between 2.5 and 8.3 s and between 10.3 and 14.4 s. In plot e) it can be noticed that the input voltage reference is constant for these first 18 s, this is due to the fact that the wind turbine is operating at high power production and that the output voltage is high. This leads to that the desired input voltage of the DC/DC converter is equal to the rated input voltage. From this it also follows that the flux reference is equal to the rated flux, with one exception. Between 2 and 5 s, the flux is reduced due to the fact that the speed is increasing and to keep the voltage constant the flux is reduced, i.e. flux weakening. From plots a) and b) it can be concluded that the input power is increasing in the beginning of the simulation and from Fig. 6.9 b), it can be seen that the current for stack 3 is decreasing slightly. This leads to an increasing output voltage of the wind turbine and from Fig. 6.11 f) it can be seen that the current reference from the output voltage controller, $i'_{\text{out,ref}}$ is decreasing. At approximately 1.5 s, the current reference from the output voltage controller gets lower than the current reference from the DC-link voltage controller and the turbine switches to VL-mode. After the change to VL-mode it can be seen in plot a) that the breaking torque of the IM, T_e , is lower than the torque from the wind and that the extra breaking torque from the pitch system increases to keep the speed reference. At 3 s the stack current decrease rapidly and, to keep the output voltage reference, the power production is also decreased rapidly, which is noticed in the decreased breaking torque by the generator. This decrease is too quick for the pitch system and therefore the overshoot in speed occurs

around 4 s. In Fig. 6.11 a), the rate limiter of the pitch system is visible between 3 and 5 s, due to the fact that the pitch torque increases with a constant rate. At 6 s, the stack current starts to increase, which means that the breaking torque also increases, and at 8.3 s the breaking torque of the IM is greater than the torque reference from the speed controller and the wind turbine changes to N-mode. However, the output voltage stays close to the rated voltage, which leads to that at 10.3 s, when the speed reference decreases, that the power production increases and to a too high output voltage, and the turbine switches back to VL-mode again. At 14 s, the stack current increases and this leads to that the turbine switches to N-mode at approximately 15 s and, due to the higher stack current the output voltage drops. It should once more be stated, that these occasions are not very frequent, but are treated here in order to show the stability of the system.

6.3 Energy Capture vs Output Voltage

As mention before, when the wind turbine switch to VL-mode due to over voltage, the power production is decreased to limit the output voltage to the rated voltage. This reduction will cause an energy production loss. The total energy production for a one hour simulation, with an unlimited output voltage and with the starting times used in Section 6.2, was 13.81 MWh. For this simulation the power originating from the aggregated power source was zero for the whole simulation. In Table 6.1 the energy production per unit of this unlimited production for different output voltage ratings are shown.

Table 6.1: Energy production for different rated output voltages and for 3 and 20 series-connected wind turbines.

rated output voltage [p.u.]	energy production 3 WT [p.u.]	energy production 20 WT [p.u.]
1.85	1	1
1.65	0.999	1
1.45	0.997	1
1.35	0.993	0.999
1.25	0.978	0.987
1.15	0.941	0.944

Table 6.1 shows that the energy production decreases when the rated output voltage decreases. This energy loss must be weighed against the increased cost of the higher rated voltage of the components on the high voltage side of the wind turbine transformer. As an example, a voltage output rating of 1.35 p.u. gives only a 0.5 % reduction of the produced energy for the wind farm and must be considered to be acceptable.

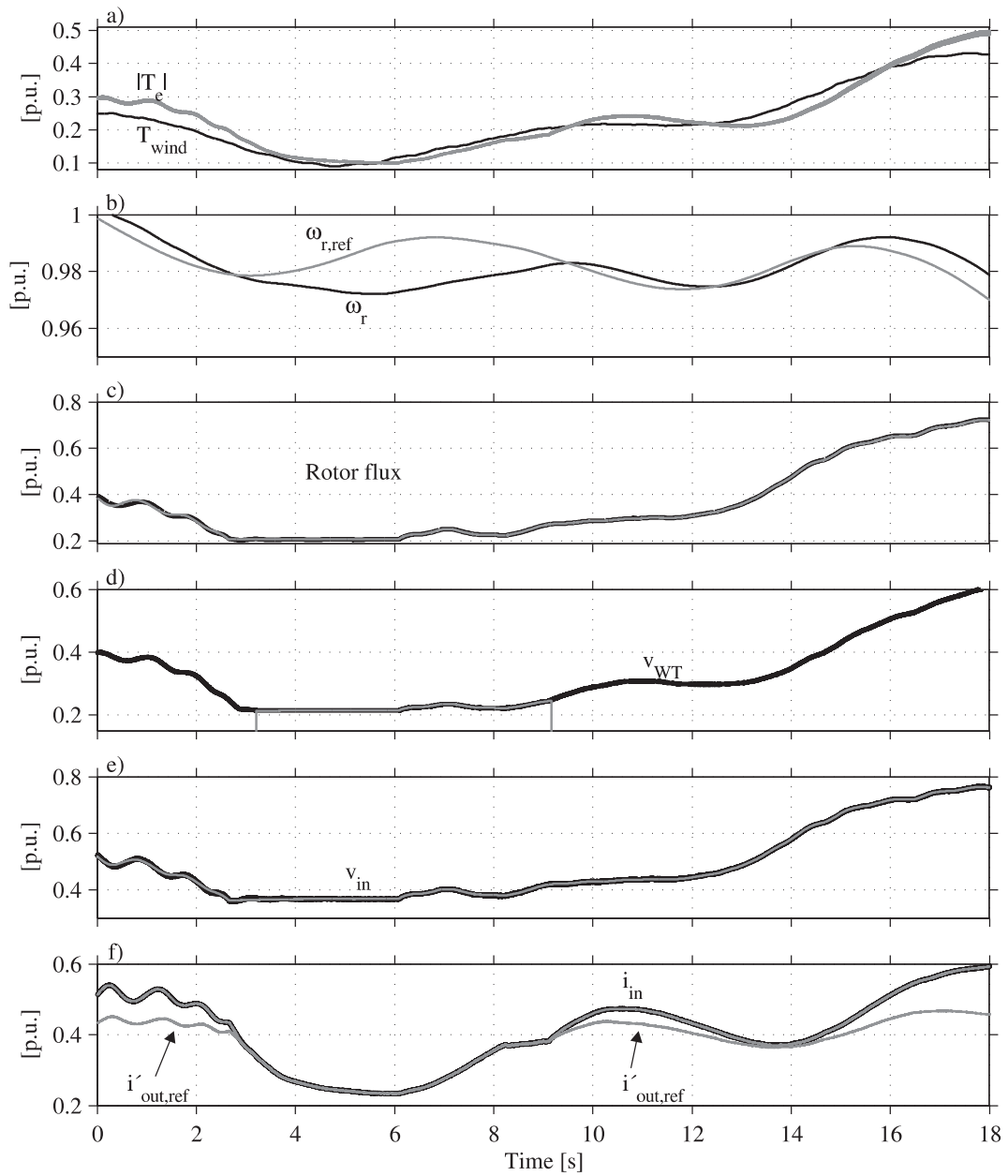


Fig. 6.10 The behavior of wind turbine 8 for the first 18 s of the simulation. a) Torque from the wind as black line and the absolute value of the torque produced by the IM as grey line, in p.u. of the rated torque. b) Speed of the wind turbine as black line and the reference as grey line, in p.u. of the rated speed of the wind turbine. c) Rotor flux in the IM as black line and the flux reference as grey line, in p.u. of the rated flux. d) Output voltage of the wind turbine as black and the output voltage reference is shown as grey when the turbine is in VL-mode. e) DC-link voltage as black and the reference as grey, in p.u. of the rated voltage. f) Input current of the DC/DC converter as black, the reference as grey and the reference from the output voltage controller as grey and marked with $i'_{out,ref}$, in p.u. of the rated input current.

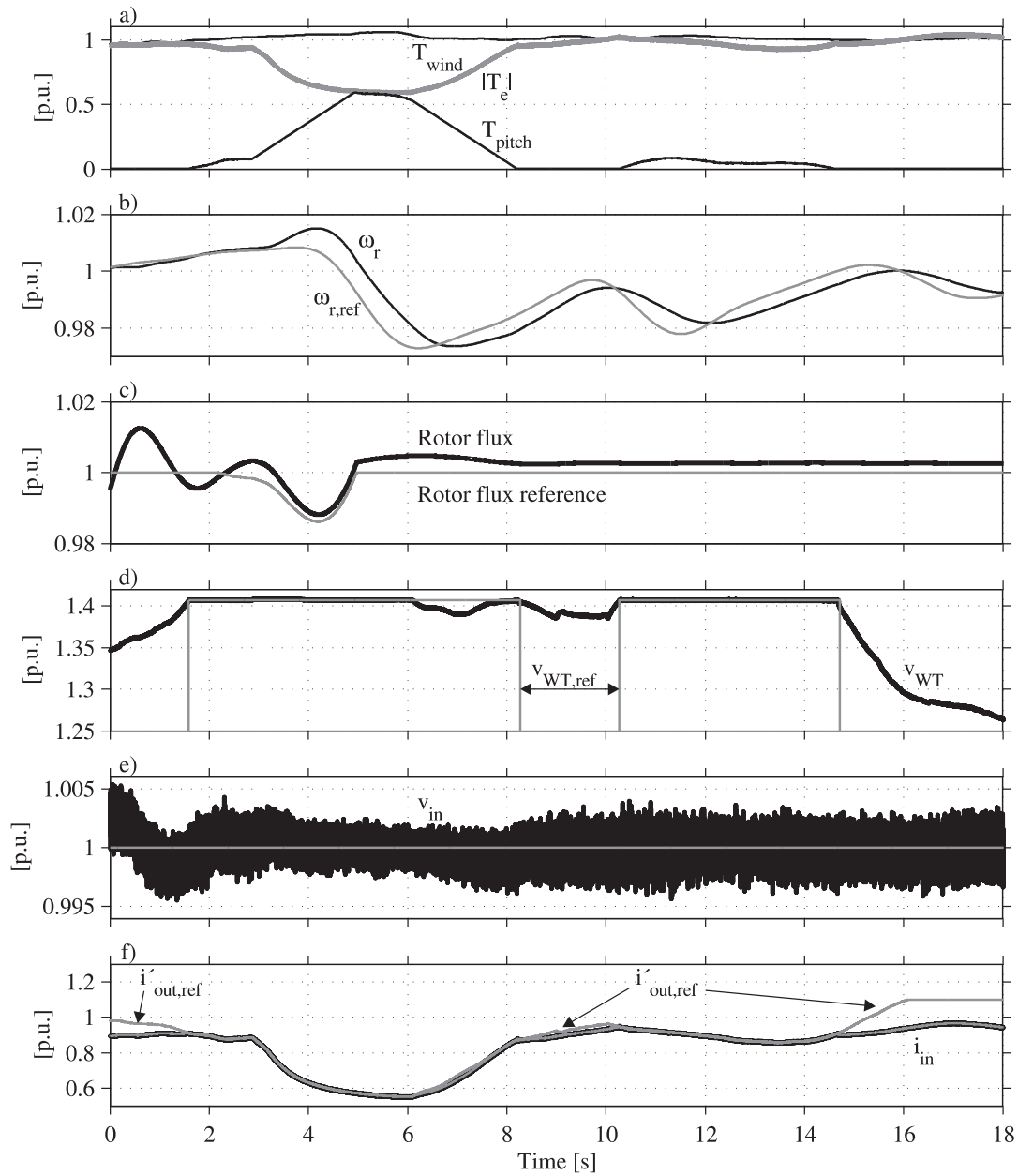


Fig. 6.11 The behavior of wind turbine 9 for the first 18 s of the simulation. See Fig. 6.10 for the description of the figure. The addition is the black line in a) for the absolute value of the pitch torque.

Chapter 7

Transformer design and measurements

7.1 Converter Design for the Series-connection

Apart from increasing the rectified voltage from the wind energy generator, the high frequency transformer in the DC/DC converter is also used for the galvanic separation of the generator side and the transmission side. This means that the common mode insulation level of the transformer must be designed for half the transmission voltage (that means $+V_{tr}/2$ or $-V_{tr}/2$), at least for the wind turbines in the top and bottom of the stack, see Figs. 4.2 and 4.1. Since the potential of the whole high-voltage side winding is close to the transmission voltage, the rating of the high voltage winding and the components on the transmission side of the DC/DC converter, only needs to be designed for the rating of the converter. The prerequisite is of course that all "objects" (windings, components) can be placed or encapsuled so they can withstand the transmission voltage to ground. If not, encapsuling for a higher voltage level needs to be used. In Fig. 7.1, a possible solution for the layout of the transformer and the transmission side is shown.

The core geometry is a toroid. In Fig. 7.1, the top side view is shown and in Fig. 7.2, the cross section of the toroid is shown. The angle θ_w indicates the sector of the core which is used by the windings. The advantage of the toroid shape is that it is smooth, or can be made smooth, in all directions, which from a high voltage point of view is to prefer. Otherwise, there will be a risk of locally high electric fields that might result in corona discharges. The space that needs to be filled, to get a circular cross section of the core, is used for cooling. The core is grounded. The semiconducting layers are used to smoothen out the geometry, to avoid sharp edges and thereby high electrical fields. The winding to be placed closest to the core, is the generator side winding, since it is almost on ground potential. Accordingly, the insulation layer for the generator side does not need to be as thick as the layer used for the transmission winding insulation, which has to be designed to withstand the transmission voltage potential.

Another problematic area from the high voltage design point of view, where there is a risk for high fields, is at the point where the transmission side winding ends, at the dashed

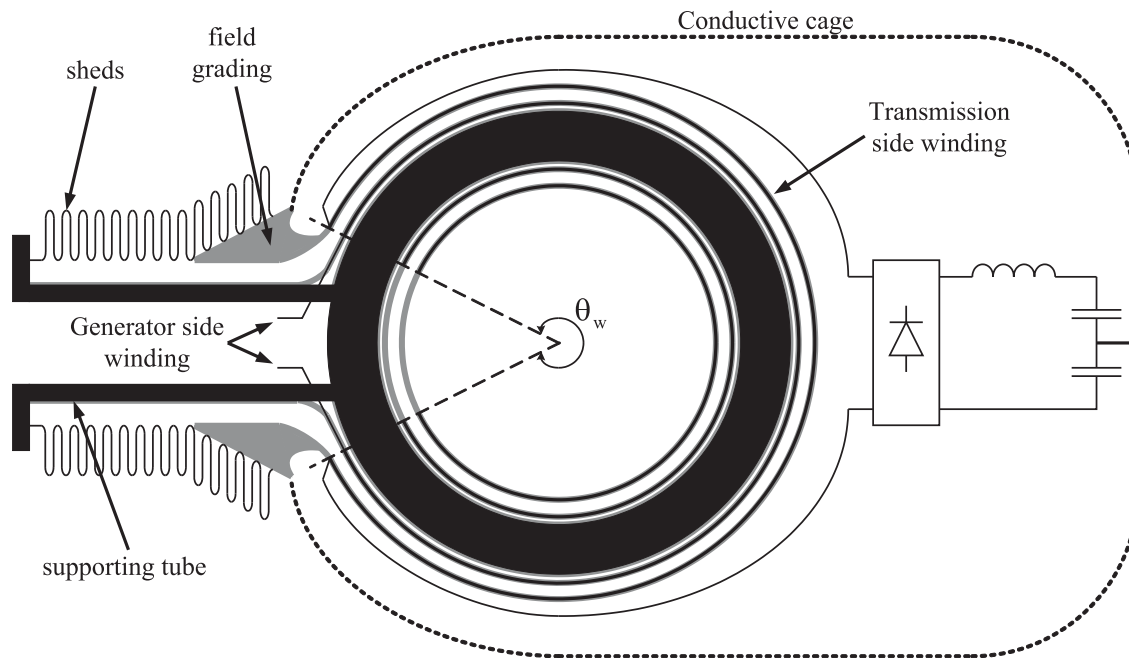


Fig. 7.1 A possible solution for the layout of the high frequency transformer and of the transmission side of the DC/DC converter for the series-connected wind turbine. Top side view of the cross section of the transformer. Grey indicates semiconducting layers.

lines which indicates the sector used by the windings. A possible solution for preventing this is to use a semiconducting layer to create a field grading area, like the one used in high voltage cable terminations. This field grading is indicated in Fig. 7.1. To have a sufficiently long creepage distance from the field grading to the end of the supporting tube, sheds on the insulator are used. The minimum creepage distance needed depends on the pollution level. For light pollution levels the minimum distance is 16 mm/kV and for very heavy it is 31 mm/kV, [28].

To decrease the voltage potential between the components on the transmission side of the transformer and ground, a conductive cage is used. The cage is attached to the field grading material/area and surrounds the transformer and the components on the transmission side. The cage is connected to the middle point of the output capacitors. In this way the cage isolates the components from the ground. The highest potential from the components to the surrounding (in this case the cage) will in this case be half of the rated output voltage of the turbine. This is a substantial reduction compared to half the transmission voltage, which will be the case for the turbines closest to the transmission cables if no cage is used. This reduces the problems caused by the fact that sharp edges produces corona and discharges. The cage is made as a round and smooth shape, so that, again, no problems with corona and discharges appears. The potential from the cage to the surrounding is approximately the potential of the stack cable, in the point where the investigated wind turbine is located. The result is that the distance from the cage to the surroundings must

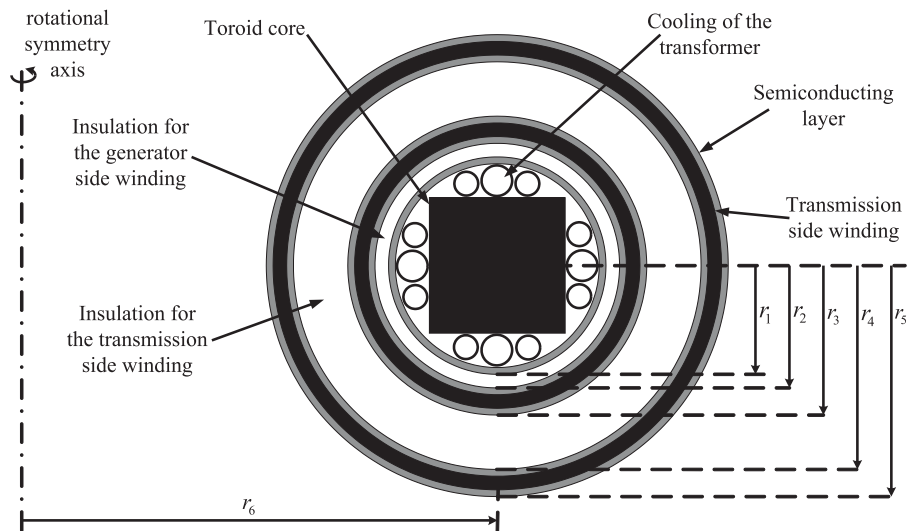


Fig. 7.2 Cross section of the toroid in Fig. 7.1. Grey areas indicates semiconducting layers.

be long enough to take up half the transmission voltage.

7.1.1 Cooling of the Transformer and the Components

As mention before, the space that needs to be filled to change the square core cross section to a circular one, is used for cooling. The cooling medium thought to be used here, is water. Since the core is grounded there is no need of using deionized water, which is the case if the object to be cooled is on high potential. For the transmission side winding and for the components on the transmission side, forced air cooling is thought to be used. The idea here is to have the fan on ground potential and use nonconductive tubes to guide the air flow to the components and transformer. In this way the expensive apparatus for the deionization of the water, which is needed if water cooling is used on this side, can be avoided.

7.1.2 Electric Field in the Transformer

In Fig. 7.3, the simplified geometry of the transformer, that is used for calculating the electrical field between the windings, is shown. The figure is drawn as a two dimensional figure with a rotational symmetry axis. Accordingly, in order to obtain the three dimensional figure, the drawn geometry is rotated 360 degrees around the rotational symmetry axis. This means that the electrical field at the end of the windings is not described with this geometry (at the end of the windings means the angle $360 - \theta_w$ in Fig. 7.1. The electrical field in a straight, long, coaxial cable, ($r_6 \rightarrow \infty$ in Fig. 7.3), can be expressed

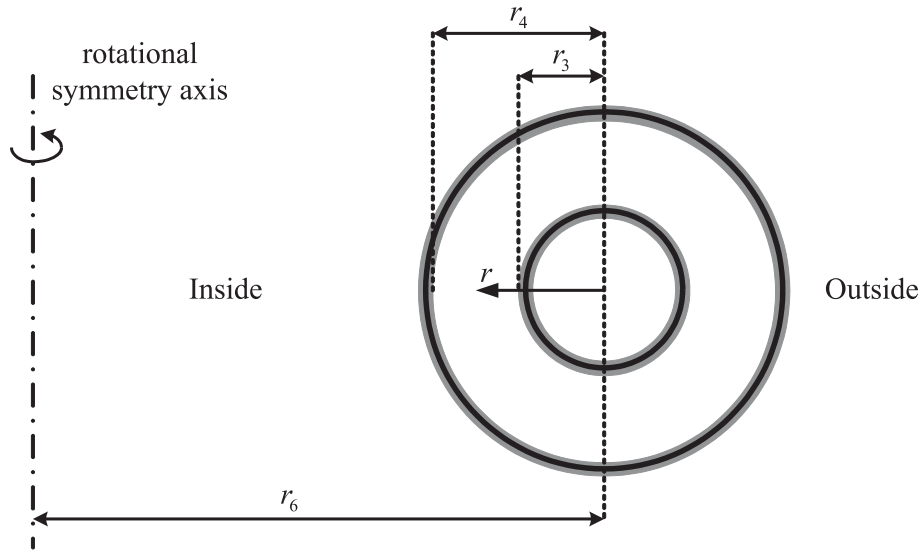


Fig. 7.3 Simplified geometry of the transformer, used for calculating the electrical field between the windings. The figure is drawn as a two dimensional figure with an rotational symmetry axis.

as

$$E_r(r) = \frac{U}{r \ln \left(\frac{r_4}{r_3} \right)} \quad (7.1)$$

where U is the voltage difference between the windings and r is the radius at which the electrical field is calculated, $r_3 < r < r_4$. From (7.1) it can be noticed that the electrical field is inversely proportional towards the radius r . This gives that the highest field is at the surface of the inner winding. But if the radius r_6 is reduced, so that it is close to r_4 , then the electrical field will be higher when $r = r_4$ than $r = r_3$, due to the higher curvature. Due to the symmetry, the electrical field will only have a component in the direction of the marked radius r , when calculated for different radii in this plane. Also due to the symmetry, the highest value of the electrical field is found in this plane (so, the plane is then a horizontal plane through the toroid when it is laying down). In Fig. 7.4, the magnitude of the electrical field is shown for the case with $r_3 = 0.09$ m, $r_4 = 0.12$ m, $r_6 = 0.14$ m and 1 V between the windings. From the figure it can be seen that the electrical field is highest on the left side of the outer circle, which is due to the fact that the rotational symmetry axis is located to the left.

To approximately take the radius r_6 into account when calculating the maximum electrical field, it is assumed that the electrical field on the inside is inversely proportional to $r(r_6 - r)$ and that it on the outside is inversely proportional to $r(r_6 + r)$. Integrating the electrical field from r_3 to r_4 gives the voltage between the inner and outer winding. This

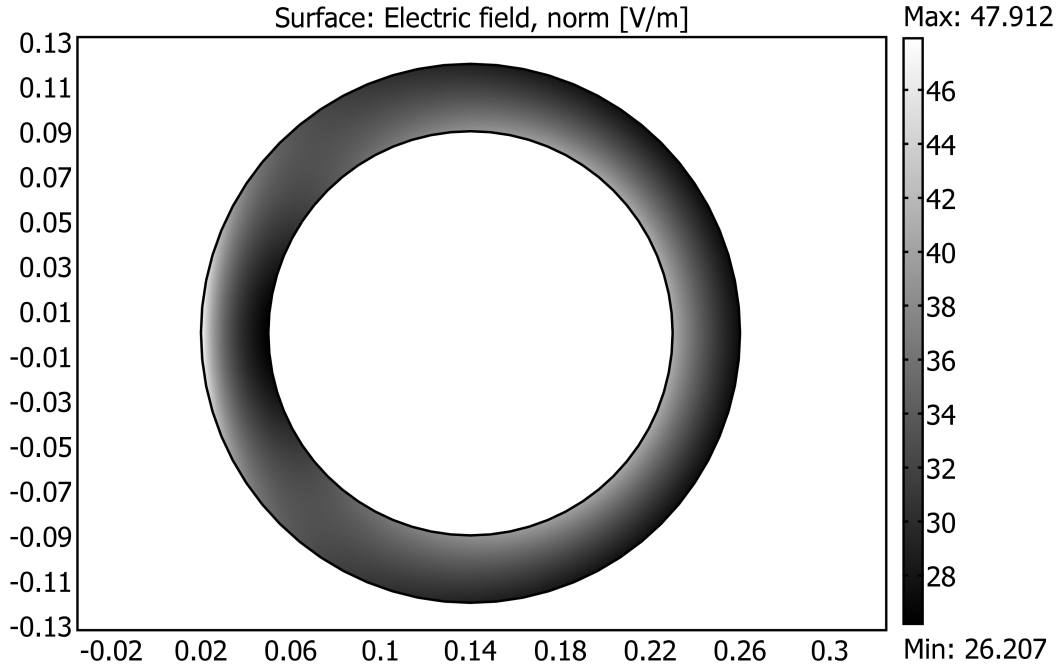


Fig. 7.4 The magnitude of the electric field between the windings for $r_3 = 0.09$ m, $r_4 = 0.12$ m, $r_6 = 0.14$ m and 1 V between the windings.

gives that the magnitude of the electrical field in the plane can be expressed as

$$E_{\text{inside}}(r) = \frac{U r_6}{r(r_6 - r) \ln \left(\frac{r_4(r_6 - r_3)}{r_3(r_6 - r_4)} \right)} \quad (7.2)$$

$$E_{\text{outside}}(r) = \frac{U r_6}{r(r_6 + r) \ln \left(\frac{r_4(r_6 + r_3)}{r_3(r_6 + r_4)} \right)}. \quad (7.3)$$

In Fig. 7.5 the magnitude of the electric field for different radii r_6 in p.u. of the maximum field obtained when $r_6 \rightarrow \infty$ are shown. Solid lines shows the field from FEM calculations and dotted lines shows the simplified model described with (7.2) and (7.3). The grey line is for when $r_6 \rightarrow \infty$. The radii are $r_3 = 0.09$ m, $r_4 = 0.12$ m, the lines marked with 1 is for $r_6 = 0.14$ and then the following lines towards the grey are for $r_6 = 0.25, 0.5$ and 0.75 respectively. From the figure it can be noticed that the simplified model describes the magnitude of the electric field well. It is when r_6 is close to r_4 that the mismatch between the FEM calculations and the model starts to be visible. The model gives in this case a somewhat too high maximum value. It should be mention that the model have been compared with FEM calculations for other values of r_3 and r_4 , that can be expected for the transformer. From these comparisons similar results that is shown in Fig. 7.5 where

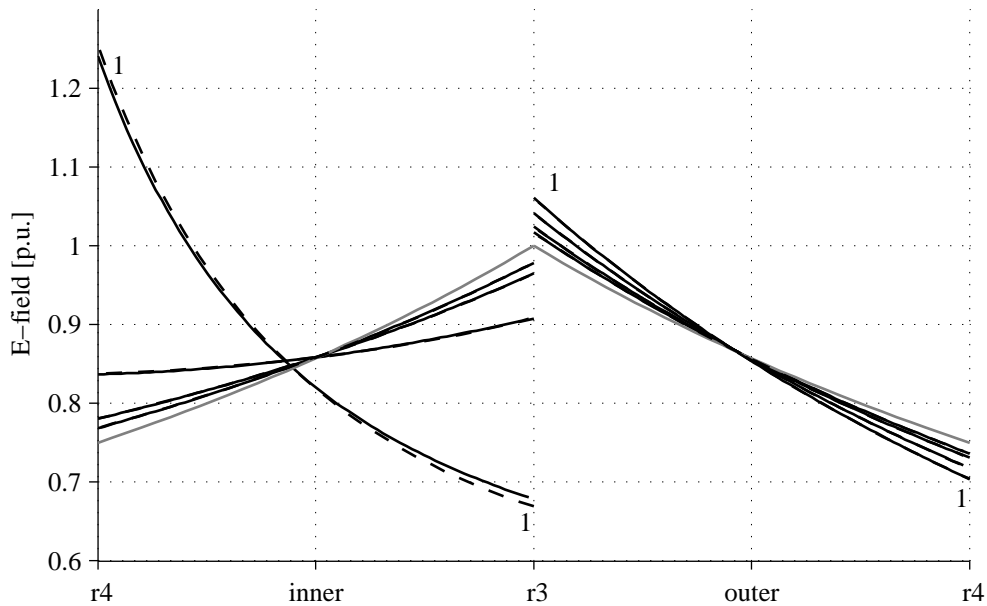


Fig. 7.5 The magnitude of the electric field for different radii r_6 in p.u. of the maximum field obtained when $r_6 \rightarrow \infty$. Solid lines shows the field from FEM calculations and dotted lines shows the simplified model described with (7.2) and (7.3). The grey line is for when $r_6 \rightarrow \infty$. The radii are $r_3 = 0.09$ m, $r_4 = 0.12$ m, the line marked with 1 is for $r_6 = 0.14$ and then the following lines towards the grey is for $r_6 = 0.25, 0.5$ and 0.75 respectively.

found. It should also be mention that the case with r_6 close to r_4 is not that realistic, since the space for the transmission side winding on the inside will be too small to fit the winding.

It should be mentioned that the electric field distribution for DC is controlled by the resistivity of the insulating material. Unfortunately the resistivity is usually very temperature dependent. The consequence is that for DC-cables, the electric field distribution can be altered due to the higher temperature inside the cable, i.e. the highest electrical field can be at the outer screen and the lowest occurring on the surface of the conductor. This effect is not taken into consideration when the simplified model is derived.

7.1.3 Full Scale FBPS Converter, 5MW

The rated power of the full scale converter is chosen to be 5 MW, although the simulations in the previous chapters have been carried out for a rated power of 2 MW. The higher rated power is selected due to the fact that the rating of wind turbines is increasing all the time and that there are experimental wind turbines installed with rated power of 6 MW. The 5 MW converter has the following ratings:

Quantity	Rated value
Input voltage	3.6 kV
Input current	1.4 kA
Output voltage	20.25 kV
Output voltage	15 kV (nominal)
Output current	0.33 kA.

The input voltage is selected in such a way that IGBTs with a rated voltage of 6.5 kV can be used without series connections of IGBTs. To avoid the need of series connected diodes on the transmission side and parallel connecting IGBTs on the generator side, the DC/DC converter can be made into 6 smaller modules. Each with a 1:1 transformer, which on the generator side can be connected in parallel to the DC-link and on the transmission side they can be connected in series. The result is one large converter with an ideal transformation ratio of 6, the needed is in this case 5.625. One interesting feature, is that by having a supporting tube with a sufficiently large radius (see Fig. 7.1), the IGBTs could be fitted inside the tube and be water cooled with the same water that is used to cool the transformer. In this way the transformer module with its casing becomes a complete DC/DC transformer. Another advantage with the modularization is that if one module breaks down, it can be short circuited on the transmission side and the production can continue, but with a lower rated output voltage and power.

The rating of these 6 modules are:

Quantity	Rated value
Power	0.83 MW
Input voltage	3.6 kV
Input current	0.23 kA
Output voltage	3.6 kV
Output voltage	2.5 kV (nominal)
Output current	0.33 kA.

The transformer rated current is 0.28 kA RMS. The transformer design for this 0.83 MW converter is based on that the core material used is Metglas alloy 2605SA1 with longitudinal field annealed. One option for the insulation is to use some type of silicone or rubber based insulating material and then to vacuum mould the different layers. These materials can have a breakdown stress of approximately 15 to 30 kV/mm. For this design, a maximum electric field of 10 kV/mm and an insulation voltage of 300 kV are used. These selections resulted in $r_6 = 0.46$ m, $r_3 = 0.08$ m and $r_4 = 0.12$ m.

7.2 Down Scaled Converter

In order to test this design a down-scaled converter was designed, built and put into operation.

For the down scaled converter the voltages and currents are scaled with a factor of 12, giving:

Quantity	Rated value
Power	5.8 kW
Input voltage	300 V
Input current	19.3 A
Output voltage	300 V
Output voltage	200 V (nominal)
Output current	29 A
Transformer current	23 A RMS
Diode current	10 A AVG
Diode current	16 A RMS.

For the down scaled converter it was decided that only two modules should be build. The reason for this is that the output voltage should not be too high, the number of components is kept low and with two modules the series connection of the modules could still be functionally checked. The IGBT bridge SEMICRON SKM400GB125D and SKHI23 driver circuits where used for creating the high frequency voltage for both transformers. The rating of the IGBTs are 1200 V and 400 A, which is well beyond what is needed. For the diode rectifier on the transmission side, SGS-Thomson Microelectronics BYT230PIV-1000 diodes where used. The rating of these diodes are 1000 V, 70 A RMS or 30 A AVG. The diodes are mounted on the same heat sink as the IGBTs, a SEMICRON P16/300 with a SKF16A-230-11 fan. This gives a thermal resistance of the heat sink of 0.024-0.036 K/W. From this it can be realized that the heat sink also is overrated for this application. The input capacitor and the two output capacitors are from RIFA and the ratings are 400 VDC and 3300 μ F. For the output capacitances it can be noticed that this is much more then what is used in the simulations. The idea of having this high capacitance was to have long time constants for the system in the testing stage.

The currents are measured with LEM LA-100S current transducers, which can measure up to ± 100 A with a bandwidth of 0 to 150 kHz (-1dB). The input voltage and output voltage are measured using an isolating amplifier from Analog Devices, AD210BN, which has a bandwidth of 20 kHz. All measuring signals go to a level adjusting card before the signal is connected to the control computer. On this card it is also possible to set protection levels, that if they are reached, turns off all IGBTs. Between the controller and the driver circuits there is also a conversion card. It is to this card the error signal form the card for the measuring signals goes and turns off the IGBTs. In Fig. 7.6 the heat sink with the IGBTs and the diodes, the driver circuits and the rack with the card for the measurement and control signals to the driver circuits are shown. In the figure also the two transformers, two output inductors and the output capacitors are shown. To control the converter the dSPACE DS1103 is used. It is a digital signal processor system, which for this application is programmed with C-code. The control system has among other things

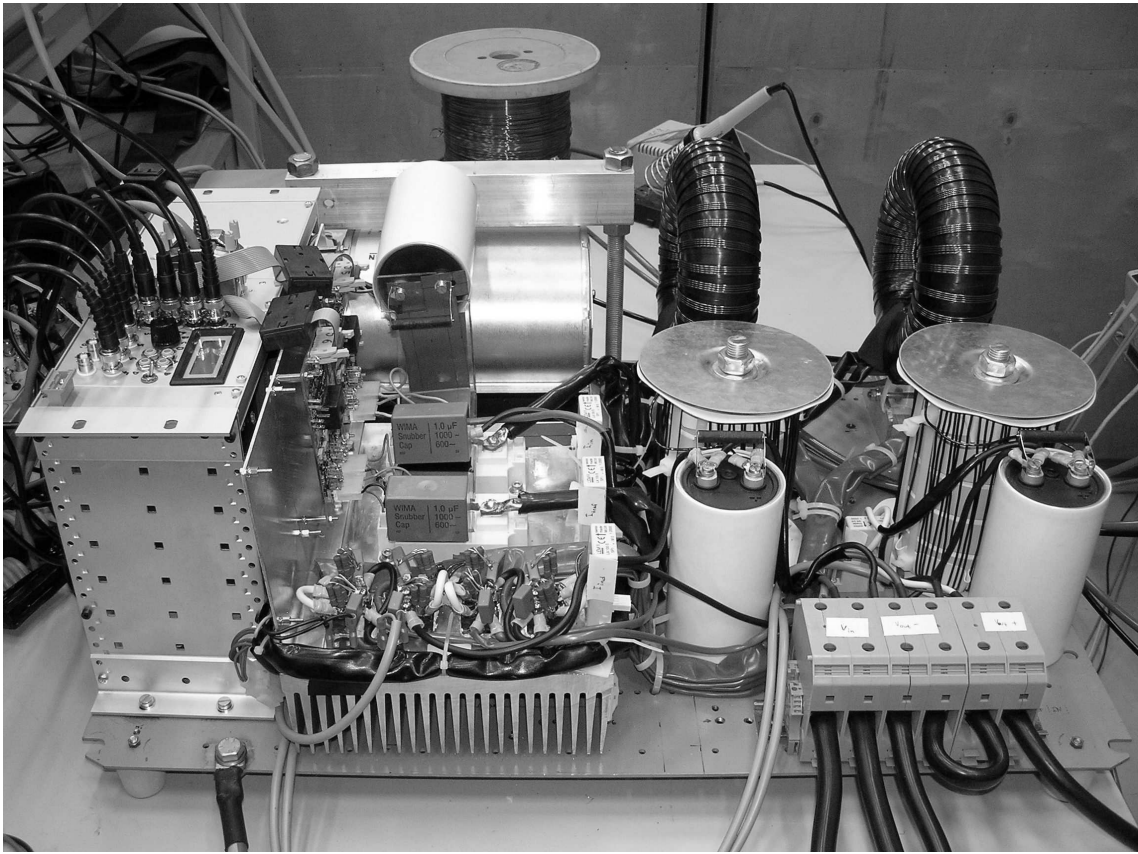


Fig. 7.6 The down scaled 11.2 kW converter.

built in A/D-converters for sampling of the measured quantities and control signals for the valves as outputs.

For the output filter inductances, iron powder cores from Amidon, model T-400A-26, are used. Five such cores are stacked on top and 74 turns of 1.8 mm copper wire is wound around them. This gives an inductance of 7.1 mH and an approximate resistance of 0.2Ω .

The material for the transformer cores that were available was Metglas alloy 2605SA1, not annealed, with a width of 30 mm. The cores that were ordered had an inner diameter of 120 mm and an outer diameter of 180 mm. The fill factors for the cores are 0.76 and 0.82. The size of the cores are big for the power rating, but since there was an uncertainty in how good the windings would become, the core was oversized to be sure that the windings should fit. From the manufacture of the core there were some protective plastic around the cores. This was left on the core. To create a circular cross section of the core, a 8 mm tube and two 6 mm tubes were put on each side of the core. Heat glue was used to fill the rest. Fig. 7.7 left photo shows the transformer core with the cooling tubes and heat glue. In the right photo shows when the insulation is applied, this will be discussed later. Before the generator winding was wound on the core, a layer of tape was put on,

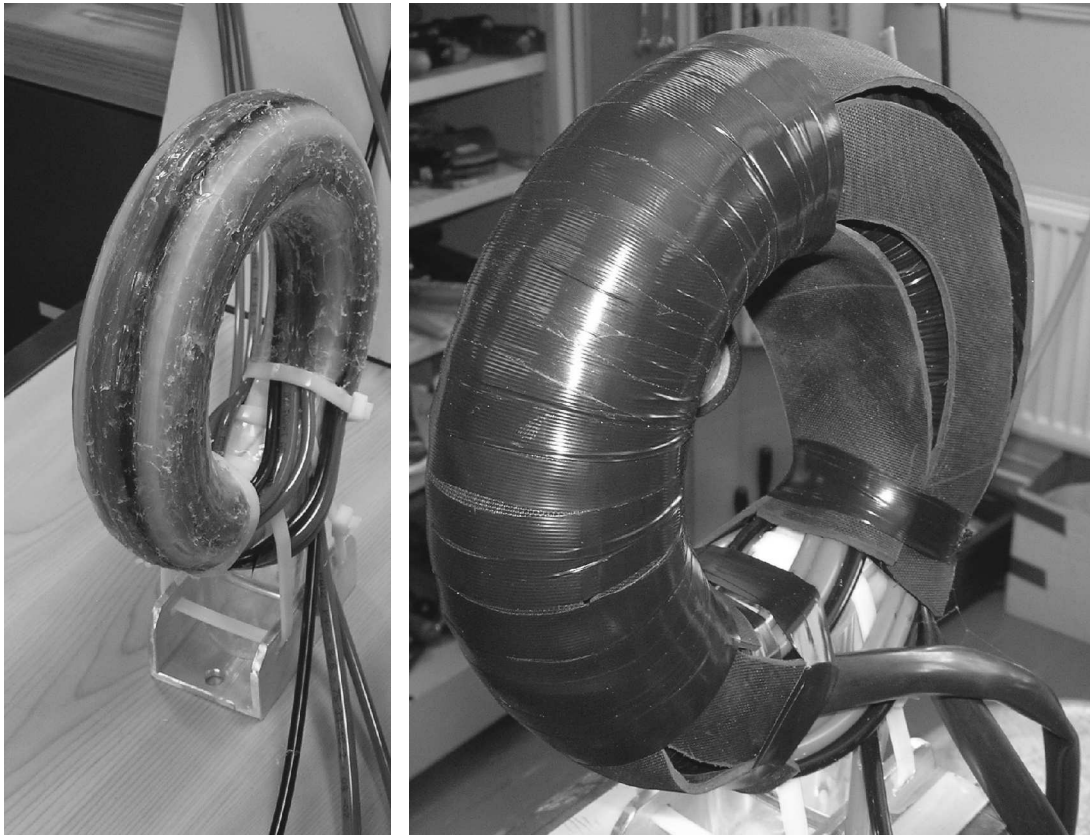


Fig. 7.7 The down scaled 11.2 kW converter.

to even out small unevenness. The generator side winding is wound with four 1.5 mm copper wires and 33 turns are applied. This gives a current density of 3.3 A/mm^2 which is approximately the value for a standard 50 Hz transformer. But for a larger transformer this is a high value. It was thought to be too complicated to wound the transformer with more than 4 wires and in order to avoid a problem with the skin effect, thicker conductors were not considered. This also gave that the winding could be wound in one layer only, which also made it simpler to wound the transformer. The winding was fixed with a layer of tape and then two layers of 6 mm rubber was put around the core. This is shown in the right photo of Fig. 7.7. this construction was done in order to resemble the insulation for the transmission voltage. The thickness of only 7 mm was chosen to keep the ratios between the radii similar as for the 5 MW transformer. Finally the transmission side winding was wound on top of the rubber insulation. The transmission side winding was made identical to the generator side winding. In Fig. 7.8, the finished transformer is shown. The geometry of the down scaled transformers are:



Fig. 7.8 The finished down scaled 5.6 kW transformer.

r_1	25 mm
r_2	25 mm
r_3	26.5 mm
r_4	33 mm
r_5	34.5 mm
r_6	75 mm

With the geometries the resistance of the generator side and transmission side resistances can be calculated to, $R_{\text{gen}} = 4.1\text{m}\Omega$ and $R_{\text{trans}} = 5.4\text{m}\Omega$ respectively. The magnetizing inductance can be approximately calculated by assuming a relative permeability of the core material of 20000 to $L_{\text{m, tr}} = 40\text{mH}$. Even though this is a very rough figure it indicates a high value of the magnetizing inductance.

7.3 Measurements

7.3.1 Converter in steady-state

No-load test

Fig. 7.9 shows measurements from one module of a no-load test at rated input voltage. In Fig. 7.9 a), the input voltage, v_1 , to the transformer is shown as a black line in p.u. of the rated input voltage. The grey line shows the input current, i_1 , magnified 10 times, in p.u. of the rated output current. From the figure it can be noticed that the current is almost in phase with the voltage, which means that it is almost only active power which is transferred to the transformer, and this current corresponds to the losses. This is also seen in Fig 7.9 b) where the input power to the transformer is shown in p.u. of the rated power of the transformer.

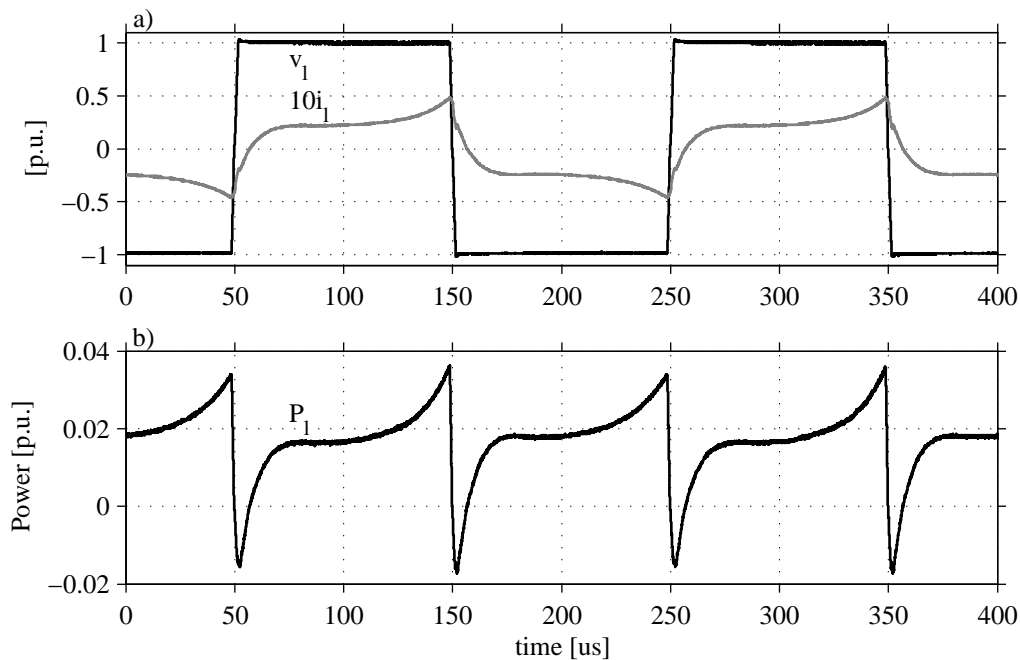


Fig. 7.9 No-load test of the down scaled 5.6 kW transformer. a) The black line shows the input voltage, v_1 , to the transformer in p.u. of the rated input voltage. The grey line shows the input current, i_1 , magnified 10 times, in p.u. of the rated output current. b) The input power to the transformer in p.u. of the rated power.

With the approximate magnetizing inductance calculated previously the magnetizing current can be calculated, for this case to be 0.01 p.u peak. Due to the, in comparison with the "active loss current", low magnetizing current, it can hardly be noted in plot a). The peak flux for this case is approximately 0.5 T. The average power loss for the no-load case is found to be 1.7 % of rated power, which is higher than the 0.9 % estimated. This

estimation was made from data sheets for this material in a longitudinal field anneal form, which differs from the non-anneal form used.

Load test

The load test for the converter was performed at a lower voltage, approximately 0.17 p.u. input voltage. The low input voltage was used in order to keep the derivative of the transformer current low, so that a good reading of it could be obtained in order to determine the leakage inductance for the transformer. In Fig. 7.10 the input voltage and input current to the transformer is shown, as black and grey lines respectively.

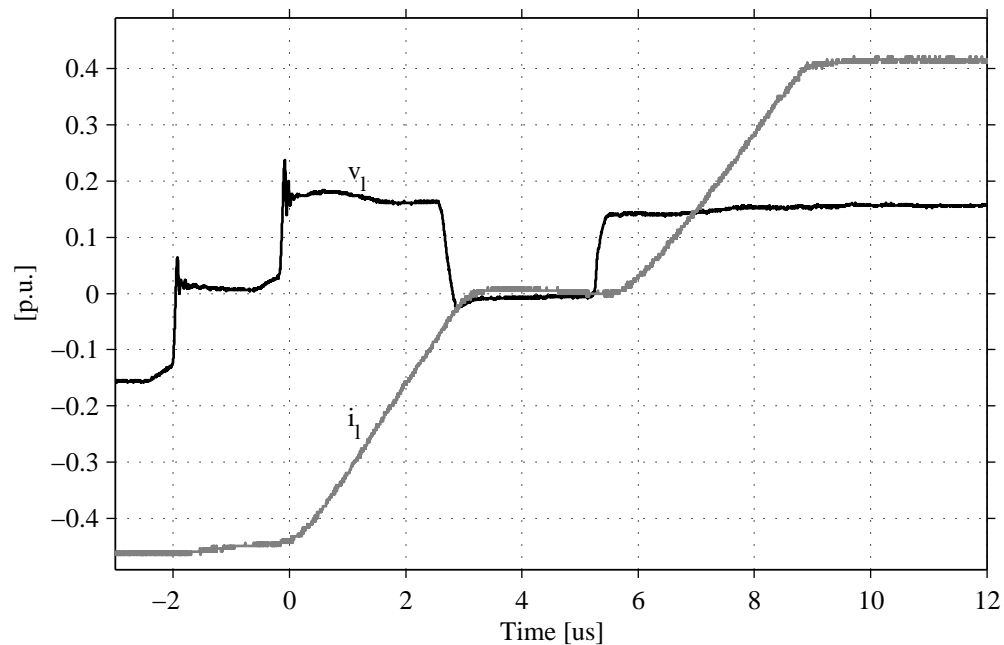


Fig. 7.10 Load test of the down scaled transformer. The black line shows the input voltage, v_1 , to the transformer and the grey line shows the input current, i_1 .

From the figure it can be seen that between 0 and 2.5 μs the voltage across the transformer is 0.16 p.u. and the current changes 0.36 p.u. This gives a leakage inductance of approximately 12 μH .

Diode snubber

For this measurement, RC-snubbers are mounted over the diodes in one module, and for the other module, the diodes are without snubber. In Fig. 7.11, the black line shows the voltage over the diode with RC-snubber and the grey displays the diode voltage without snubber in p.u. of rated input voltage. The input voltage was 1 p.u., the output voltage 1 p.u. and the output current were 0.5 p.u. in this measurement. From the figure it can

be seen that for the diode without snubber, the peak voltage is 2.8 p.u. and it should be remembered that the rating of the diode is 3.3 p.u. Due to the fact that this overvoltage increases with the current, 0.5 p.u. current was considered too high clearly motivating the need for using a snubber circuit. For the diode with a snubber circuit, the peak voltage is reduced to 1.2 p.u. in this case.

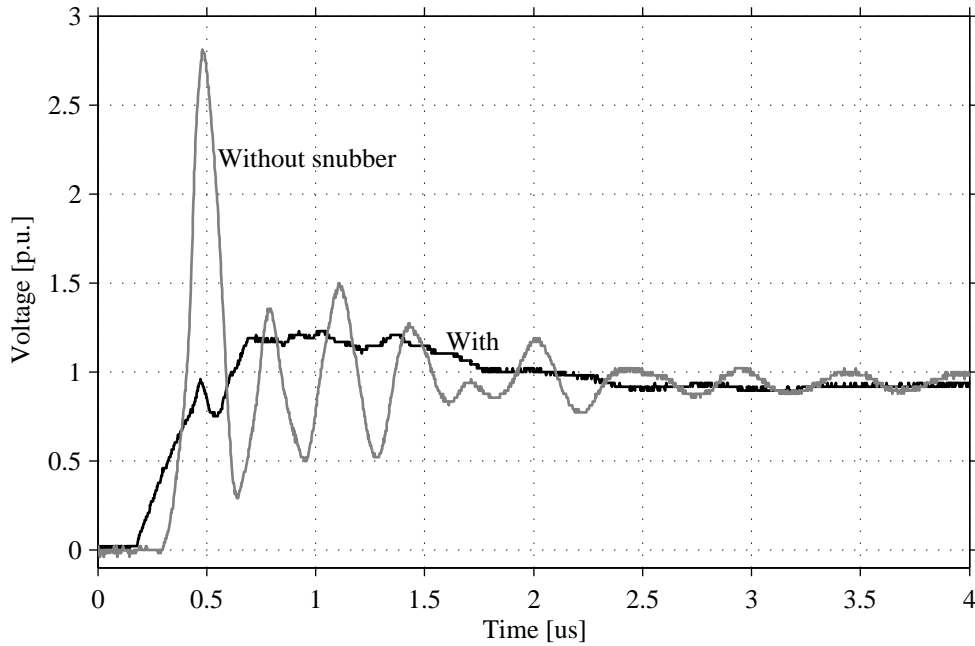


Fig. 7.11 The voltage across one diode in the diode bridge on the transmission side for an input voltage of 1 p.u., output voltage of 1 p.u. and an output current of 0.5 p.u. For this measurement RC-snubbers are mounted over the diodes in one module and for the other module the diodes are without snubber. The black line shows the voltage over the diode with an RC-snubber and the grey for the diode without snubber in p.u. of rated input voltage.

The snubber is designed as described in [37], and with an estimate of the peak reverse recovery current, I_{rr} of 10 A the base values of the snubber can be calculated as

$$C_{\text{base}} = L_{\text{Leakage}} \left[\frac{I_{rr}}{v_{\text{WT, rated}}} \right]^2 \approx 7 \text{ nF} \quad (7.4)$$

$$R_{\text{base}} = \frac{v_{\text{WT, rated}}}{I_{rr}} = 30 \text{ } \Omega. \quad (7.5)$$

The recommended selection of snubber values are, $C_s = C_{\text{base}}$ and $R_s = 1.3R_{\text{base}} = 39 \text{ } \Omega$. The implemented values are $C_s = 10 \text{ nF}$ and $R_s = 55 \text{ } \Omega$.

7.3.2 Current controller

The step performance of the current controller is shown in Fig. 7.12. It can be noticed from the figure that the rise time of the current is approximately 0.8 ms which corresponds well to the theoretically ordered one of 0.7 ms. This case is for a small current step, if larger steps are made the converter goes into voltage saturation and the increase of the current becomes limited. When the converter goes into voltage saturation, the rise time becomes longer than the theoretical one.

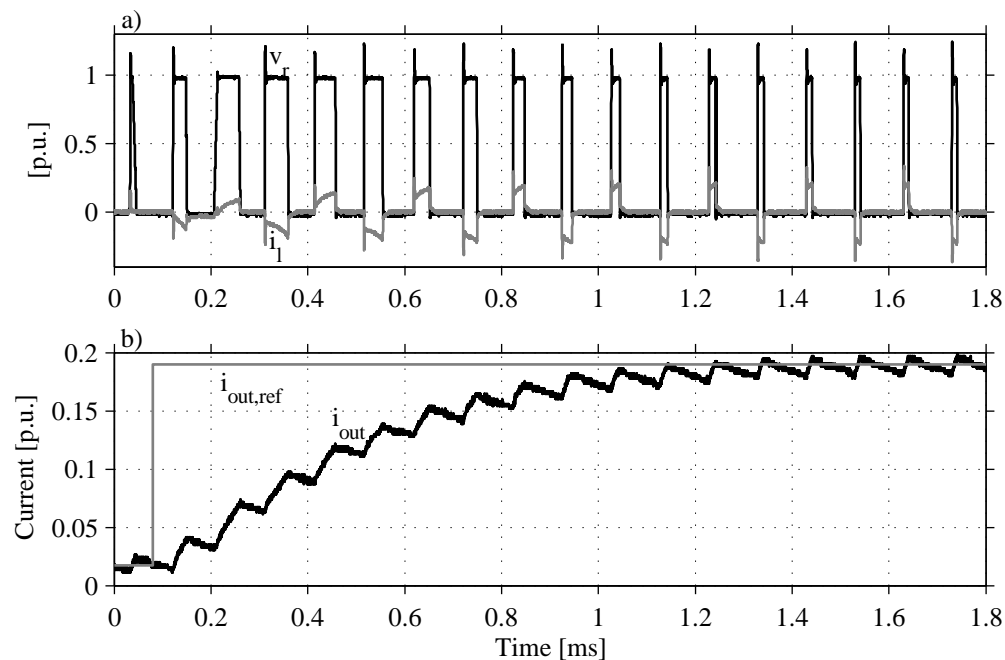


Fig. 7.12 Step response of the current controller for a step size of 0.17 p.u. and with an input voltage of 1 p.u. and an output voltage of 0.25 p.u. a) The rectified voltage, v_r , in p.u. of rated input voltage as black line and the transformer input current, i_1 , as grey in p.u. b) Inductor current as black line and the reference as grey, in p.u. of rated output current.

7.3.3 DC/DC transformer flux controller

Due to that the applied voltages during the positive and negative cycle are not perfectly equal, it was necessary to use a flux controller with the purpose of centering the current around 0. The bandwidth, $\alpha_{tr,eq}$, used for the flux controller was 40 rad/s and the cutoff frequency for the low pass filter was 125 Hz. In Fig. 7.13 the transformer input current is shown for two cases: black with the DC/DC transformer flux controller in operation and the grey without. These measurements are performed at a low input and output voltage, 0.2 and 0.18 p.u. respectively. From the figure it can be seen that the flux controller manages to keep the flux (transformer current), centered around zero. In this presented case, the

equalization voltage, $v_{tr,eq,ref}$, from the flux controller was around 0.2 % of the input voltage. For the case with the flux controller disabled, it can be seen that the transformer current has a DC-offset of approximately -0.05 p.u. The same operation conditions were used in both the cases.

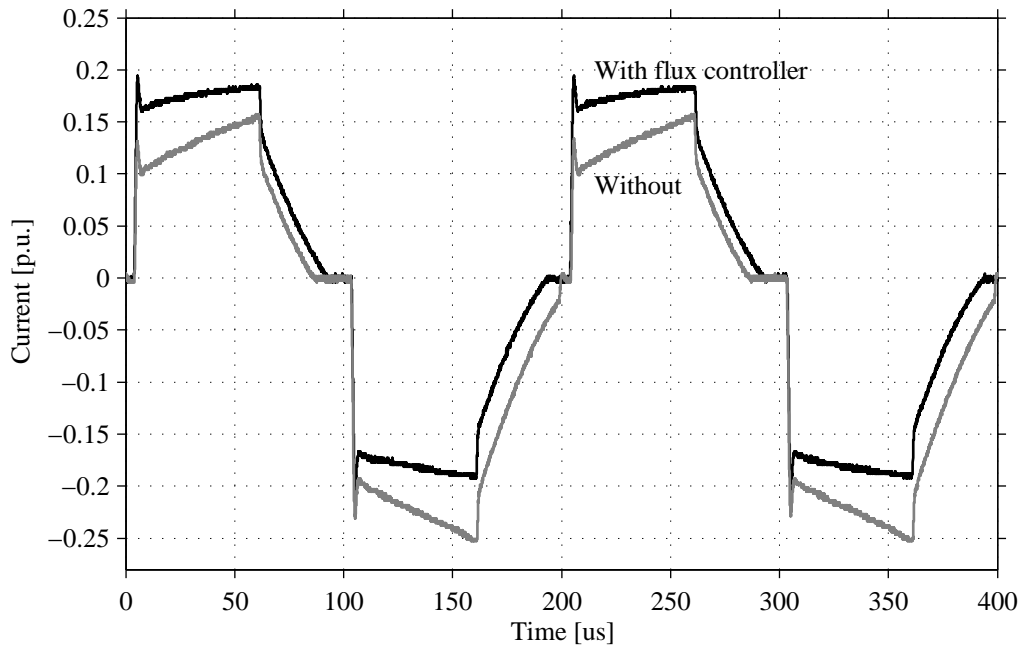


Fig. 7.13 Transformer input current in p.u. for the case with the DC/DC transformer flux controller, black line, and without, grey line. The measurements are made for an input voltage of 0.2 p.u. and an output voltage of 0.18 p.u.

From Fig. 7.12 a) it can be seen that the flux controller also can manage steps in the current. The method presented in Section 5.5.2 was implemented in the experimental setup. From the figure, the initial limitation of the change of voltage can be observed. The first voltage pulse after the reference step is approximately half of the second one which is as desired.

Chapter 8

Conclusions

8.1 Results from present work

In this thesis aspects regarding wind park design and grid connection has been treated.

Various wind turbine systems were investigated from an energy capture point of view. It was found that the difference in energy capture between the investigated systems was quite small, given a specific rotor diameter, the energy capture is almost the same regardless of the system used. The selection of the system to be used thus depend on other factors.

Using these results, six different electrical configurations of wind parks were investigated for the energy production cost. The investigation was done for various wind park sizes, different transmission lengths and different average wind speeds.

It should be stressed that the energy efficiency in itself is of little importance, instead it is the energy production cost that is the interesting quantity. The results regarding the energy production cost for the AC wind parks was as expected. The small AC wind park was best for short transmission distances (up to approximately 20km) and the AC/DC wind park was best for long distances (above approximately 130km). The large AC wind park is best in between the small AC and the AC/DC wind park. The series DC wind park showed a good potential to be cost effective, due to the possibility to operate without a platform. It was found that an increased investment cost of 13% can be allowed for the series DC park before the production cost of this park is equal to that of the large AC park.

Moreover, the electrical limiting factors when wind installations are connected to the grid were investigated. It was found that it is the line capacity and the voltage limitations that sets the limits for the installations. However, for small wind parks using wind turbines of fixed-speed types, care must be taken so that the flicker emission limits, which are set by the utilities, are not exceeded. An interesting observation was found regarding the summation of flicker from individual wind turbines: it was found that the summation formula for flicker given in IEC 61400-21, can result in that the flicker prediction is too low.

The main part of the thesis dealt with the dynamic investigation of the series-connected DC wind park concept. It was found that the proposed control strategy for the series-connected wind turbines proved to operate the wind farm successfully in spite of large variations in the individual turbine powers. However, the wind turbine controllers need a control structure that can handle the operation of the turbine when the input power to the turbines varies strongly. In order to avoid too high energy production loss, the output voltage rating of the wind turbine must be at least 35 % higher than the nominal output voltage (the transmission voltage divided by the number of series-connected wind turbines).

As wind turbine unit DC/DC converters, two candidates were investigated. The Full-bridge isolated boost converter was used in the park simulations, since it is the most difficult one to operate in this application. The full bridge converter was chosen for a design analysis. A down-scaled version of this converter was built and the base current controller functions were experimentally verified.

8.2 Future Research

There are several items regarding the series DC-converter that is worthy of further investigation.

The experimental prototype should be used also to test under and over voltage limitation operation.

A good idea is also to include a better model representation of the wind turbine, with an appropriate pitch and speed controller.

The generating system should also be more looked in to. In particular, a synchronous generator with a diode rectifier, instead of the induction machine and the IGBT rectifier, could lead to a reduction of energy production cost. It would also be nice to build the isolated boost converter and compare the performance with the full bridge converter.

The last item mentioned, but most certainly not the least interesting is the fault handling and protection design. This is a topic that also should be studied further.

References

- [1] ABB Power Technologies AB, “It’s time to connect - Technical description of HVDC Light technology,” Brochure, 2005.
- [2] T. Ackermann, R. Leutz, and J. Hobohm, “World-wide offshore wind potential and european projects,” in *Power Engineering Society Summer Meeting, 2001. IEEE*, Vancouver, BC, Canada, 15-19 June, 2001, pp. 4–9 vol.1.
- [3] T. Ackermann, “Transmission systems for offshore wind farms,” *Power Engineering Review, IEEE*, vol. 22, no. 12, pp. 23–27, Dec. 2002.
- [4] V. Akhmatov, H. Knudsen, and A. Nielsen, “Advanced simulation of windmills in the electric power supply,” *Electrical Power and Energy Systems*, vol. 22, no. 6, pp. 421–434, 2000.
- [5] L. Ängquist, “Synchronous voltage reversal control of thyristor controlled series capacitor,” Ph.D Thesis, Royal Institute of Technology, Department of Electrical Engineering, Stockholm, Sweden, 2002.
- [6] K. Åström and T. Hägglund, *PID controllers; theory, design and tuning*. Research Triangle Park, NC: Instrument Society of America, 1995.
- [7] K. Åström and B. Wittenmark, *Computer Controlled Systems, Theory and Design*. Prentice-Hall, Inc., 1984.
- [8] R. Barthelmie and S. Pryor, “A review of the economics of offshore wind farms,” *Wind engineering*, vol. 25, no. 3, pp. 203–213, 2001.
- [9] P. Bauer, S. de Haan, C. Meyl, and J. Pierik, “Evaluation of electrical systems for offshore windfarms,” in *IEEE Industry Applications Conference 2000*, 8-12 Oct. 2000, pp. 1416 –1423 vol.3.
- [10] E. Bossanyi, “The design of closed loop controllers for wind turbines,” *Wind Energy*, vol. 3, no. 3, pp. 149–163, July/September 2000.

References

- [11] C. Bryan, J. Smih, J. Taylor, and B. Zavadil, "Engineering design and integration experience from cape wind 420 MW," in *Fourth International Workshop on Large-Scale Integration of Wind Power and Transmission Networks for Offshore Wind Farms*, Billund, Denmark, 20-21 October, 2003.
- [12] K. Burges, E. van Zuylen, J. Morren, and S. de Haan, "DC transmission for offshore wind farms: Concepts and components," in *Second International Workshop on Transmission Networks for Offshore Wind Farms*, Stockholm, Sweden, 30-31 March, 2001.
- [13] J. Claassens and I. Hofsjager, "A flux balancer for phase shift zvs dc-dc converters under transient conditions," in *Applied Power Electronics Conference and Exposition, 2006. APEC '06*.
- [14] G. Demetriades, "On small-signal analysis and control of the single- and dual-active bridge topologies," Ph.D Thesis, Royal Institute of Technology, Department of Electrical Engineering, Stockholm, Sweden, 2005.
- [15] Elsam A/S, "Horns Rev Offshore Wind Farm, Ground-breaking wind power plant in the north sea," Information folder. [Online]. Available: http://www.hornsrev.dk/nyheder/brochurer/Horns_Rev_GB.pdf
- [16] —, "Horns Rev Offshore Wind Farm, The world's largest offshore wind energy project," Information folder. [Online]. Available: <http://www.hornsrev.dk>
- [17] Eltra, "Eltra's 150 kV-kabelanlaeg Blåvand-Karlgårde," Information folder. [Online]. Available: http://www.eltra.dk/media/1030_12817.pdf
- [18] A. Grauers and S. Landström, "The rectifiers influence on the size of direct-driven generators," in *European Wind Energy Conference and Exhibition (EWEC '99)*, Nice, France, March 1-5, 1999.
- [19] A. Grauers and A. Lindskog, "PM generator with series compensated diode rectifier," in *2000 IEEE Nordic Workshop on Power and Industrial Electronics (NORpie/2000)*, Aalborg, Denmark, 13-16 June, 2000, pp. 59–63.
- [20] A. Grauers, "Design of direct-driven permanent-magnet generators for wind turbines," Ph.D Thesis, Chalmers University of Technology, Department of Electric Power Engineering, Göteborg, Sweden, October 1996.
- [21] L. H. Hansen, L. Helle, F. Blaabjerg, E. Ritchie, S. Munk-Nielsen, H. Bindner, P. Sørensen, and B. Bak-Jensen, "Conceptual survey of generators and power electronics for wind turbines," Risø National Laboratory, Roskilde, Denmark, Tech. Rep. Risø-R-1205(EN), December 2001, ISBN 87-550-2743-8.

- [22] L. Harnefors and H.-P. Nee, "Model-based current control of ac machines using the internal model control method," *IEEE Transactions on Industry Applications*, vol. 34, no. 1, pp. 133–141, January. 1998.
- [23] L. Harnefors, *Control of Variable-Speed Drives*. Department of electronics, Mälardalen University, Västerås, Sweden: Applied signal processing and control, 2002.
- [24] M. Häusler and F. Owman, "AC or DC for connecting offshore wind farms to the transmission grid?" in *Third International Workshop on Transmission Networks for Offshore Wind Farms*, Stockholm, Sweden, 11-12 April, 2002.
- [25] G. Johnson, *Wind Energy Systems*. Prentice-Hall, 1985.
- [26] N. Kirby, L. Xu, M. Luckett, and W. Siepman, "HVDC transmission for large offshore wind farms," *Power Engineering Journal*, vol. 16, no. 3, pp. 135 –141, June 2003.
- [27] H. Klug, T. Osten, and J. Gabriel, "Noise from wind turbines or: How many megawatts can you get for a 100dB(A)?" in *European wind energy conference*, Dublin Castle, Ireland, October 1997, pp. 124–127.
- [28] Z. W. Kuffel, E. and J. Kuffel, *High Voltage Engineering: Fundamentals*. Butterworth-Heinemann, 2000.
- [29] M. Kuhn and S. T., "Utgrunden offshore wind farm - first results of design verification by measurements," in *European Wind Energy Conference 2001*, Copenhagen, Denmark, 2-6 July 2001, pp. 545 – 548.
- [30] S. Lundberg, "Evaluation of wind farm layouts," in *Nordic Workshop on Power and Industrial Electronics (NORPIE 2004)*, Trondheim, Norway, 14-16 June, 2004, p. CD.
- [31] —, "Electrical limiting factors for wind energy installations," Diploma thesis, Chalmers University of Technology, Department of Electric Power Engineering, Göteborg, Sweden, December 2000.
- [32] —, "Configuration study of large wind parks," Licentiate Thesis, Chalmers University of Technology, Department of Electric Power Engineering, Göteborg, Sweden, October 2003.
- [33] —, "Performance comparison of wind park configurations," Department of Electric Power Engineering, Chalmers University of Technology, Department of Electric Power Engineering, Göteborg, Sweden, Tech. Rep. 30R, August 2003.

References

- [34] K. Macken, L. Driesen, and R. Belmans, "A DC bus system for connecting offshore wind turbines with the utility system," in *European Wind Energy Conference 2001*, Copenhagen, Denmark, 2-6 July 2001, pp. 1030 – 1035.
- [35] O. Martander and J. Svensson, "Connecting offshore wind farms using DC cables," in *Wind Power for the 21st Century*, Kassel, Germany, 25-27 September 2000.
- [36] O. Martander, "DC grids for wind farms," Licentiate Thesis, Chalmers University of Technology, Department of Electric Power Engineering, Göteborg, Sweden, June 2002.
- [37] N. Mohan, T. Underland, and R. W.P., *Power Electronics Converters, Applications, and Design*. John Wiley and Sons, Inc., 2003.
- [38] R. Ottersten, "On control of back-to-back converters and sensorless induction machine drives," Ph.D Thesis, Chalmers University of Technology, Department of Electric Power Engineering, Göteborg, Sweden, 2003.
- [39] M. Papadopoulos, S. Papthanassiou, N. Boulaxis, and S. Tentzerakis, "Voltage quality change by grid-connected wind turbines," in *European Wind Energy Conference*, Nice, France, 1-5 March 1999, pp. 782–785.
- [40] A. Petersson and S. Lundberg, "Energy efficiency comparison of electrical systems for wind turbines," in *Nordic Workshop on Power and Industrial Electronics (NORpie 2002)*, Stockholm, Sweden, August 12-14, 2002, pp. CD-ROM.
- [41] T. Petru, "Modeling of wind turbines for power system studies," Ph.D Thesis, Chalmers University of Technology, Department of Electric Power Engineering, Göteborg, Sweden, June 2003.
- [42] S. Rehman, T. Halawani, and M. Mohandes, "Wind power cost assessment at twenty locations in the kingdom of saudi arabia," *Renewable Energy*, vol. 28, pp. 573–583, 2003.
- [43] F. Santjer, L.-H. Sobeck, and G. Gerdes, "Influence of the electrical design of offshore wind farms and of transmission lines on efficiency," in *Second International Workshop on Transmission Networks for Offshore Wind Farms*, Stockholm, Sweden, 30-31 March, 2001.
- [44] M. Schubert and J. Molly, "Megawatt wind turbines - lessons learned," in *European wind energy conference*, Dublin Castle, Ireland, October 1997, pp. 193–196.
- [45] T. Schütte, M. Ström, and B. Gustavsson, "The use of low frequency AC for offshore wind power," in *Second International Workshop on Transmission Networks for Offshore Wind Farms*, Stockholm, Sweden, 30-31 March, 2001.

- [46] SEAS, “Nysted Havmøllepark,” Information folder. [Online]. Available: <http://uk.nystedhavmoellepark.dk/upload/pdf/NystedDK.pdf>
- [47] W. Siepmann, “AC transmission technology for offshore wind farms,” in *Second International Workshop on Transmission Networks for Offshore Wind Farms*, Stockholm, Sweden, 30-31 March, 2001.
- [48] C. Skaug and C. Stranne, “HVDC wind park configuration study,” Diploma thesis, Chalmers University of Technology, Department of Electric Power Engineering, Göteborg, Sweden, October 1999.
- [49] A. Skytt, P. Holmberg, and L. Juhin, “HVDC light for connection of wind farms,” in *Second International Workshop on Transmission Networks for Offshore Wind Farms*, Stockholm, Sweden, 30-31 March, 2001.
- [50] K. Smith and G. Hagerman, “The potential for offshore wind energy development in the united states,” in *Second International Workshop on Transmission Networks for Offshore Wind Farms*, Stockholm, Sweden, 30-31 March, 2001.
- [51] P. Sørensen, G. Gerdes, F. Santjer, N. Robertson, W. Davy, M. Koulouvari, E. Morfiadakis, and Å. Larsson, “Standards for measurements and testing of wind turbine power quality,” in *European Wind Energy Conference*, Nice, France, 1-5 March 1999, pp. 721–724.
- [52] P. Sørensen, J. Tande, L. Söndergaard, and J. Kledal, “Flicker emission levels from wind turbines,” *Wind Engineering*, vol. 20, no. 1, pp. 39–46, 1996.
- [53] J. Svenson and F. Olsen, “Cost optimising of large-scale offshore wind farms in the danish waters,” in *1999 European Wind Energy Conference*, Nice, France, 1-5 March, 1999, pp. 294–299.
- [54] Sveriges elleverantörer, “Anslutning av mindre produktionsanläggningar till elnätet (AMP),” in Swedish, 1999.
- [55] T. Thiringer and J. Linders, “Control by variable rotor speed of a fixed-pitch wind turbine operating in a wide speed range,” *IEEE Transactions on Energy Conversion*, vol. 8, no. 3, pp. 520–6, Sept. 1993.
- [56] T. Thiringer and A. Petersson, “Control of a variable-speed pitch-regulated wind turbine,” Department of Energy and Environment, Chalmers University of Technology, Department of Energy and Environment, Göteborg, Sweden, Tech. Rep., 2005.
- [57] T. Thiringer, “Research program of the utgrunden demonstration offshore wind farm, final report: Part 3, wp 2, electrical,” Department of Energy and Environment, Chalmers University of Technology, Department of Energy and Environment, Göteborg, Sweden, Tech. Rep. STEM P11518-2, 2005.

References

- [58] R. Thomas, A. Phadke, and C. Pottle, “Operational characteristics of a large wind-farm utility-system with a controllable AC/DC/AC/Interface,” *IEEE Transactions on Power Systems*, vol. 3, no. 1, pp. 220–225, Feb. 1988.
- [59] T. van Engelen, E. van der Hooft, and P. Schaak, “Development of wind turbine control algorithms for industrial use,” in *European Wind Energy Conference 2001*, Copenhagen, Denmark, 2-6 July 2001, pp. 1098 – 1101.
- [60] L. Weimers, “New markets need new technology,” in *Power System Technology, 2000. Proceedings. PowerCon 2000*, 4-7 Dec. 2000, pp. 873–877 vol.2.
- [61] L. Weixing and O. Boon-Teck, “Optimal acquisition and aggregation of offshore wind power by multiterminal voltage-source HVDC,” *Power Delivery, IEEE Transactions on*, vol. 18, no. 1, pp. 201 –206, Jan 2003.
- [62] “PSCAD/EMTDC power system simulation software,” Version 3.0.8, Manitoba HVDC Research Centre Inc., winnipeg, Manitoba, Canada.

Appendix A

Data for the implemented models

Turbine parameters	Symbol	Value
Turbine inertia (high speed side)	J	457 kgm ²
Rated speed (electrical speed)		314 rad/s

Induction machine parameters	Symbol	Value
Rated voltage		400 V
Rated current		3.5 kA
Stator resistance	R_s	0.73 m Ω
Stator leakage inductance	L_σ	56 μ H
Rotor resistance	R_R	0.58 m Ω
Magnetizing inductance	L_M	0.96 mH
Pole pair number	n_p	2

DC-link	Symbol	Value
DC-link capacitance	C_{in}	30 mF

Appendix A. Data for the implemented models

FBIB converter	Symbol	Value
Rated input voltage	v_{in}	0.73 kV
Rated input current	i_{in}	3.0 kA
Nominal output voltage	$v_{WT,nom}$	15 kV
Output capacitor	C_{out}	70 μ F
Input inductor	L_{IB}	0.25 mH
Inductor resistance	$R_{L,IB}$	0.5 m Ω
IGBT conduction resistance	$R_{on,IGBT}$	1.1 m Ω
IGBT conduction voltage drop	$V_{on,IGBT}$	2 V
Diode conduction resistance	$R_{on,diode}$	42 m Ω
Diode conduction voltage drop	$V_{on,diode}$	12 V
Snubber resistance	R_{snubb}	450 Ω
Snubber capacitance	C_{snubb}	200 μ F
FBIB transformer parameters	Symbol	Value
Rating		2 MVA
Frequency		5 kHz
Leakage inductance		0.001 p.u.
Magnetizing current		10 %
Turns ratio		10

Appendix B

Selected Publications

Paper I

A. Petersson, S. Lundberg, T. Thiringer, "A DFIG Wind-turbine Ride-Through System Influence on the Energy Production," *Wind Energy*, vol. 8, issue 3, pp. 251-263, July/September 2005.



I

Paper II

A. Petersson, S. Lundberg, "Energy Efficiency Comparison of Electrical Systems for Wind Turbines," *Nordic Workshop on Power and Industrial Electronics (NORpie 2002)*, Stockholm, Sweden, August 12-14, 2002, CD-ROM.



Paper III

S. Lundberg, T. Petru, and T. Thiringer, "Electrical limiting factors for wind energy installations in weak grids," *International Journal of Renewable Energy Engineering*, vol. 3, no. 2, pp. 305 - 310, August, 2001.



Paper IV

T. Thiringer, T. Petru, S. Lundberg, "Flicker Contribution from Wind Turbine Installations," *IEEE Transactions on Energy Conversion*, vol. 19, no. 1, pp. 157-163, March 2004.



IV

Paper V

S. Lundberg, "Evaluation of wind farm layouts," *EPE Journal*, vol. 16, no. 1, pp. 14-21, February 2006.



Paper VI

O. Carlsson, **S. Lundberg**, “Integration of Wind Power by DC-Power Systems,”
PowerTech Conference, St. Petersburg, Russia, June 2005, Panel session paper.

A black square containing the white Roman numeral VI.

Paper VII

L. Max and **S. Lundberg**, "System efficiency of a DC/DC converter based wind turbine grid system," *Nordic Wind Energy Conference*, Espoo, Finland, 22-23 May, 2006.



VII